MASSEY UNIVERSITY

Instructions:

(1) Please complete two of these forms, by providing title details and striking out one option from each of the sections 1-3.

(2) If you select option b of any section you must include a specific time period. The maximum permitted period is 24 months.

(3) Include the two forms with the copies of your thesis submitted to your supervisor.

(4) The Library must receive the original of your thesis.

(5) We strongly recommend that you provide the Library with two copies of your thesis if it has colour plates.

Massey University Library. Thesis Copyright Form

Title of thesis: The Effect of Added Electrolyte on the Phase Behaviour of a Micellar Liquid Crystal System

(1) (a) I give permission for my thesis to be made available to readers in the Massey University Library under conditions determined by the Librarian.

~~(b)~~ I do not wish my thesis to be made available to readers without my written consent for _____ months.

(2) (a) I agree that my thesis, or a copy, may be sent to another institution under conditions determined by the Librarian.

~~(b)~~ I do not wish my thesis, or a copy, to be sent to another institution without my written consent for _____ months.

(3) (a) I agree that my thesis may be copied for Library use.

~~(b)~~ I do not wish my thesis to be copied for Library use for _____ months.

Signed A. N. Parker
M. J. N. Malcolm
Professor of Chemistry

Date 26-3-90

The copyright of this thesis belongs to the author. Readers must sign their name in the space below to show that they recognise this. They are asked to add their permanent address.

NAME AND ADDRESS DATE

Th
Par

THE EFFECT OF ADDED ELECTROLYTE ON THE PHASE BEHAVIOUR OF THE MICELLAR LIQUID CRYSTAL SYSTEM CAESIUM PENTADECAFLUOROOCTANOATE / WATER.

A thesis presented in the partial fulfilment
of the requirements for the degree
of Master of Science
in Chemistry at
Massy University

Ashok Neil Parbhu

1990

ABSTRACT

This thesis is a study of the effects of added electrolyte (CsCl) on the aggregate structure and hence on the macroscopic phase behaviour of the micellar liquid crystal system caesium pentadecafluorooctanoate / heavy water. The techniques used were ^{2}H, ^{133}Cs and ^{35}Cl N.M.R. spectroscopy. The relationship between the quadrupole splittings of these nuclei and the structure and order of the liquid crystal mesophase is discussed in detail. A partial phase diagram for the CsPFO / CsCl / $^{2}H_2O$ system at a fixed 1 : 1 weight ratio of CsPFO to $^{2}H_2O$ is presented. The phase behaviour has been compared with that for a hydrocarbon surfactant. The changes in phase transition temperatures with added salt has been shown to be due to an increase in the micellar size. This increases with added electrolyte but is constant along the lamellar to nematic transition line. It is shown that there is a strong coupling between micelle size and the micellar fractional surface charge.

Specifically the effect of caesium chloride on the CsPFO / $^{2}H_2O$ system was investigated using ^{2}H, ^{133}Cs and ^{35}Cl N.M.R. spectroscopy to probe the micellar structure and identify the phase transitions. A full description of the N.M.R theory pertaining to this work is presented.

Acknowledgements

I would like to express my appreciation to my supervisor, Associate Professor Ken Jolley, for his encouragement and guidance both within and out of the NMR laboratory and especially for his patience.

I would also like to thank my colleagues Dr David Parker and Mr Mark Smith for their advice, encouragement and invaluable contribution to my research.

Thank you to Mr Grant Platt, the glassblower, for his assistance in the sealing of my NMR tubes.

I wish to thank all my friends for their interest and help, especially I want to thank Karen for her support to the end to get this thesis finished.

Finally I would like to acknowledge my appreciation to my family; Mum, Dad, Bharat and Ramela, for basically just being there for me over the years.

TABLE OF CONTENTS

1. INTRODUCTION

Lyotropic liquid crystals were known to the ancient world in the form of concentrated soap solutions. These viscous solutions are now refered to as smectic (Greek: σμῆγμα = soap) phases. Until recently however scientists have paid little attention to them other than to "rough out" phase diagrams for mainly the commercial purposes of soap and detergent manufacturing.

Lyotropic liquid crystals are composed of two or more components, where one of the components is a an amphiphile and the other essential component is a solvent (usually water). An amphiphile is a molecule which consists of a polar head group and non-polar hydrophobic chain. Examples of amphiphile molecules are soaps, phospholipids, synthetic detergents and some proteins. Other components of lyotropic liquid crystals system can be alcohols and/or inorganic salts. Phase transitions in these systems can be brought about by both temperature and composition changes.

Historically the general belief was that amphiphiles on dissolution in water, would form small discrete micelles in dilute solutions [1], and liquid crystals with extended aggregate structures in concentrated solutions [2,3,4]. The small discrete micelles can be spherical, disc or rod shaped, while the extended aggregate structures are cylinders or bimolecular layers of indefinite size. As a result of this artificial separation research into micellar solutions and lyotropic liquid crystals has evolved as separate fields of endeavour.

Another type of liquid crystal which was only discovered in 1888 [5] are the thermotropic liquid crystals, which typically consist of long lathe-like molecules or disk shaped molecules. These systems can be single components, or mixtures of similar types of molecules. As their name suggests phase changes are brought about by temperature

changes. The long thin molecules undergo a sequence of phase transitions from isotropic where there is no long range orientational order to nematic (Greek: νῆμα = thread) where there is long range orientational order, to smectic where there is long range orientational and translational order of the symmetry axes of the molecules, on decreasing the temperature. The corresponding sequence for disk shaped molecules is isotropic to nematic to columnar. The commercially exploitable phase is the nematic phase, and the closely related cholesteric phase formed from molecules with chiral centres. The useful property of these phases is that they can be aligned in a magnetic or electric field as a consequence of anisotropy in their diamagnetic or dielectric susceptibilities. The molecules therefore align themselves in the force field so as to minimize their energy by aligning along (+ve susceptibility) or at 90^0 to (-ve susceptibility) the direction of the field. This property has resulted in massive commercial exploitation of thermotropic liquid crystals starting in the early 70's .

At the end of the 60's a magnetically orientatable lyotropic phase was discovered [6] which by analogy with the thermotropic liquid crystals was given the title nematic phase. This discovery has lead (albeit slowly at first) to renewed interest in lyotropic liquid crystals. Several more lyotropic nematic phases have now been discovered.

The early reported nematic phases were located over narrow concentration ranges in complex mixtures of amphiphile, solvent and salts or alcohols such as the sodium decyl sulfate/decanol/water system which exhibits a nematic phase, for a fixed weight fraction of decanol of 0.07, over an amphiphile weight fraction range w from 0.34 to 0.39 [7]. For a long time it was thought that a third component (salt or alcohol) was essential for the production of stable nematic phases. However, several binary systems which exhibit nematic phases have now been observed. The decylammonium chloride(DACl)/water system for example, which was long thought to require salts to form a stable nematic

phase, exhibits such a phase over the range w = 0.42 to 0.49 [8]. The disodium cromoglycate/water system also exhibits a nematic phase from w = 0.10 to 0.15 [9]. These are examples of hydrocarbon amphiphiles where the nematic range is typically limited to very small concentration ranges. On the other hand fluorocarbon amphiphiles have been observed to exhibit nematic phase regions over large temperature and concentration ranges in aqueous solutions. These include the caesium , ammonium and tetramethylammonium salts of pentadecafluorooctanoic [10,11,12] and heptadecafluorononononoic acids [12,13]. To date the only system for which a high resolution phase diagram has been published is the caesium pentadecafluorooctanoate (CsPFO) / water system [10,14]. It is likely that other soaps of the perfluorinated carboxylic acids will produce nematic phases but solubility limitations can prevent these from being observed [12].

The obvious question is, what is the molecular property which allows the phase to become oriented in a magnetic field? Thermotropics become orientated in the nematic phase as a result of the diamagnetic anisotropy of the molecules. In lyotropic liquid crystals, in the nematic phase, it has been shown that the structural unit consists of anisotropic micelles. The first report of a micellar nematic phase [15,16] has been followed by many more and it is now clear that uniaxial nematic micellar phases can be prepared from both ionic [17] and non-ionic [18] amphiphiles.

Nematic micellar mesophase are classified in terms of the micellar structure. There are three distinct structural varieties of anisotropic micelle: rod shaped, disc shaped, or biaxial micelles. Rod shaped micelles, maybe actual rods with semi-spherical end caps or prolate ellipsoids, form a nematic mesophase designated as 'canonic' (Greek : κανων = rod) and denoted N_C. The disc shaped micelles, maybe flat discs, discs with hemispherical rims or oblate ellipsoids, form a nematic mesophase designated as discotic

(Greek : δισχοξ = quoit) and denoted N_D. There are also biaxial micelles, maybe asymmetric ellipsoids or biaxial platelets, which form biaxial nematic mesophases denoted as N_B [19]. These classifications can be sub-classified as either + or - depending upon the diamagnetic susceptibility anisotropy of the aggregate, defined by $\Delta\chi = \chi_{//} - \chi_{\perp}$. $\chi_{//}$ and $\chi_{\perp}$ are respectively the components of the aggregate diamagnetic susceptibility parallel and perpendicular to the director. A micelle with a positive diamagnetic susceptibility anisotropy will align with its symmetry axis parallel to a magnetic field and one with a negative anisotropy will align perpendicular to the field.

Recently the CsPFO / water system has been shown to undergo a series of order-disorder transitions analogous to the isotropic to nematic to smectic A series of transitions in thermotropic liquid crystals. Other systems also exhibit this behaviour [20]. In all of these systems there exists a concentration regime where the nematic to lamellar transition simply involves the imposition of translational order on decreasing the temperature. There is no reason to suppose that this behaviour is unique to the above systems and it is quite possible that there is universal behaviour in both thermotropic and lyotropic liquid crystals.

The nature of the interaggregate interactions which drive the phase transitions must however be different as the fundamental structural unit in thermotropics is an anisotropic molecule while in lyotropics it is an anisotropic charged aggregate. The driving force of thermotropic organization is attraction between cores of lathe-like or disc-shaped molecules while for lyotropics it is the repulsive interaction between charged aggregates that dominates (+ve or -ve depending on the nature of the head group) [21] , although there is evidence that long range attractive potentials are also involved [22]. Another complication in lyotropic liquid crystals is that the size and shape of the aggregate varies with temperature and composition, i.e. it does not have fixed dimensions, and the

packing fraction of the micelles is relatively low compared with that for thermotropics. By modifying the shape and size of the micelle (aggregate) it should be possible to produce liquid crystals with "designer" properties, and in particular nematic phases with exploitable qualities. One possible way to effect micelle size and shape is to alter the counter-ion binding at the micellar surface. This will alter the charge density at the surface and will also moderate the intermicellar interactions.

The aim of this study was to examine the effect of added salt on the phase behaviour of the CsPFO / ^2H_2O system. In addition it was hoped to relate the phase behaviour to the changes in the size and/or shape of the micelles, and to see if these changes could be related to the degree of counter-ion binding.

The CsPFO/CsCl/^2H_2O system was chosen for this study because as a system it has many attractive features. Firstly, the CsPFO/^2H_2O system exhibits an N_D^+ phase over a wide range of both concentration (0.225 to 0.632 weight fraction, w, of CsPFO) and temperature (285.3 to 351.2 K) [10] . This phase lies between an isotropic micellar solution phase I to higher temperatures and a lamellar phase to lower temperatures. There is no detectable change in the size of the discoid micelle at the transition from N_D^+ to lamellar phase [21,23] which suggests that in the lamellar phase the small discoid micelle is stable with respect to the classical bilayer, i.e. it is an L_D phase. Secondly, because it is a simple two component system the effect of added salt will be clear and thirdly, the phase transitions are a simple series of order-disorder transitions as demonstrated in figure 1 .

Another advantage of the system is that because the nematics phase has positive diamagnetic susceptibility the local director will align along the director of a magnetic field to give a macroscopically aligned uniaxial mesophase. This is a particularly useful

Figure 1. Schematic representation of order-disorder transitions in a system of discoidal micelles. The director **n** represents the preferred orientation of the micelle symmetry axis. In the nematic phase there is the imposition of orientational ordering of the symmetry axes and in the lamellar phase positional ordering of the centre of masses is also present.

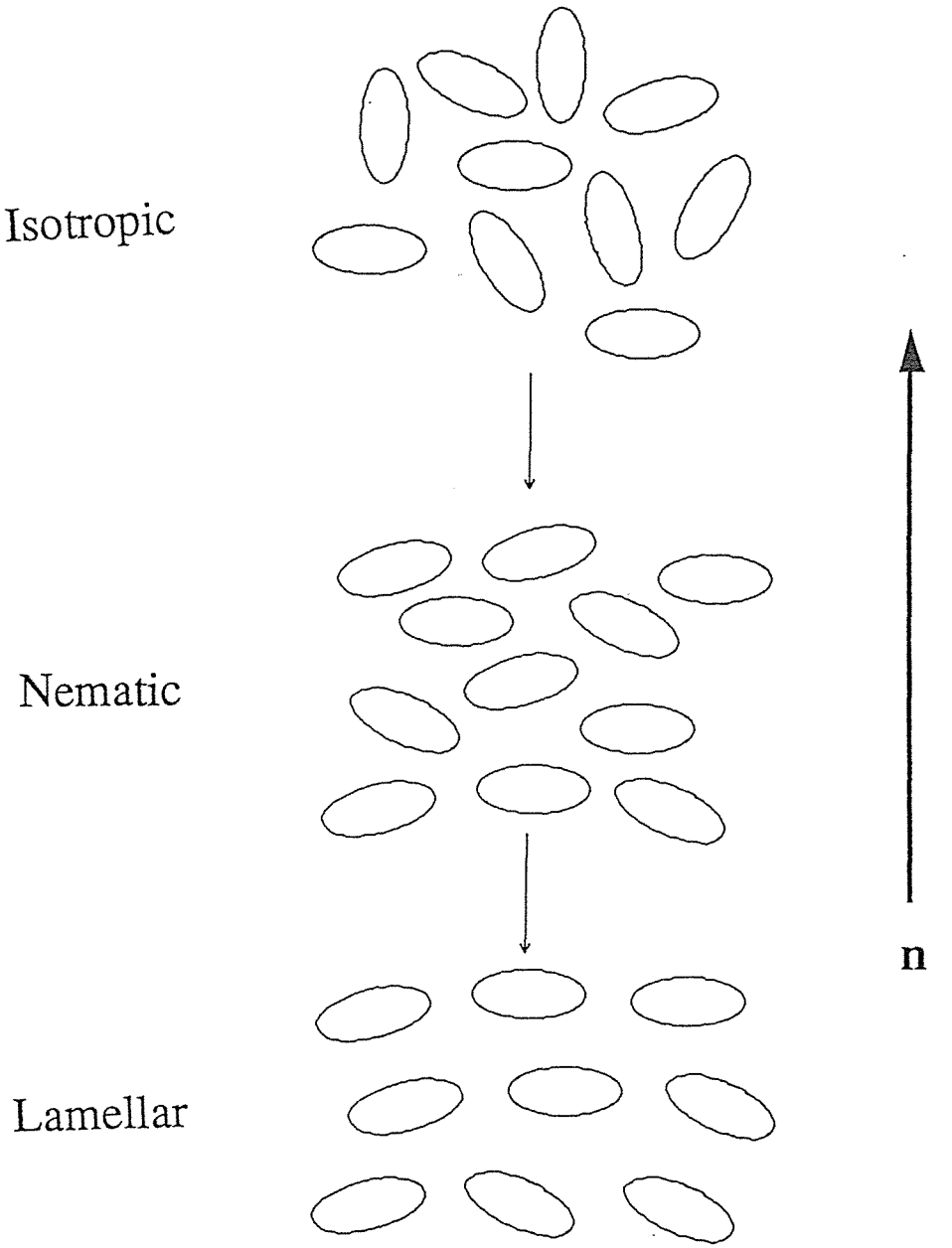
Isotropic
Nematic
Lamellar
n

property for the detection of phase transition temperatures. These features have obviously appealed to many other researchers as the CsPFO/^2H_2O system and some of its analogs have been extensively investigated. The main reason for its popularity is the published high resolution phase diagram of the system which is the only one so far published [10]. In particular the system has attracted the attention of physicists who have studied the effect of the counter-ion, alcohols, salts, and mixed amphiphiles on the pretransitional behaviour at the I to N_D^+ transition [24,25,26]. The N_D^+ to L_D transition on the other hand has received little attention to date. The concentration chosen to study the effects of added salt was w = 0.5, at this concentration the N_D^+ to L_D transition is first order. In the binary system the transition becomes second order on decreasing w at a tricritical point Tcp (w = 0.43, T = 304.80 K). We have chosen CsCl as the salt to examine the effect of an electrolyte, because in having a common cation for the salt and the amphiphile, there are no complications from the effects of competitive (selective) ion binding at the micellar surface.

All investigations into both the mesophase behaviour and the micellar structure were conducted by examining the NMR of quadrupole nuclei, of which there are three useful ones in the CsPFO/^2H_2O/CsCl system. The ^2H quadrupole splittings of ^2H_2O have been shown to reflect mesophase order as well as aggregate shape and size [10] and ^{133}Cs quadrupole splittings in addition to the above depend also on the degree of counter-ion binding [14]. The ^{35}Cl quadrupole splittings will reflect the degree of coion binding.

A major part of this work involved the elucidation of a precise phase diagram. A strong criticism of previous work on lyotropic liquid crystals is that they have been done on poorly defined systems with inadequate (at best) phase diagrams. In this report the phase diagram for the system CsPFO/^2H_2O/CsCl will be presented first. The weight ratio of CsPFO to ^2H_2O is held constant at 0.5 (which represents a mole ratio of 1 to 27.3) and

the phase transition temperatures are plotted against the weight fraction of CsCl (w_e). Samples will be identified in the text according to their w_e values. The techniques used to define the phase diagram will follow its presentation.

2. EXPERIMENTAL

2.1 SAMPLE PREPARATION

Caesium pentadecafluorooctanoate (CsPFO) was synthesized by the neutralization of a pentadecafluorooctanoic acid (Aldrich-Chemic) solution with caesium carbonate (BHD). The neutralized solution was then dried in an oven at 80 C. The resulting CsPFO was purified by recrystallization from a 1:1 (v/v) solution of n-butanol / n-hexane, after which the CsPFO was further purified by recrystallization from ethanol. To remove any solvents the crystals were dried under vacuum (0.5 mmHg) for up to 36 hours. The crystals recovered were white and glossy, indicative of high purity. No melting point of the crystalline salt could be established because the crystals start to decompose at 495 K. An indication of the purity of the sample was the transition temperatures for the $w_e = 0$ sample which agreed to within 0.1 K to those previously determined [10,14].

A bulk standard 0.5 weight fraction CsPFO /^2H_2O was prepared from ^2H_2O (Sigma, 99.8% ^2H) and CsPFO. This was done by weighing directly into a glass ampule, which was then immediately flame sealed to avoid concentration changes due to either evaporation or the absorption of H_2O by the hygroscopic ^2H_2O. The sample was then heated in an oven to 80 C and mixed repeatedly until a homogeneous isotropic phase was formed.

NMR samples were prepared by weighing both the caesium chloride (A.R. grade, Lonover scientific, London) ,which had previously been dried under vacuum and then used without further purification, and the standard 0.500 weight fraction CsPFO/^2H_2O, directly into 5 mm o.d. NMR tubes. Before the CsPFO/^2H_2O solution was unsealed it was heated into the isotropic phase and then mixed to ensure homogeneity. Having the

sample in the isotropic phase facilitated the transfer of the CsPFO/^2H_2O into the NMR tubes. This was achieved using a constant volume micropipettor with a long hypodermic syringe needle, so that the sample could be placed in the base of the tube. The CsCl was added through a long glass funnel which fitted inside the NMR tube. Both of these methods avoided contact of the sample constituents with the upper section of the NMR tube. This is essential so as to prevent any alterations in concentration due to evaporation of ^2H_2O or the decomposition of CsPFO when the tubes are flame sealed. Following the weighings the tubes were immediately flame sealed. Thus all samples had a constant weight fraction ratio of 0.5 (mole ratio of 1: 27.3), of CsPFO to ^2H_2O. To enable the sample to be mounted in the sample cell (see next section) the tubes were extended, with 5 mm o.d. glass tubing, to a total length of 65.5 cm .

2.2 TEMPERATURE CONTROL

In determining phase transition temperatures it is important to have both stable and accurate temperature control of the sample. Temperature control was maintained by mounting the extended sample tube into a double pass water flow sample cell (see figure 2). The cell was constructed by the glassblower of the department of Chemistry and Biochemistry to fit the dimensions of the Oxford Instruments 6.34 T wide-bore magnet. The cell can be easily customized to suit the dimensions of other magnets, either superconducting or iron. The sample cell was connected to a Colora wk3 cryo-thermostat via thermally insulated silicone tubing . The control water had a relatively high flow rate so that there was no measurable temperature gradient over the sample length. The importance of this temperature homogeneity will be considered in detail in section 5.1.1.

Figure 2. Double pass water flow sample cell used to control temperature during NMR experiments.

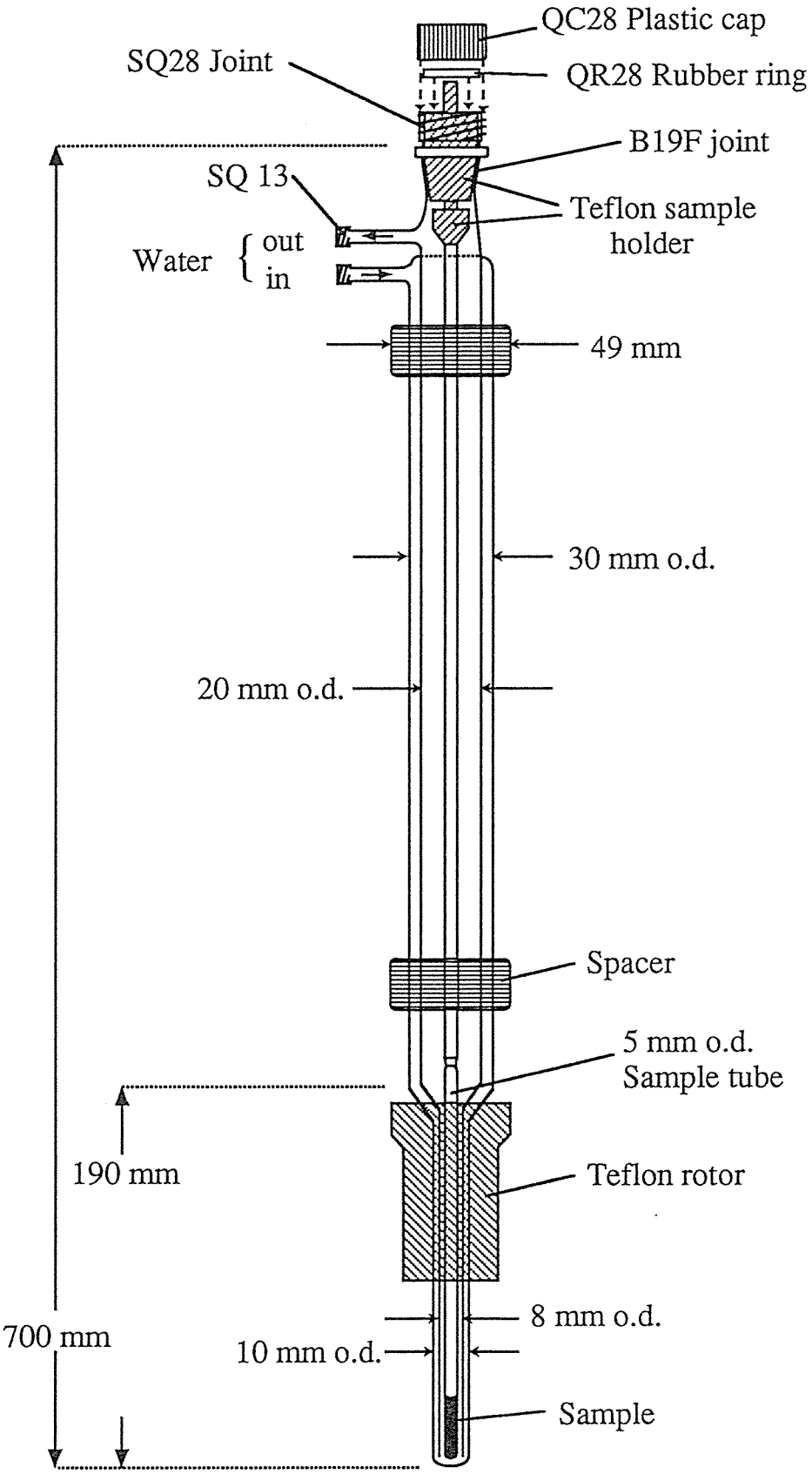
QC28 Plastic cap
SQ28 Joint
QR28 Rubber ring
B19F joint
SQ 13
Teflon sample holder
Water
out
in
49 mm
30 mm o.d.
20 mm o.d.
Spacer
5 mm o.d.
Sample tube
190 mm
Teflon rotor
8 mm o.d.
700 mm
10 mm o.d.
Sample

The temperature was measured by a copper / constantan thermocouple using an ice slurry reference point. The thermocouple was placed as close to the sample as was consistent with good resolution. The thermocouple potential was measured with a Philips PM2535 systems multimeter, to an accuracy of 0.1 μV. The thermocouple was calibrated at 2 K intervals to an accuracy of 1 mK, against a Hewlett-Packard 2801A digital quartz thermometer with a 2805A temperature probe, which had been calibrated at the Physics and Engineering Laboratory of DSIR, Wellington. The measured thermocouple potential was transformed into temperature (K) by linear interpolation between the calibration points, using a Hewlett-Packard HP85 computer.

2.3 NMR MEASUREMENTS

All NMR measurements were obtained using a Jeol JNM GX270W Pulse Fourier Transform spectometer using an Oxford Instruments 6.34 T wide bore magnet. The tuneable 10mm multinuclear probe (NM-G27T10) was used to observe ^{133}Cs nuclei, while a the tuneable 10mm low frequency multinuclear probe (NM-G27T10L) was used to observe ^{35}Cl nuclei. The G27T10 probe was tuned to the ^{133}Cs nucleus to give a 90° pulse width of 19 μs. Surprisingly it was possible to observe ^{2}H spectra under the same tuning conditions by simply increasing the pulse width to about 200 μs. ^{2}H spectra with good signal to noise ratio were obtained using this pulse width and limitations associated with pulse power distribution over the frequency range of the spectra did not apply since a typical observation frequency for ^{2}H spectra was 2000 Hz (effective frequency range $(1/\tau_p)$ = 5000 Hz). ^{2}H spectra were also observed using the same technique with the G27T10L tuned to the ^{35}Cl nucleus. It should be noted that it would not work the other way round since the average frequency range (see table below) for both ^{133}Cs and ^{35}Cl is much greater than 5000 Hz.

The following table contains typical experimental parameter values for the NMR measurements, although these were often slightly varied depending on the requirements of individual samples.

	Respective Values For Each Nuclei		
parameter	^{133}Cs	^{2}H	^{35}Cl
Observation Frequency /MHz	35.31	41.34	26.34
Accumulations	16	4	1000
Pulse Width /μs	19.0	200.0 *	30.0
Pulse Delay /s	1.0	2.0	0.5
Sweep Width /Hz	32051	2000	24038
Data Points	32768	4096	8192
Resolution /Hz	2	1	6

* Detuned.

3. NMR THEORY

Nuclear magnetic resonance (NMR) is a particularly useful technique for investigations of lyotropic liquid crystals, as the observation and measurement of the quadrupole splittings of quadrupole nuclei provides an insight to the system at the molecular level of the aggregate structure as well as at the macroscopic level of the mesophase structure and order.

Indeed, NMR measurements of the quadrupole splittings of either ^{2}H in heavy water or of counterions is unparalleled as an experimental method for mapping phase diagrams [14] and for studying the mechanism of phase transitions in lyotropic amphiphillic liquid crystals. This is because the quadrupole splittings acts as a signature for a particular phase and is both temperature and composition dependent. At a molecular level for micellar liquid crystal phases the quadrupole splitting is a function of the size and shape of the micellar aggregate, the fraction of bound molecules or ions, and the orientational order parameter of the micelle. To obtain useful information about these parameters it is necessary to examine in detail their contribution to the observed quadrupole splittings. In the following discussion the effect of quadrupole interactions on the Zeeman energies will be presented together with a discussion of the factors contributing to the quadrupole interaction. A brief description of ^{133}Cs chemical shift anisotropy will also be presented.

Most nuclei exhibit spin angular momentum since protons and neutrons have this property. The magnitude of the spin angular momentum vector **P** for any given nucleus, is given by

$$P = \hbar[\, I(I+1)]^{1/2}$$

where I is the nuclear spin quantum number, which can have integral or half integral values. The direction of **P** is defined by another quantum number (m_I) such that the

magnitude of **P** along a reference direction (usually defined in the z direction) is given by

$$P_Z = \hbar m_I$$

where m_I (= +I, +I-1,....-I) can have 2I+1 values. Since the nucleus is also a charged particle there is an associated magnetic moment vector μ, such that

$$\mu = \gamma \mathbf{P}$$

where γ is the nuclear magnetogyric ratio of the nucleus. This is clearly the ratio of magnetic moment to angular momentum and is a characteristic of any given nucleus.

In the absence of a magnetic field the energy of an isolated nucleus is independent of m_I (i.e. independent of orientation). But in the presence of a magnetic field **B**, the nuclear magnetic moment precesses about the magnetic field at an angle θ. It precesses with a frequency, ν, called the Larmor precession frequency, which is characteristic of a given nucleus, and is determined by **B** and γ. The interaction energies which are commonly referred to as Zeeman energies are defined by

$$\mathbf{E} = -\mu.\mathbf{B}$$

with components in the field direction of

$$E = -\gamma \hbar m_I B.$$

So on immersion of a magnetic nucleus of spin I into a magnetic field of flux density **B**, 2I+1 energy levels are generated, each separated by $|\gamma \hbar B|$, i.e.

$$\Delta E = \gamma \hbar \Delta m_I B$$

Transitions between the energy states may be brought about by electromagnetic radiation of the appropriate frequency. The selection rule of the transitions initiated in this way is $\Delta m_I = \pm 1$, giving

$$\Delta E = h\nu = \gamma \hbar B$$

and thus

$$\nu = \frac{\gamma}{2\pi} B$$

In the absence of perturbing interactions, all nuclei of a given species will have the same resonance frequency (ν), and the spectrum will consist of a single absorption line. The effects of Heisenberg uncertainty, relaxation, and inhomogeneities in the magnetic field (causing different resonance conditions through the bulk of the sample), cause the absorption line to have a finite width. A number of perturbing interactions can cause a change in the permitted energy levels, and can thus effect the observed spectrum. Of these, chemical shift and quadrupole interactions are the only perturbing interactions which are relevant to this study.

3.1 QUADRUPOLE ENERGIES FOR NUCLEI WITH ELECTRIC QUADRUPOLE MOMENTS (I> 1/2).

All nuclei with I >1/2 have an ellipsoidal distribution of charge (e), and a consequent electric quadrupole moment (Q). Electric quadrupole coupling occurs when a quadrupole nucleus minimizes electrostatic energy by appropriate alignment within an electric field gradient. For quadrupole nuclei , in the presence of an electric field gradient, the degeneracy of the Zeeman transition is lifted to give 2I transitions with a first order intensity distribution [I(I+1) - m(m+1)]. The magnitude of the interaction is determined by the magnitude of the electric quadrupole coupling constant and the magnitude of the external electric field gradient. In all the practical cases discussed in this thesis the nuclear quadrupole coupling energy is negligibly small compared with the nuclear Zeeman energy, i.e. all spectra are first order.

The nematic phase of CsPFO/^2H_2O is diamagnetically positive. Thus, the nematic director **n** undergoes spontaneous alignment along the direction of the spectrometer magnetic field **B** to give a macroscopically aligned sample. For this and, indeed, for any

other macroscopically aligned uniaxial mesophase, the first order spectrum for any spin I > 1/2 will consist of 2I equally spaced lines with separation, henceforth referred to as the quadrupole splitting, given by [27,28]

$$\Delta\nu(\phi) = \frac{3}{2I(2I-1)} |\tilde{q}_{zz}| P_2(\cos\phi) \qquad (1)$$

where the upper tilde denotes partially averaged quantities. In equation (1) $P_2(\cos\phi) = \frac{1}{2}(3\cos^2\phi - 1)$ and is a second-rank Legende polynomial describing the orientation of the mesophase director (**n**) with respect to the magnetic field. ϕ is the angle between the mesophase director and the direction of the magnetic field, which experimentally is the spectrometer magnetic field, **B**. In this study, most of the measurements were made on a uniaxially aligned sample such that $\phi = 0$ and thus $P_2(\cos\phi) = 1$. $|\tilde{q}_{zz}|$ is the partially averaged component of the nuclear quadrupole - electric field gradient interaction tensor measured parallel to **n**. It is given by

$$\tilde{q}_{zz} = \sum_n p_n \chi_n \{ S^n_{cc} + \frac{1}{3}\eta_n (S^n_{aa} - S^n_{bb}) \} \qquad (2)$$

Where S_{ij} are the elements of the Saupe ordering matrix for the principle axes (a,b,c) of the nuclear quadrupole interaction tensor at the n'th site which has statistical weight p_n. $\chi_n \equiv (\frac{e^2qQ}{h})_n$ is the corresponding quadrupole coupling constant, η_n is the asymmetry parameter for the electric field gradient tensor at that site defined as $\eta = \frac{q_{aa}-q_{bb}}{q_{cc}}$ where q_{ii} are components of the electric field gradient tensor. In the case of a uniaxial mesophase ($q_{aa} = q_{bb}$) η is zero. The actual values for p_n, χ_n and η_n in addition to being dependent on the nucleus being observed, will vary from site to site and will thus be determined by the detailed structure of the micelle.

In all cases considered in the study, the observed spectra for uniaxially aligned samples in single phase regions consist of simple multiplets which implies that the various motions of the quadrupole nuclei are fast in the time scale of the experiment. If this were not so, the spectrum would consist of a superposition of multiplets.

It has been shown [10,21] that $|q_{zz}|$ can be replaced by $|q_{zz}|_s S$ where $|q_{zz}|_s$ is solely determined by the detailed structure of the aggregate and the concentration of the solution, and S is an orientational order parameter which must be defined carefully for micellar liquid crystals. For these micellar solutions the order parameter must take into account both oscillations of the local director (**n**) about the macroscopic director (which is some type of field, **F**), and fluctuations in the micellar symmetry axis (**m**) about the local director.

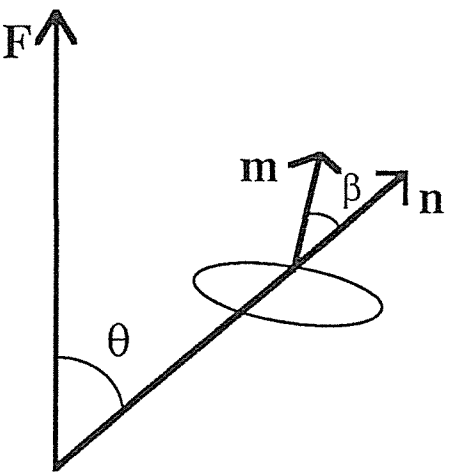

i.e. $$S = \langle P_2(\cos\theta)\rangle \langle P_2(\cos\beta)\rangle = P_{2n}.P_{2m}$$

Where S is the order parameter, and P_{2n} and P_{2m} represent the fluctuations of the local director and the micelle, respectively. θ is the angle between the director and the field while β is the angle between the symmetry axis of the micelle and the director and the

angular brackets indicate it is an ensemble average. S = 0 when there is no order present in the system (isotropic phase) and S = 1 when there is complete alignment.

In the following sections where the specific expressions for $\Delta\nu$ and $|q_{zz}|_s$ for the three nuclei studied here are considered $P_2(\cos\phi)$ is taken to have the value of unity (i.e. the angle between the nematic director and the field is zero for a uniaxial macroscopically aligned diamagnetically positive mesophase).

3.1.1 ^2H (I=1)

The spectrum for a ^2H nuclei in labelled water will be a symmetrical doublet with separation given by

$$\Delta\nu = \frac{3}{2} |q_{zz}|_s S \qquad (3)$$

where

$$|q_{zz}|_s = \langle P_2(\cos\alpha) \rangle_s \chi_D \left(\frac{x_A}{x_W}\right) n_b S_{OD} \qquad (4)$$

In transforming equation (2) into equation (4) it has been assumed that all χ_n (given by χ_D) are equivalent, and that for all the water molecules not bound directly to the surface of the micelle $|q_{zz}|_s = 0$. The factor $\langle P_2(\cos\alpha) \rangle = \langle \frac{3}{2} \cos^2\alpha - \frac{1}{2} \rangle_s$, where α, as shown below,

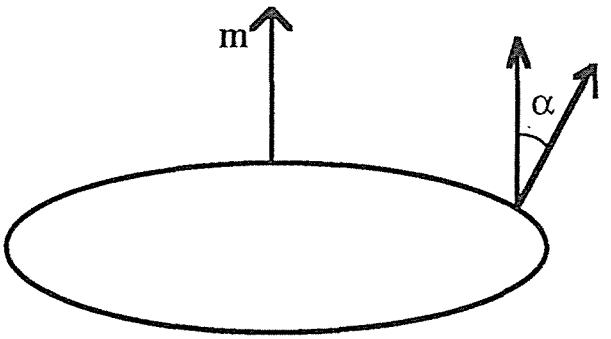

is the angle between the normal to the surface and the symmetry axis of the micelle and the angular brackets denote an average over the micelle surface, accounts for the motional averaging of the quadrupole splitting arising from the translational diffusion of the water molecules across the micellar surface. n_b is the number of water molecules bound per molecule of amphiphile,while x_A and x_W are, respectively , the mole fraction of amphiphile and water. S_{OD} is a "order parameter " which represents the averaging due to the local reorientational motion of bound water molecules at a particular site.

3.1.2 ^{133}Cs ($I = \frac{7}{2}$)

The spectrum for ^{133}Cs , will consists of seven equally spaced lines of relative intensities: 7: 12: 15 : 16 : 15 : 12 : 7 , and with peak separation given by

$$\Delta\nu = \frac{1}{14} |q_{zz}|_s \, S \quad (5)$$

where

$$|q_{zz}|_s = \langle P_2(\cos\alpha) \rangle_s \chi_{Cs} \beta_{Cs} \quad (6)$$

Here β_{Cs} is the fraction of ions bound to the micelle. The field gradient of the Cs^+ ion probably arises from distortion of the symmetry of the hydration shell [28], since the mole ratio of ^2H_2O to CsPFO for the $w_e = 0$ sample is $\approx$ 27 : 1. Furthermore this distortion and the surface coverage are assumed to be independent of the angle α. Thus a single value for χ_{Cs} obtains.

3.1.3 ^{35}Cl ($I = \frac{3}{2}$)

The spectrum for ^{35}Cl will consist of three equally spaced lines of relative intensities : 3 : 4 : 3 , and with peak separation given by

$$\Delta\nu = \frac{1}{2} |q_{zz}|_s \, S \qquad (7)$$

where

$$|q_{zz}|_s = \langle P_2 (\cos\alpha) \rangle_s \, \chi_{Cl} \, \beta_{Cl} \qquad (8)$$

where β_{Cl} is the fraction of ions bound to the micelle. The assumptions relating to the Cs^+ ions also apply to the Cl^- ion.

3.2 ^{133}Cs CHEMICAL SHIFT ANISOTROPIES.

The ^{133}Cs spectra show chemical shift anisotropies in addition to quadrupole splittings. These can be quite large and are revealed in the -1/2 to +1/2 Zeeman transition which, to first order , contains no contribution from quadrupole interactions. This comparatively large change is associated with the ease of polarizing the large $^{133}Cs^{+}$ ion [29,30]. No comparable shifts were observed for either ^{2}H or ^{35}Cl.

The chemical shift of a nucleus in an anisotropic liquid crystalline phase is composed of an isotropic and an anisotropic part [29,30]. In an ordinary liquid only the isotropic part is visible owing to rapid isotropic rotation. The ^{133}Cs has a shift range sufficiently large that in a liquid crystal sample both the isotropic and the anisotropic shift may be observed. In our system the anisotropic part always dominates and we can write (c.f. to equations (5) and (6)) for nematic and lamellar phases

$$\Delta\sigma = S\langle P_2(\cos\alpha)\rangle_s(\sigma_{//}-\sigma_{\perp})\beta_{Cs} \quad (9)$$

Where $\Delta\sigma$ is the observed chemical shift anisotropy and $\sigma_{//}$ and $\sigma_{\perp}$ are the components of the chemical shift shielding tensor σ parallel and perpendicular to the symmetry axis of the micelle.

For a polycrystalline sample, i.e. a sample with a isotropic distribution in the director orientation, $\Delta\sigma$ can be determined directly from the spectrum [31]. For ordered samples where the nematic or lamellar director is parallel to **B** only the parallel component of σ contribute to the shift. In the isotropic phase it is the trace of σ which determines the observed shift. Since the isotropic shift can be ignored $\Delta\sigma$ can be

calculated for ordered samples from the chemical shift difference between the Zeeman transition of the ordered phase ($\sigma^{*}_{//}$) and that of the isotropic phase (σ_i)

i.e. $$\sigma^{*}_{//} - \sigma_i = S\langle P_2(\cos\alpha)\rangle_s \beta_{Cs} \left(\sigma_{//} - \frac{2}{3}\sigma_{\perp} - \frac{1}{3}\sigma_{//}\right) \qquad (10)$$

$$= S\langle P_2(\cos\alpha)\rangle_s \beta_{Cs} \frac{2}{3}(\sigma_{//} - \sigma_{\perp}) = \frac{2}{3}\Delta\sigma$$

Note that the above relationship only applies if there is no background isotropic contribution to the shift. This will be demonstrated to be the case.

The presence of this chemical shift anisotropy turns out to be extremely useful because the m = +1/2 to m = -1/2 transition has different chemical shifts in isotropic and anisotropic environments.This makes it possible to identify phases according to their chemical shifts as will be discussed in detail in the following section.

4. PHASE DIAGRAM

A partial phase diagram of the CsPFO/^2H_2O/CsCl system is presented in figure 3. The weight ratio of CsPFO to ^2H_2O is fixed at 1:1, which is a constant mole ratio of 1 to 27.3. The phase diagram shows an N_D^+ phase intermediate to an isotropic micellar solution phase I and what is probably a discotic lamellar phase L_D. The N_D^+ phase is stable between w_e= 0 to 0.078 ± 0.002 and temperature of 316.3 and 343.7 K.

All the phase transition temperatures are seen to increase with increasing weight fraction of CsCl, but not to the same extent. The initial effect of adding electrolyte is to increase the temperature range of the nematic region, but as the CsCl concentration increases the nematic range diminishes until it disappears altogether at w_e= 0.078 ± 0.002. This behaviour is illustrated in figure 4, where the temperature range of the N_D^+ region (T_{NI} - T_{LN}), is plotted as a function of w_e.

There are two interesting features of the phase diagram. The first is the occurrence of a tricritical point along the L_D to N_D^+ line, where the transition crosses over from first to second order behaviour. It is not possible to locate this point precisely with the w = 0.5 sample. For the w_e = 0 sample the transition is weak (the width of the N_D^+ / L_D coexistence region is 100 mK). On addition of a small amount of CsCl (w_e = 0.0015), ^{133}Cs NMR shows the transition to be second order, i.e. it is not possible to identify coexisting N_D^+ and L_D phases. This places Tcp between w = 0 and 0.0015. The fact that it is there at all is exciting since it indicates that the addition of salt weakens the L_D to N_D^+ transition to such an extent that it becomes second order. Tricritical points along the N_D^+ to L_D transition line have also been observed in the binary systems CsPFO / water [10,14] and APFO/ water [11]. In these systems the transition changes from first to second order with decreasing amphiphile concentration, here we have an inverse of that

Figure 3. Partial phase diagram of the CsPFO/CsCl/^2H_2O system, where the mole ratio of CsPFO to water is fixed at 1 : 27.3 and the weight fraction of CsCl w_e is varied between 0.00 and 0.13. Nomenclature: I, Isotropic micellar solution phase; N_D^+, nematic phase with positive diamagnetic susceptibility anisotropy and discoidal micelles; L_D , lamellar phase with discoidal micelles; Tcp, lamellar-nematic tricritical point; Cep, the lamellar-nematic critical end point. The temperatures of the phase boundary curves are estimated to have errors of $\pm$ 0.04 K.

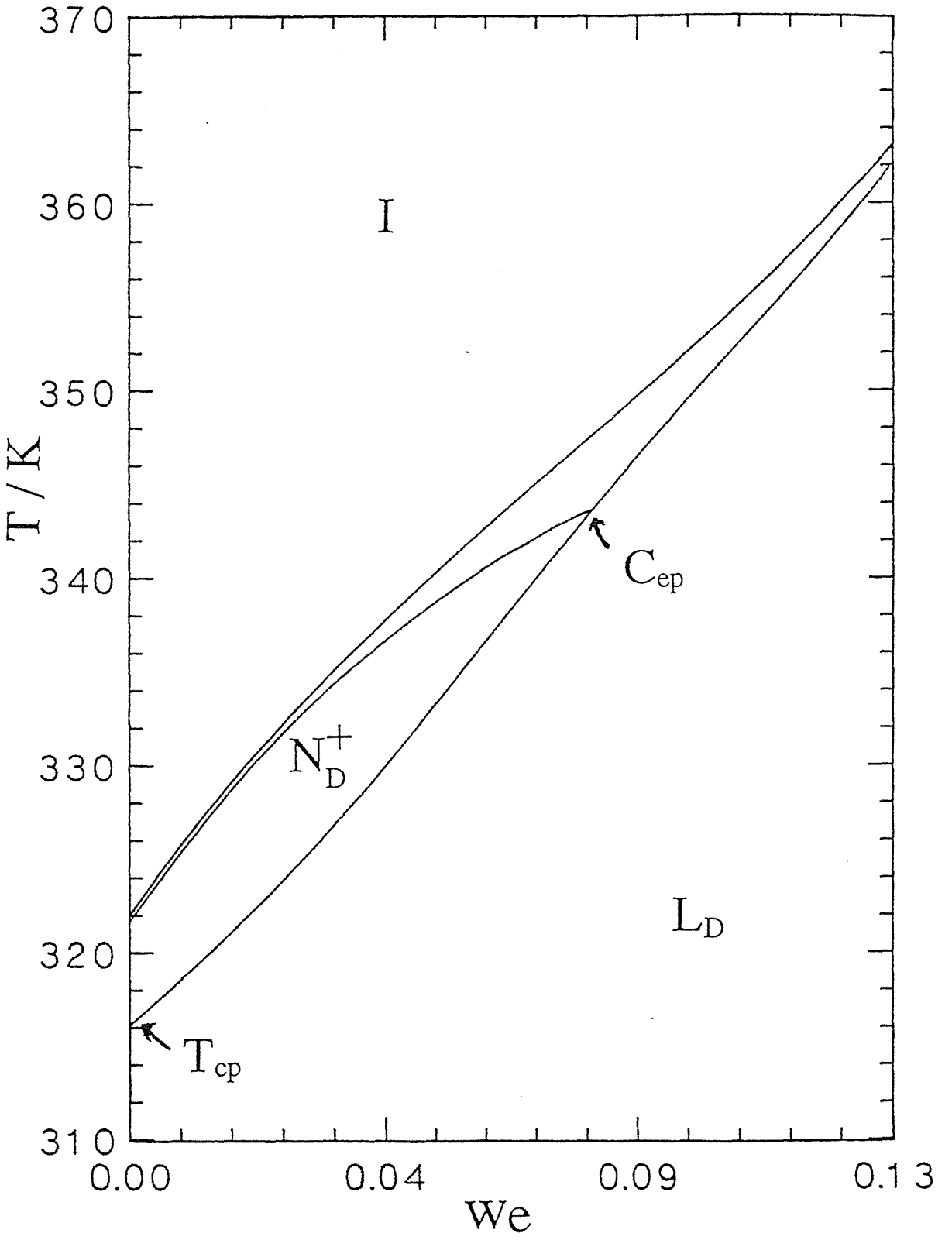
370
360
350
340
330
320
310
T / K
I
N_D^+
C_{ep}
L_D
T_{cp}
0.00
0.04
0.09
0.13
We

Figure 4. Plot of the temperature width of the nematic phase, T_{NI} - T_{LN}, versus the weight fraction of CsCl, w_e . After an initial increase in the width of the nematic phase with the addition of salt T_{NI} - T_{LN} decreases and the nematic phase disappears altogether at Cep. (w_e =0.078(2) T = 343.7 K)

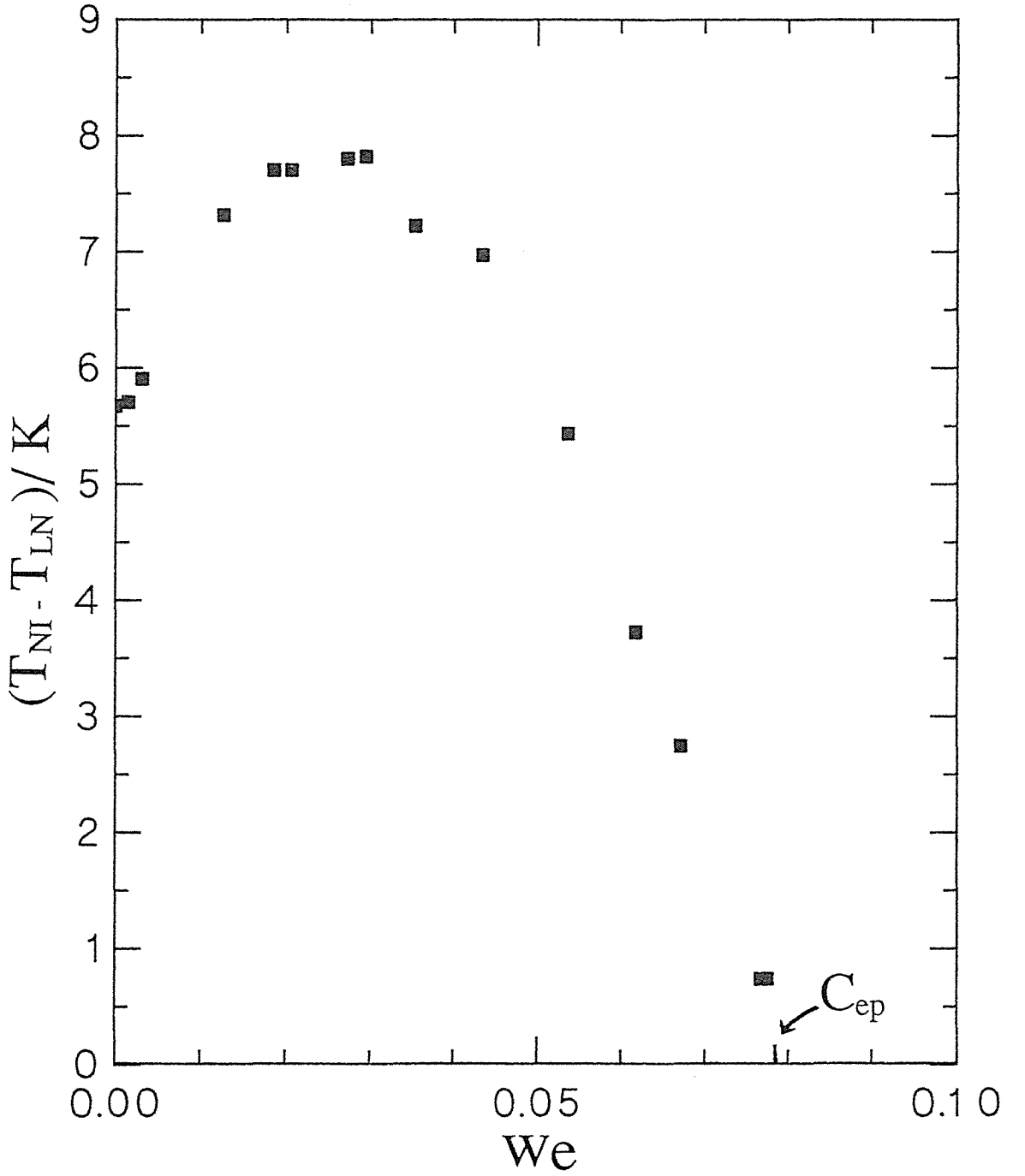
9
8
7
6
5
4
3
2
1
0
0.00
0.05
0.10
We
$(T_{NI} - T_{LN})$ / K
C_{ep}

behaviour in that the transition from first to second order occurs on increasing the electrolyte concentration. The presence of the lamellar-nematic tricritical point is an indication that the I to N_D^+ to L_D sequence of transitions is analogous to the isotropic to nematic to smectic A sequence observed for thermotropics calamitic liquid crystals [32,33]. This suggests that the transition is a simple order-disorder one and does not involve any significant change in the structure of the micelles at the nematic to lamellar transition. Hence the transition from the nematic to the lamellar phase simply involves the introduction of translational order and the lamellar phase is an L_D phase. The second point of interest is the critical end point (Cep, w_e = 0.078 ±0.002 T = 344.0 ±0.05 K) where the line of second order L_D to N_D^+ transitions intersect with the lines of first order N_D^+ to I and L_D to I transitions.

The significance of the two singular points is best illustrated in the schematic plot of temperature verses chemical potential figure 5. On such a diagram mixed phase regions appear as a single line since the chemical potentials of the coexisting phases are equal. At Tcp the transition changes from first (continuous line) to second order (dotted line). At Cep the line of second order L_D to N_D^+ transitions intersects the line of first order N_D^+ to I and L_D to I transitions.

Figure 5. Schematic phase diagram of the CsPFO/CsCl/^2H_2O system in temperature, chemical potential space, illustrating the significance of the two singular points, Tcp and Cep. Continuous lines represent first order transitions and the broken line represents a line of second order transitions.

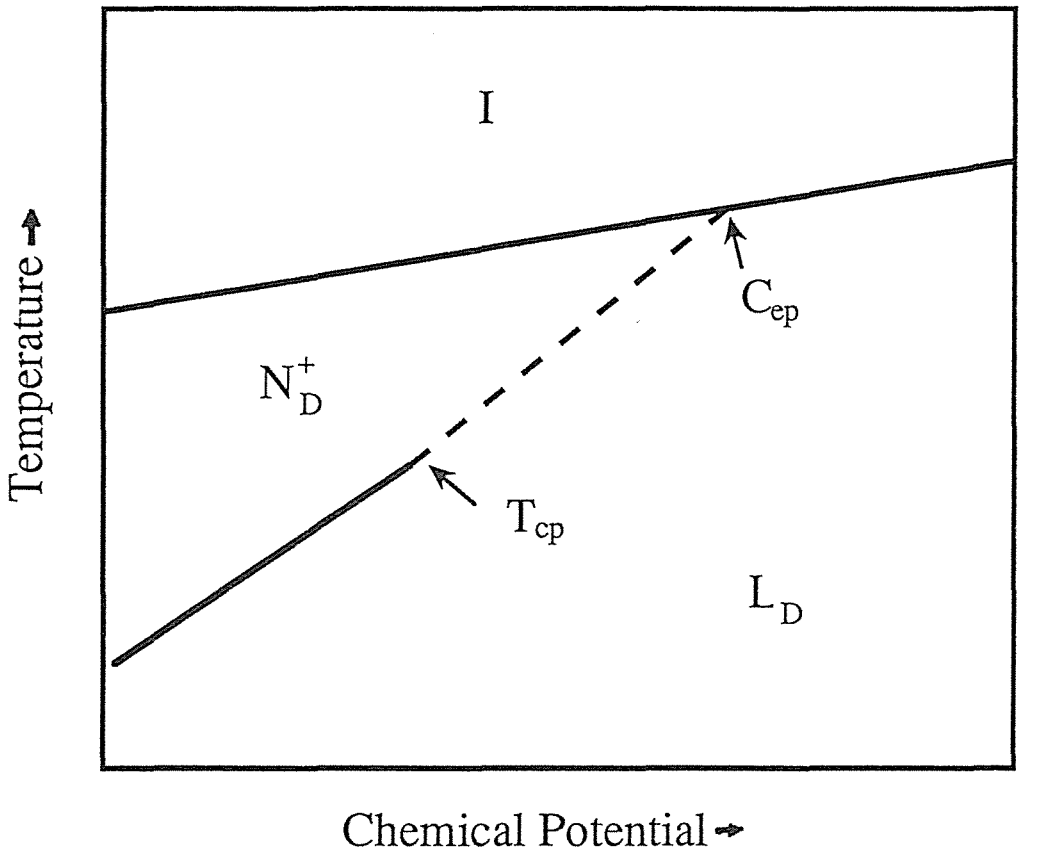
I
C_{ep}
N_D^+
T_{cp}
L_D
Temperature
Chemical Potential

5. NMR MEASUREMENTS AND DETERMINATION OF PHASE TRANSITION TEMPERATURES IN THE CsPFO/CsCl/^2H_2O SYSTEM

5.1 NMR MEASUREMENTS

Illustrations of spectra in the isotropic phase I, nematic phase N_D^+, and polycrystalline lamellar phase L_D for ^2H, ^{133}Cs and ^{35}Cl nuclei are given in figures 6, 7 and 8 respectively. In the isotropic micellar solution phase the order parameter S is zero. Thus only the Zeeman interaction is observed and the spectra of all three nuclei consist of a single peak.

For macroscopically ordered nematic and lamellar mesophases $0 < S < 1$ and the quadrupole splitting for ^2H, ^{133}Cs and ^{35}Cl spectra are given by equations (3), (5) and (7) respectively. Thus the ^2H spectrum of heavy water consists of a symmetrical doublet (figure 6b), the ^{133}Cs spectrum consists of seven equally spaced lines (figure 7b), and the ^{35}Cl spectrum is composed of three equally spaced lines (figure 8b) with the expected intensity distributions.The ordered spectra shown is for the nematic phase in each case. The appearance of the spectrum of a macroscopically aligned lamellar phase is identical to that of the corresponding nematic phase spectrum but the magnitude of the quadrupole splittings are greater in the L_D phase.

Macroscopically ordered lamellar phases are easily prepared by cooling from the isotropic micellar solution phase, through the nematic phase, where the nematic director aligns along the magnetic field, into the lamellar phase where the lamellar director becomes locked into the mesophase. If the cooling takes place outside of a magnetic field a polycrystalline sample is obtained in which there is a random orientation of local lamellar

Figure 6. ^2H NMR spectra of ^2H_2O for a sample with $w_e = 0.0434$.

(a) Isotropic micellar solution phase

(b) Nematic phase

(c) Lamellar phase with an isotropic distribution of local directors.

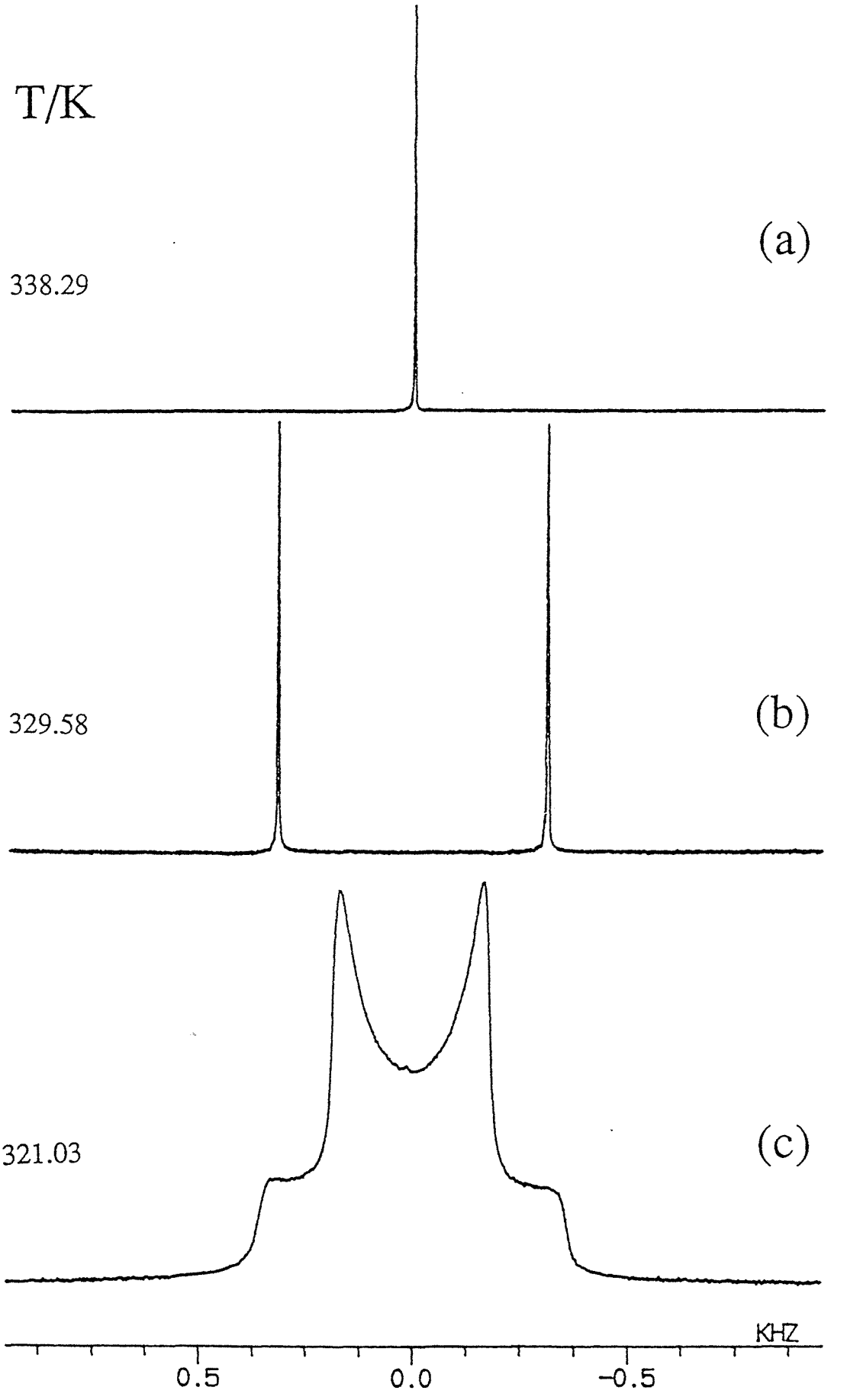
T/K
338.29
(a)
329.58
(b)
321.03
(c)
KHZ
0.5
0.0
-0.5

Figure 7. ^{133}Cs NMR spectra for a sample with $w_e = 0.0434$.

(a) Isotropic micellar solution phase

(b) Nematic phase

(c) Lamellar phase with an isotropic distribution of local directors.

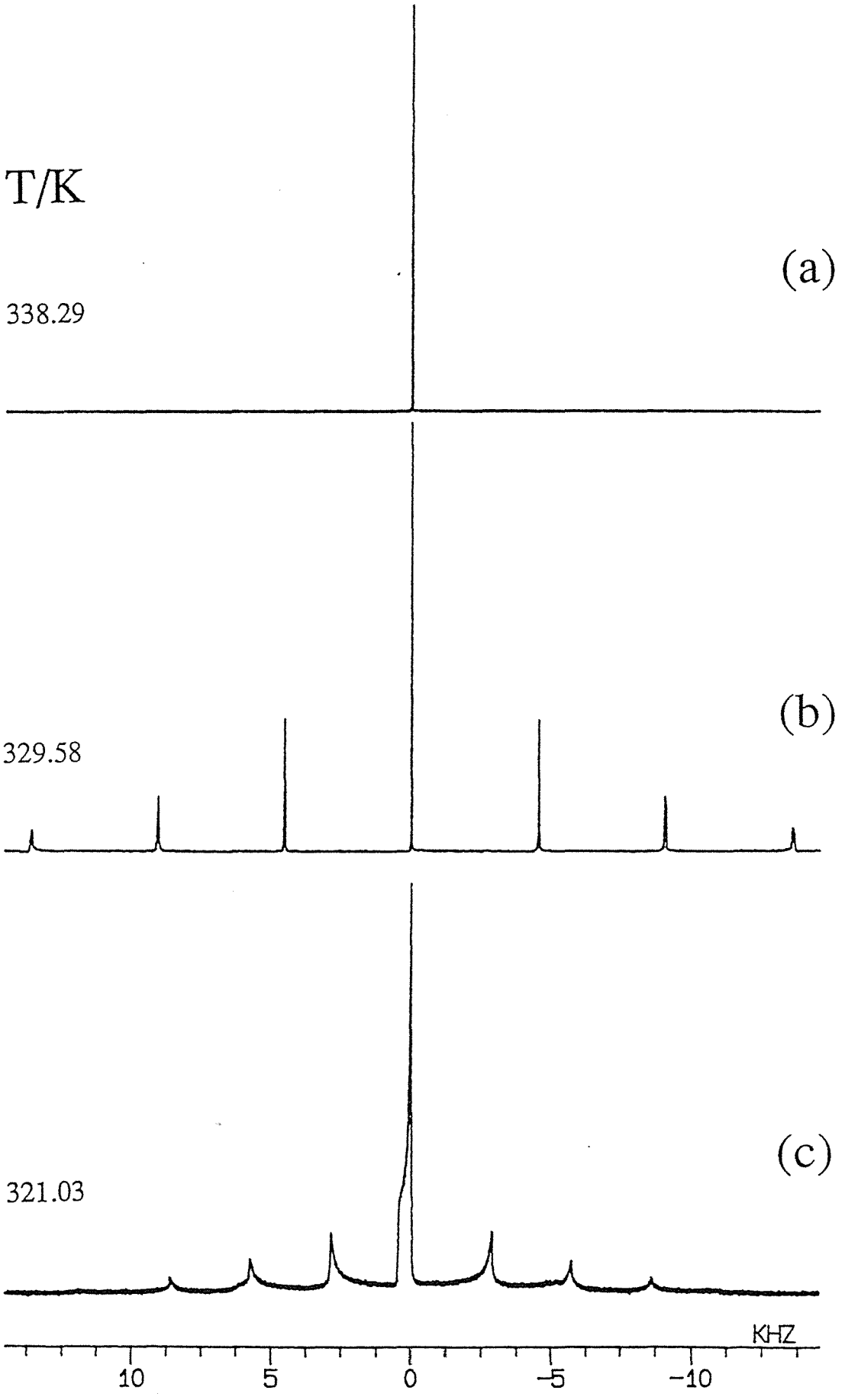
T/K
(a)
338.29
(b)
329.58
(c)
321.03
KHZ
10
5
0
-5
-10

Figure 8. ^{35}Cl NMR spectra of for a sample with $w_e = 0.0434$.

(a) Isotropic micellar solution phase

(b) Nematic phase

(c) Lamellar phase with an isotropic distribution of local directors.

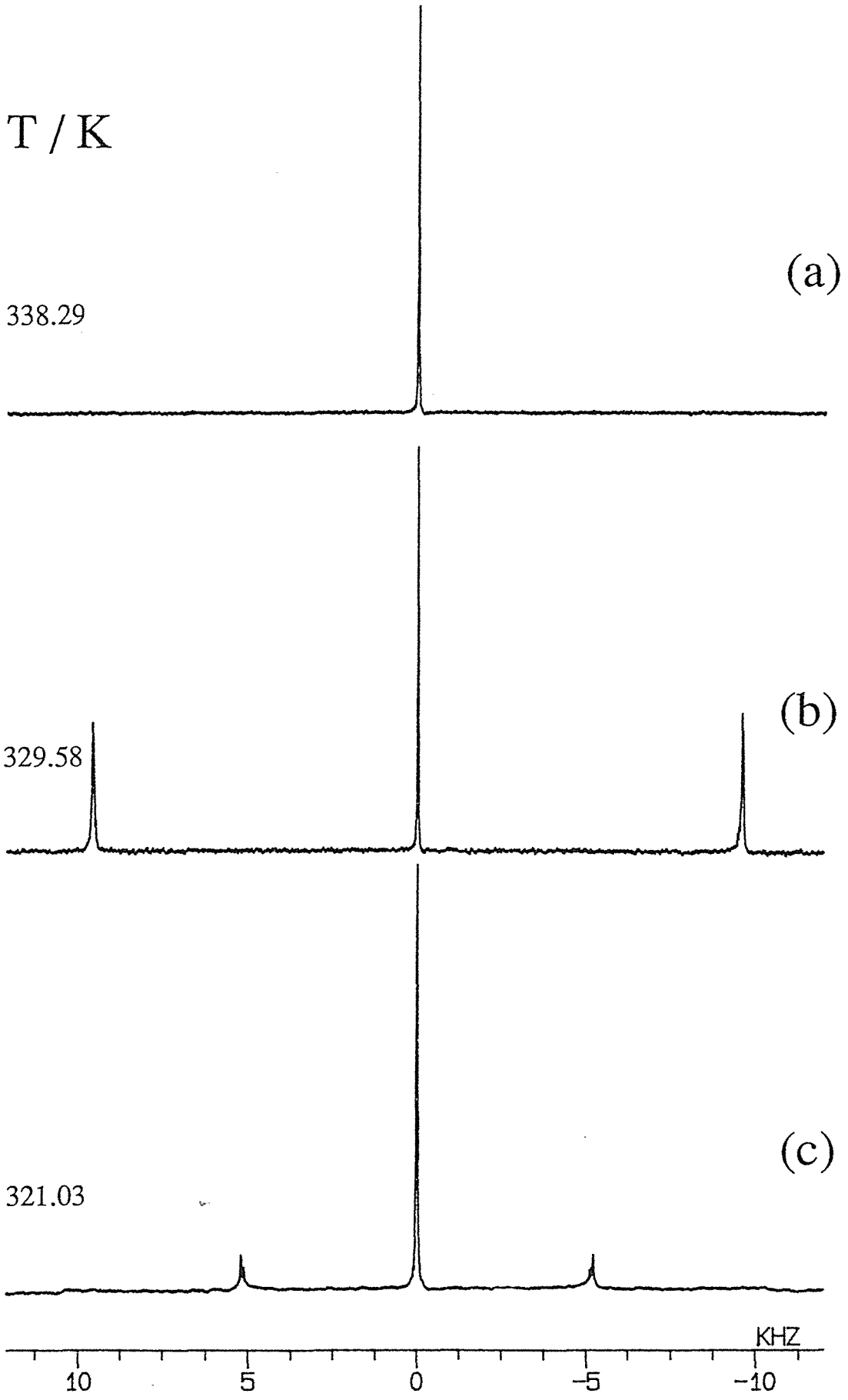
T / K
(a)
338.29
(b)
329.58
(c)
321.03
KHZ
10
5
0
-5
-10

directors. Since the lamellar phase will not reorientate in a magnetic field (i.e. it has an infinite valued rotational viscosity coefficient [34]), the observed spectra reflects an isotropic distribution of director orientation. For ^{2}H (figure 6c) the polycrystalline spectrum consists of a "Pake" doublet, where singularities are evident at $\phi=90^{o}$ (central doublet) and $\phi = 0^{o}$ (outer doublet). Thus the quadrupole splittings as defined in equation (3) ($\phi=0$) can easily be extracted from this spectrum. The ^{133}Cs polycrystalline spectrum (figure 7c) has a singularity at $\phi=90^{o}$ and so the splitting between adjacent lines is half that of the quadrupole splittings as defined in equation (5). Similarly for the ^{35}Cl polycrystalline spectra (figure 8c). So quadrupole splittings can be readily abstracted from both ordered and polycrystalline spectra. Mostly it is better to work with ordered samples but occasionally it is convenient and quicker to examine polycrystalline samples in the lamellar phase.

From the spectra of all three nuclei it is thus possible to distinguish between isotropic and ordered phases. Furthermore in biphasic regions separate signals for the coexisting phases can be observed which enables the precise determination of the upper and lower boundaries to these transitions. However when the mixed phase region covers only a small temperature range the composition of the two phases (e.g. N_{D}^{+} or L_{D}) will be similar and in practice it becomes difficult to resolve the separate signals.

Experimentally it was ascertained that ^{133}Cs was the most useful nucleus in the detection of phase transition temperatures and the resolution of coexisting phases, despite the fact that ^{133}Cs, and ^{2}H have similar electric quadrupole moments, while the quadrupole moment of ^{35}Cl is approximately a order of magnitude larger than both of them. The quadrupole splittings for ^{133}Cs in the $w_{e} = 0.0434$ sample are seen to be an order of magnitude greater than those for ^{2}H, figure 9. This difference can be understood by

Figure 9. ^{2}H, ^{35}Cl and ^{133}Cs NMR spectra for a $w_e = 0.0434$ sample within the nematic phase 329.582 K, illustrating the difference in magnitudes of their respective quadrupole splittings.

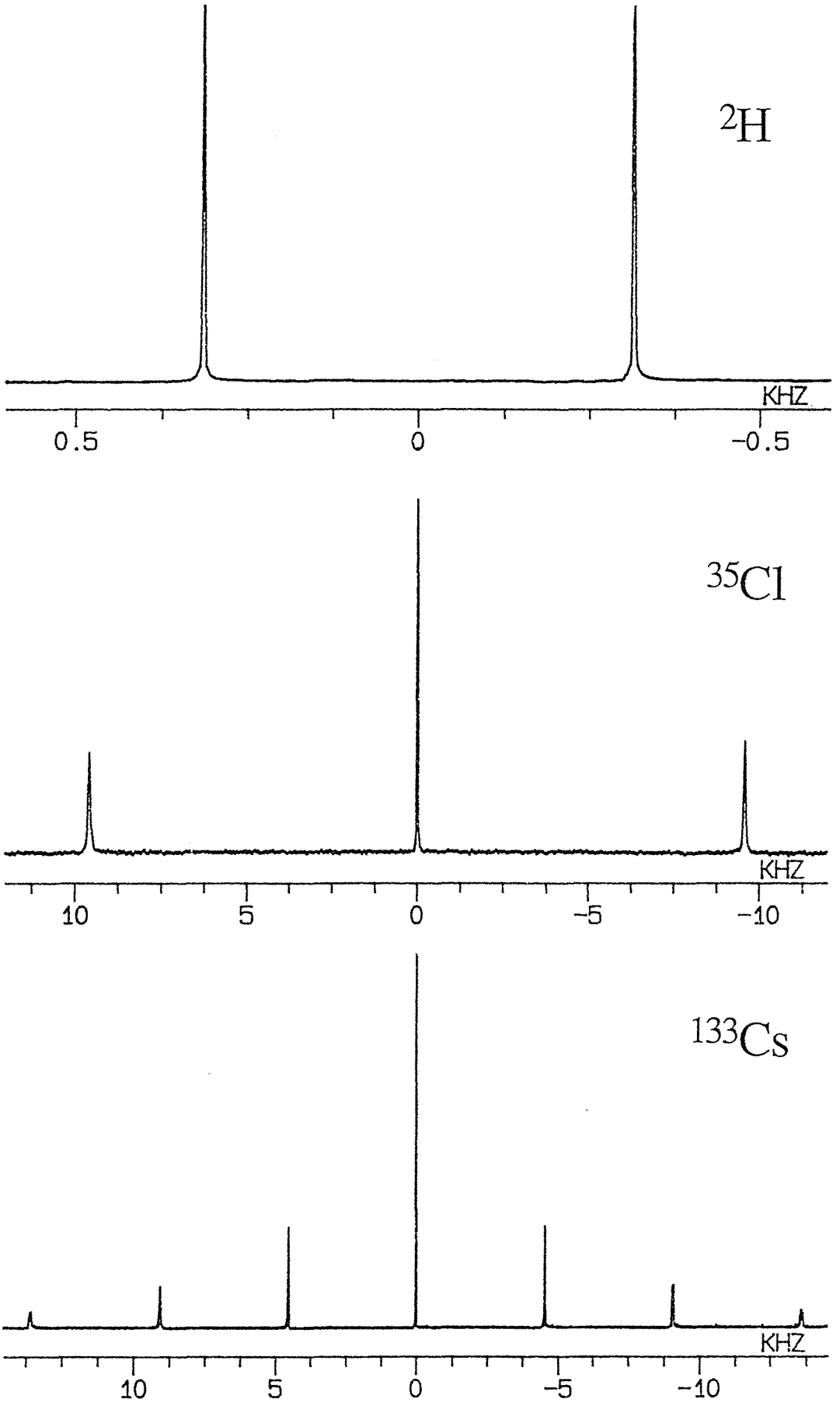
^{2}H
KHZ
0.5
0
-0.5
^{35}Cl
KHZ
10
5
0
-5
-10
^{133}Cs
KHZ
10
5
0
-5
-10

considering the values for $|q_{zz}|_s$ for the two nuclei (equations (4) and (6) respectively). For the $w_e = 0.0$ sample the values for β_{Cs} and $(\frac{X_A}{X_W})n_b S_{OD}$ are approximately, 0.6 and 0.004, respectively [10]. Substitution of these values for $|q_{zz}|_s$ into equations (3) and (5), and assuming $\chi_D = \chi_{Cs}$, predicts a $\Delta\nu$ (^{133}Cs) / $\Delta\nu$ (^{2}H) ratio of 7:1. Thus practically all the difference in quadrupole splittings is accounted for by the difference in β_{Cs}+ and $(\frac{X_A}{X_W})n_b S_{OD}$, indicating that $\chi_D \approx \chi_{Cs}$. This is not surprising since their magnitudes of the electric quadrupole moments(Q) are 2.875 x 10^{-27} and 3.0 x10^{-27} cm^2 for ^{2}H and ^{133}Cs respectively. ^{133}Cs spectra therefore offer an order of magnitude improvement over ^{2}H spectra in the resolution of spectra from coexisting phases since the line-widths are of the same order. Another useful property of ^{133}Cs is that it exhibits chemical shift anisotropy, as discussed previously. So when traversing from an isotropic to an anisotropic environment the chemical shift anisotropy is large enough to enable accurate determination of the phase transition. This method of phase detection is discussed in section 5.2.1.

The ^{35}Cl splittings are about two times greater than those for ^{133}Cs (figure 9). A comparison of equations (5) and (7) show that the ratio of the quadrupole splittings at any given temperature is given by

$$\frac{\Delta\nu\ (^{35}\mathrm{Cl})}{\Delta\nu\ (^{133}\mathrm{Cs})} = \frac{7\chi_{Cl}\beta_{Cl}}{\chi_{Cs}\beta_{Cs}}$$

and since the ratio of the electrical quadrupole moment of the two nuclei $Q(^{35}Cl)$ / $Q(^{133}Cs)$ is 27.3, this would suggest a β_{Cl} / β_{Cs} ratio of $\approx$ 0.011. Thus for the sample (w_e =0.0434) at 321.03 K, only a small fraction of the Cl^- ions are bound to the surface. This Cl^- ion binding will be considered in more detail in the discussion section In spite of this low value for β_{Cl} the large magnitude for the ^{35}Cl splitting with respect to that for ^{133}Cs would suggest that the ^{35}Cl nucleus would be better able to resolve coexisting

phases. The increase in quadrupole splitting is however offset by the increase in the line width of the ^{35}Cl signals as a consequence of the larger electrical quadrupole moment. Furthermore the relative sensitivity of ^{35}Cl is an order of magnitude less than that for ^{133}Cs.

Phase transitions are often determined by observing the temperature dependence of the quadrupole splittings and it is instructive to consider the observed behaviour here. Figure 10 shows the temperature dependence of the ^{133}Cs quadrupole splittings for the $w_e = 0.0$ sample on cooling from the isotropic to the lamellar phase. Across the I / N_D^+ coexistence region the quadrupole splittings are roughly constant which is a result of a constant value of S at T_{NI} for the nematic phase. In the N_D^+ phase there is a rapid increase in $\Delta\nu$ close to T_{NI} which eases off as cooling continues. This increase has been shown to reflect increases in S (equation (5)) and $\langle P_2(\cos\alpha)\rangle_s$ (equation (6)) [10,21]. β_{Cs} (equation (6)) also increases with decreasing temperature as will be demonstrated in section 6.1.2. T_{LN} and T_{NL} are identified from discontinuities in the temperature dependence of the quadrupole splittings. $\Delta\nu$ continues to increase in the lamellar phase due to an increase in $\langle P_2(\cos\alpha)\rangle_s$ and β_{Cs}. The value of S has been shown to increase only slowly with decreasing temperature in the L_D phase [21].

5.1.1 Sample Homogeneity

It is essential for the precise determination of phase transition temperatures that the sample must be homogeneous.This is particularly important for lyotropic liquid crystals since phase transitions are both temperature and composition dependant. NMR is a particularly sensitive technique for the detection of inhomogeneities of composition within a sample. In a homogeneous sample the singlet of the isotropic micellar solution and the -1/2 to +1/2 transition of the ordered nematic or lamellar mesophases, are

Figure 10. Partially averaged ^{133}Cs quadrupole splitting $\Delta\nu$ observed on cooling a sample of $w_e = 0.00$ from the isotropic micellar solution phase to the nematic phase and then from the nematic phase into the lamellar phase. The dotted lines correspond to the phase transitions at T_{IN} (321.15 K), T_{NI} (320.82 K), T_{NL} (315.63 K) and T_{LN} (315.62 K).

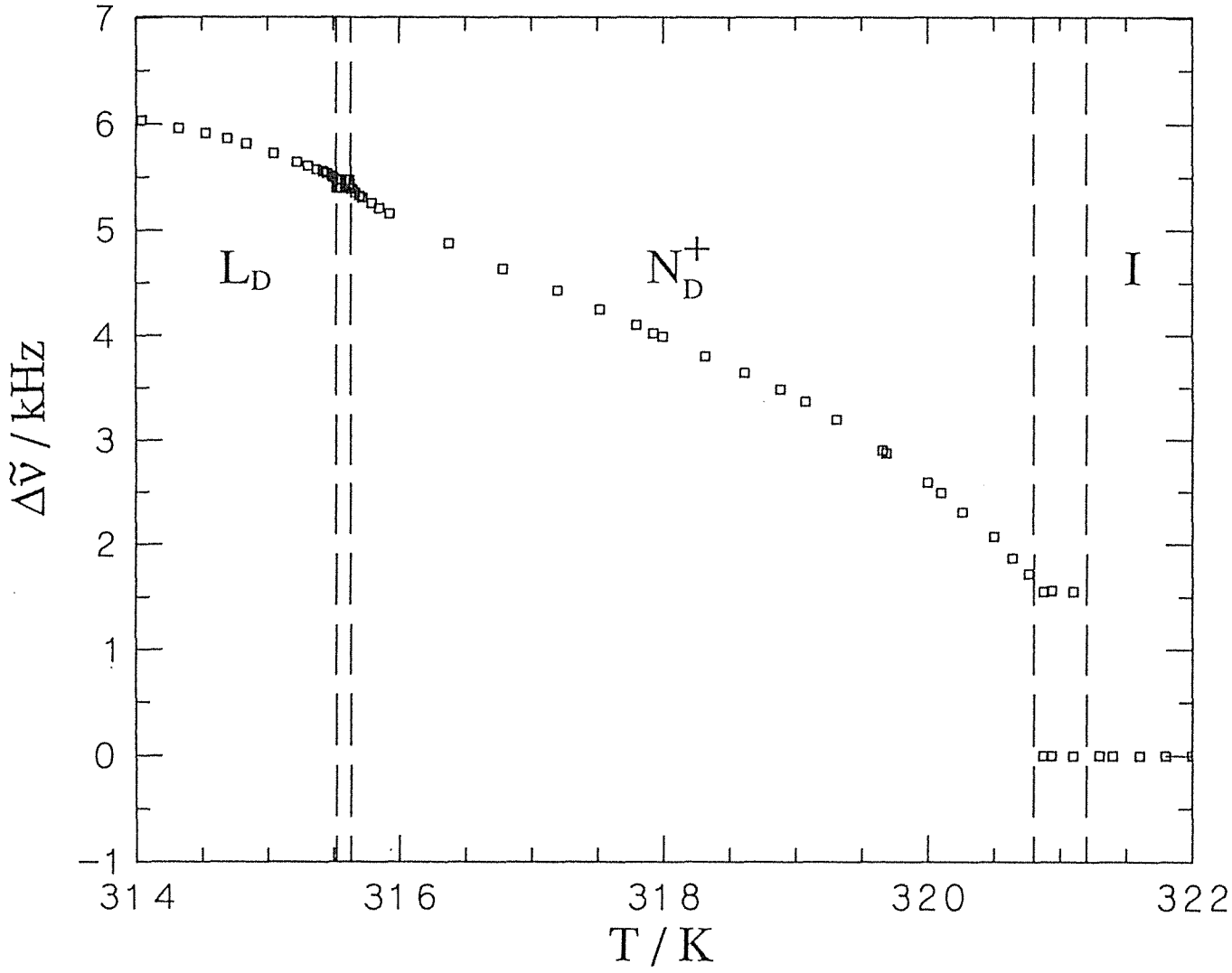
7
6
5
4
3
2
1
0
−1
$\Delta\tilde{\nu}$ / kHz
L_D
N_D^+
I
314
316
318
320
322
T / K

Lorentzian in shape, and have typical widths at half height of approximately 4 Hz for ^{133}Cs. Any deviations, such as broadening of the peaks or the presence of additional peaks, from these simple spectrum are indicative of inhomogeneities in temperature and/or composition. A particularly sensitive indicator of sample homogeneity is the symmetry of the spectrum. In the case of ^{2}H for example the spectrum should consist of two lines of equal intensity. Often this is not the case and the literature has many examples of asymmetric ^{2}H spectra in lyotropic liquid crystals [12,35]. Those asymmetric spectra are a result of temperature and/or composition gradients in the presence of a magnetic field gradient as illustrated in figure 11. In the example given there is a temperature gradient along the long axis of the NMR tube. This is a common situation with conventional air flow temperature control systems where the warm air flows from the bottom to the top of the tube. The schematic spectra illustrates two extremes. The inner doublet is generated by ^{2}H nuclei in the base of the sample which is at a higher temperature than the ^{2}H nuclei at the top of the sample, which give rise to the outer doublet. In the absence of a field gradient ($\delta B = 0$) there will simply be a broadening of both peaks due to the distribution of quadrupole splittings along the length of the sample. In the presence of a field gradient however an asymmetric spectrum is generated. As it is illustrated, the field at the top of the sample is greater than that at the base. The outer doublet (top of the sample) will thus be displaced to higher frequencies while the inner doublet (bottom of sample) will be displaced to lower frequencies. This will result in the sharpening of the low frequency peak and a broadening of the high frequency peak. Of course, the same arguments apply to any quadrupole nuclei and the quadrupole splitting distribution could be the result of a concentration as well as a temperature gradient. If a concentration gradient was the cause the splittings at the top of the tube would be less than those at the bottom but the argument is not affected.

Figure 11. Illustration of how asymmetric spectra can be generated from samples with a temperature gradient δT along axis of the sample tube and a magnetic field gradient δB.

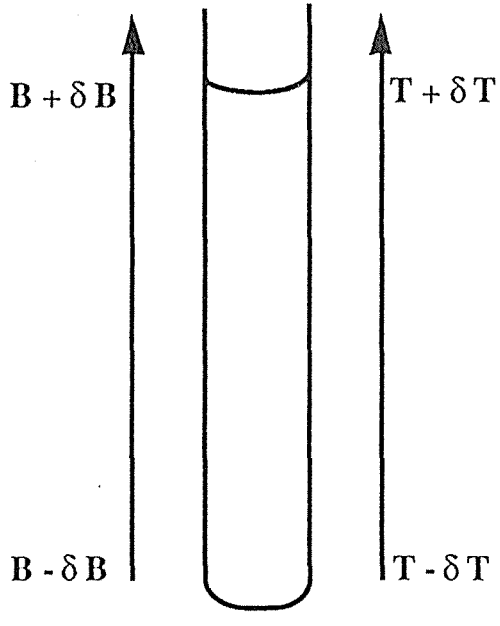
B + δB
T + δT
B - δB
T - δT

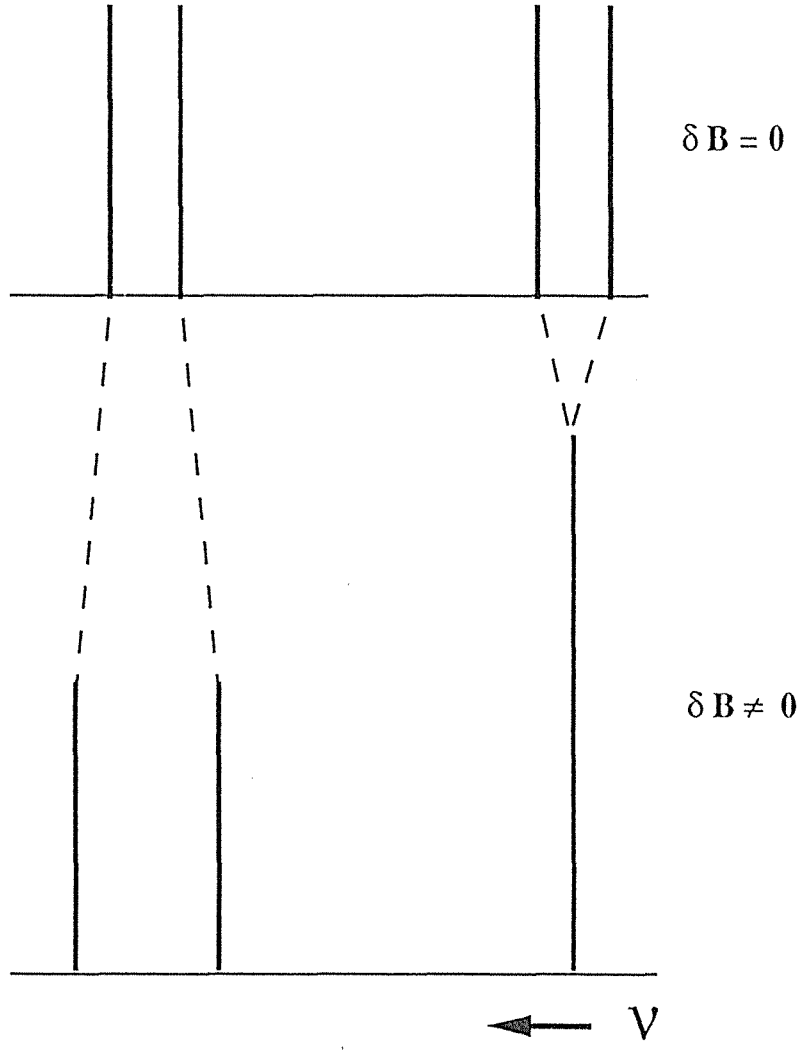
δ B = 0
δ B ≠ 0
V

With our temperature control system all pure phases give symmetric spectra for all three nuclei (see figures 6b, 7b and 8b) , indicating the absence of significant temperature gradients. If asymmetric spectra are observed then a concentration gradient is indicated. This can arise from two main causes. Firstly, a concentration gradient can be established along the long axis of the sample tube by the evaporation of $^2H_20$ from the solution with subsequent condensation onto the glass walls, and thence back into solution. This process can occur within a uniform temperature environment, but could be eliminated with the removal of the vapour space above the sample. It is convenient however to have a space above the solution so that the sample can be easily mixed. Secondly, a concentration gradient can be generated if a sample is kept in a biphasic region for a length of time. The composition of two phases in a biphasic region are different. This difference, which will depend upon the width of the mixed phase region, will result in different densities for the two phases, which in turn will lead to partial macroscopic separation of the phases. For this reason minimal time was spent within the biphasic regions. When a distribution in composition did occurred, the sample had to be re-mixed above the nominal T_{IN} transition temperature, since the more dense phase has a higher T_{IN} and it is necessary to make sure that all the sample is in the same phase (isotropic) before complete mixing well occur.

It is very important therefore to ensure composition homogeneity over the sample volume. To do this the sample was heated in an oven to well above the nominal T_{IN} transition temperature, and mixed by repeated inversion of the sample tube, then the sample was loaded into the sample cell which had previously been thermally equilibrated to approximately 2 K above T_{IN}. The sample was mixed again by repeated inversion of the sample cell before being loaded into the spectrometer, This procedure consistently produced homogeneous samples.

5.2 PHASE TRANSITION TEMPERATURES

In the following discussions the detection of the various phase transition boundaries is discussed in detail.The phase boundaries that were located were; T_{IN}, T_{NI}, T_{NL}, T_{LN}, T_{IL}, and T_{LI}, which are defined as follows :

T_{IN} - The upper limit of the isotropic / nematic biphasic region .

T_{NI} - The lower limit of the isotropic / nematic biphasic region .

T_{NL} - The upper limit of the nematic / lamellar biphasic region .

T_{LN} - The lower limit of the nematic / lamellar biphasic region for a first order L_D to N_D transition or the phase transition temperature for a second order transition .

T_{IL} - The upper limit of the isotropic / lamellar biphasic region .

T_{LI} - The lower limit of the isotropic / lamellar biphasic region .

5.2.1 The determination of T_{IN}.

A homogeneous isotropic sample was prepared as previously described and the sample was cooled to within about 0.5 K of T_{IN}. Cooling was then slowed to approximately 100 mK min^{-1} until the first appearance of the nematic Zeeman peak was observed superimposed on the isotropic spectrum as illustrated in the sequence of spectra in figure 12. The nematic Zeeman peak was at a higher frequency (about 100 Hz) than the isotropic micellar solution singlet. The chemical shift of the nematic Zeeman peak is determined only by the parallel component of the chemical shielding tensor since the nematic phase director is aligned parallel to the magnetic field. The chemical shift of the isotropic peak is determined by the trace of σ. The difference in the chemical shift

Figure 12. The sequence of ^{133}Cs NMR spectra of the -1/2 to +1/2 transition as observed on cooling the sample $w_e = 0.0434$ from the isotropic micellar solution I to the nematic phase N_D^+.

(a) Isotropic micellar solution phase

(b) - (d) isotropic / nematic coexistence region

(e) Nematic phase.

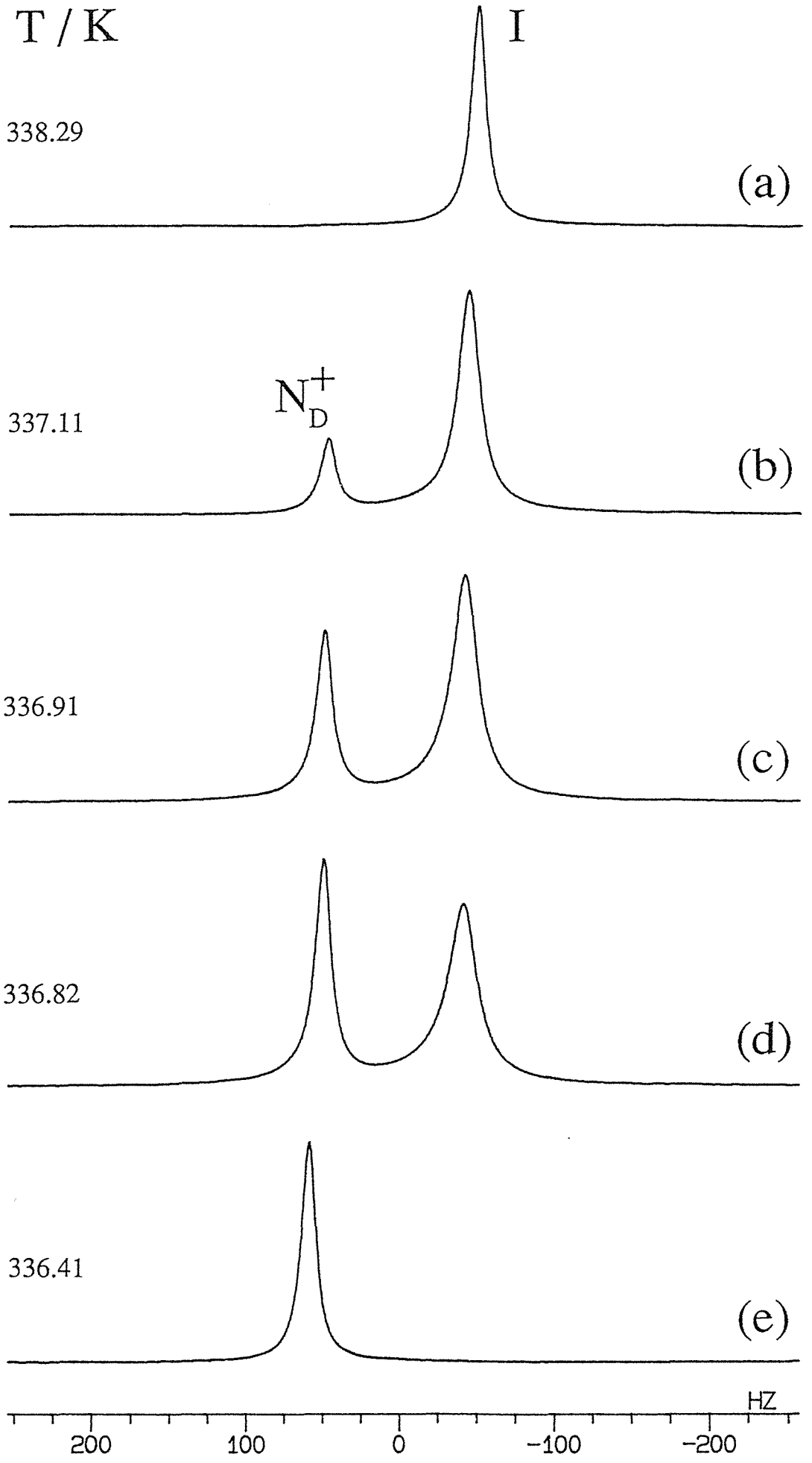
T / K
I
338.29
(a)
N_D^+
337.11
(b)
336.91
(c)
336.82
(d)
336.41
(e)
HZ
200
100
0
-100
-200

between the isotropic and nematic phases is therefore given in equation (10). The appearance of the nematic Zeeman peak indicates that the boundary into the isotropic / nematic biphasic region (T_{IN}) has been crossed. The cooling experiment was then repeated from approximately 100 mK above T_{IN}, at a slower cooling rate of approximately 20 mK min^{-1} until the reappearance of the nematic Zeeman peak. The temperature of the reappearance of this peak was taken as T_{IN} . This method determined T_{IN} to within $\pm$ 20 mK. A limitation of this method of detection is that it is dependant on the traversal of the isotropic phase into the isotropic / nematic biphasic region, i.e. to observe the nematic peak at all means that the phase boundary has been crossed. There is nothing to be done about this unless the isotropic phase exhibits pretransitional ordering (see below) but it is much easier to detect the narrow -1/2 to +1/2 transition than it is to see the first appearance of the broader satellite peaks.

For samples with low weight fraction of electrolyte from 0 to about 0.003, the appearance of the nematic Zeeman peak was preceded by a broadening of the isotropic peak. This broadening and the eventual resolution into a broad multiplet (figure 13) is due to pretransitional ordering of the micelles induced by the magnetic field [36]. It arises from a magnetic torque acting on the micelles, a torque which is enhanced by the build-up of angular correlations of the micelles as the transition is approached. The magnitude of the induced doublet splitting is related to the degree of orientational ordering of the micelles. For samples with w = 0.40 or less the induced isotropic splitting is quite large, indeed it is even clearly seen in the ^2H spectrum [36] but for the w = 0.50 sample it is quite small. This is because the induced splitting is proportional to the anisotropy in the magnetic susceptibility of the micelles which in turn depends upon the eccentricity of the discoidal micelles. This is known to decease with increasing w (and temperature) [21]. For samples with w < 0.4, use can be made of the phenomena to study pretransitional behaviour in the isotropic phase and to determine very precise values for T_{IN} and T*, the

Figure 13. The sequence of ^{133}Cs NMR spectra for the-1/2 to +1/2 transition as observed on cooling a $w_e = 0.00$ sample from the isotropic phase I into the isotropic / nematic coexistence region.

(a) Isotropic micellar solution phase

(b) Isotropic micellar solution phase with broadening of the line line as a result of pretransitional orientational ordering of the micelles.

(c) and (d) isotropic / nematic coexistence region. The structure due to the orientational ordering of the micelles in the isotropic phase is evident.

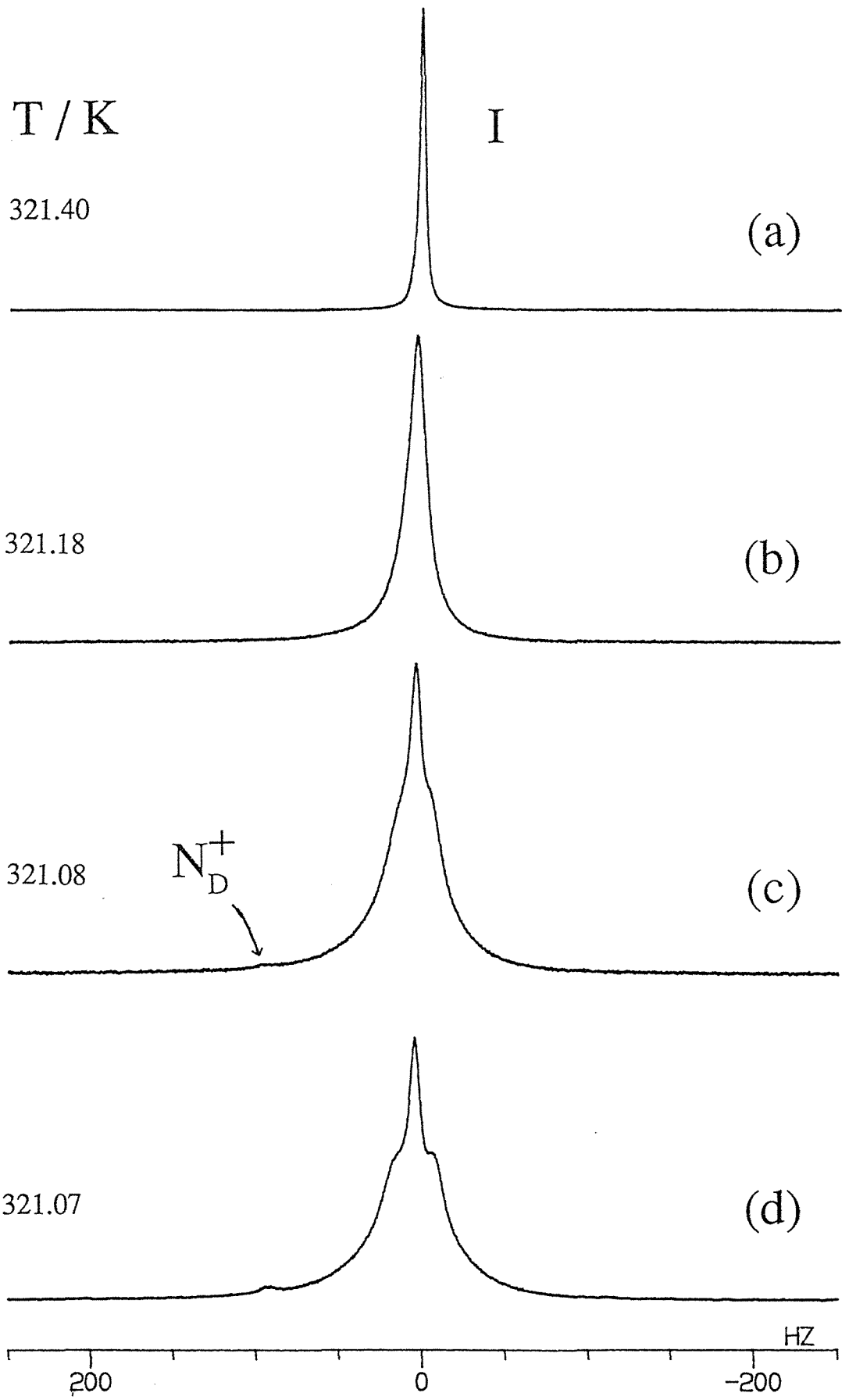
T / K
I
321.40
(a)
321.18
(b)
321.08
N_D^+
(c)
321.07
(d)
HZ
200
0
-200

supercooled lower limit of the isotropic phase [36]. In the w = 0.5 sample resolution of the broad satellites indicates that the temperature is very close to T_{IN} (within approximately 10 mK).

5.2.2 The determination of T_{IL}

T_{IL} was determined in a similar method as T_{IN}. The precision to which T_{IL} can be determined depends on the width of the isotropic/lamellar biphasic region. The greater the temperature interval (ΔT) the slower the rate of build-up of lamellar phase with decreasing temperature (Lever rule) and the greater the "supercooling" across the phase boundary preceding the appearance of the lamellar phase - 1/2 to +1/2 transition. At the critical end point (Cep) the width of the I / L_D biphasic region is 4 K and the estimated precision in the T_{IL} is $\pm$ 40 mK. As w_e increases $\Delta T(I / L_D)$ decreases and T_{IL} can be determined with a greater precision. At $w_e = 0.13$, $\Delta T(I / L_D) = 0.65$ K and T_{IL} is estimated to have a precision of $\pm$ 20 mK.

5.2.3 The determination of T_{NI} .

The disappearance of the isotropic Zeeman peak on cooling from the isotropic / nematic biphasic region (see figure 12), or the appearance of the isotropic peak on heating from the nematic phase could have been used to determine the phase transition boundary. The first method requires cooling through the isotropic /nematic biphasic region and can produce problems with phase separation, particularly for samples with large values for $\Delta T(I / N_D^+)$, while the second method would again rely on actually crossing the phase transition boundary into the mixed phase region before the isotropic peak becomes visible. A more precise method of determining T_{NI} is to plot $\Delta\nu$ versus temperature on heating from the nematic phase into the isotropic / nematic biphasic region. In order to

minimize phase separation problems the nematic phase was firstly accessed by rapidly cooling the sample in the magnet from the isotropic phase into the nematic phase. At the N_D^+ to I transition there is a discontinuity in the slope of the $\Delta\nu$ versus temperature plot which identifies T_{NI} (figure 14). Careful measurements close to the discontinuity enables T_{NI} to be measured with a precision of $\pm$ 10 mK.

For samples with $w_e > 0.05$, a homogeneous nematic phase was not accessible by cooling the sample in the magnet through the isotropic / nematic biphasic region due to the occurrence of partial phase separation while traversing the biphasic region. The maximum cooling rate of the Colora is typically 0.6 K / min. During the time required to cross the mixed phase region ($\approx$ 6 min), partial phase separation occurred. To overcome this problem, the sample was made polycrystalline by first heating into the isotropic, mixing to ensure homogeneity of the sample. and then cooling rapidly outside the magnetic field, by immersion in a beaker of cold water, into the lamellar mesophase. The rapid cooling resulted in a concentration homogeneous polycrystalline sample. This was then placed in the sample cell and heated into the N_D^+ phase. Reorientation of the nematic director occurs readily in the nematic phase to give a macroscopically aligned sample and an ordered spectrum. The N_D^+ to L_D boundary is second order in this concentration regime and so there is no possibility of phase separation on crossing this boundary.

5.2.4 The determination of T_{NL} and T_{LN}.

For the $w_e = 0.0$ sample the L_D to N_D^+ transition is first order, i.e. there is a biphasic region separating the two single phase regions. The transition is only weakly first order however with the width of the mixed phase region being only 100 mK. The presence of a biphasic region is indicated by the presence of separate signals from the coexisting

Figure 14. The temperature dependence of the the partially averaged ^{133}Cs quadrupole splitting for a $w_e = 0.0294$ sample. The discontinuity in $\Delta\nu$ identifies T_{NI}.

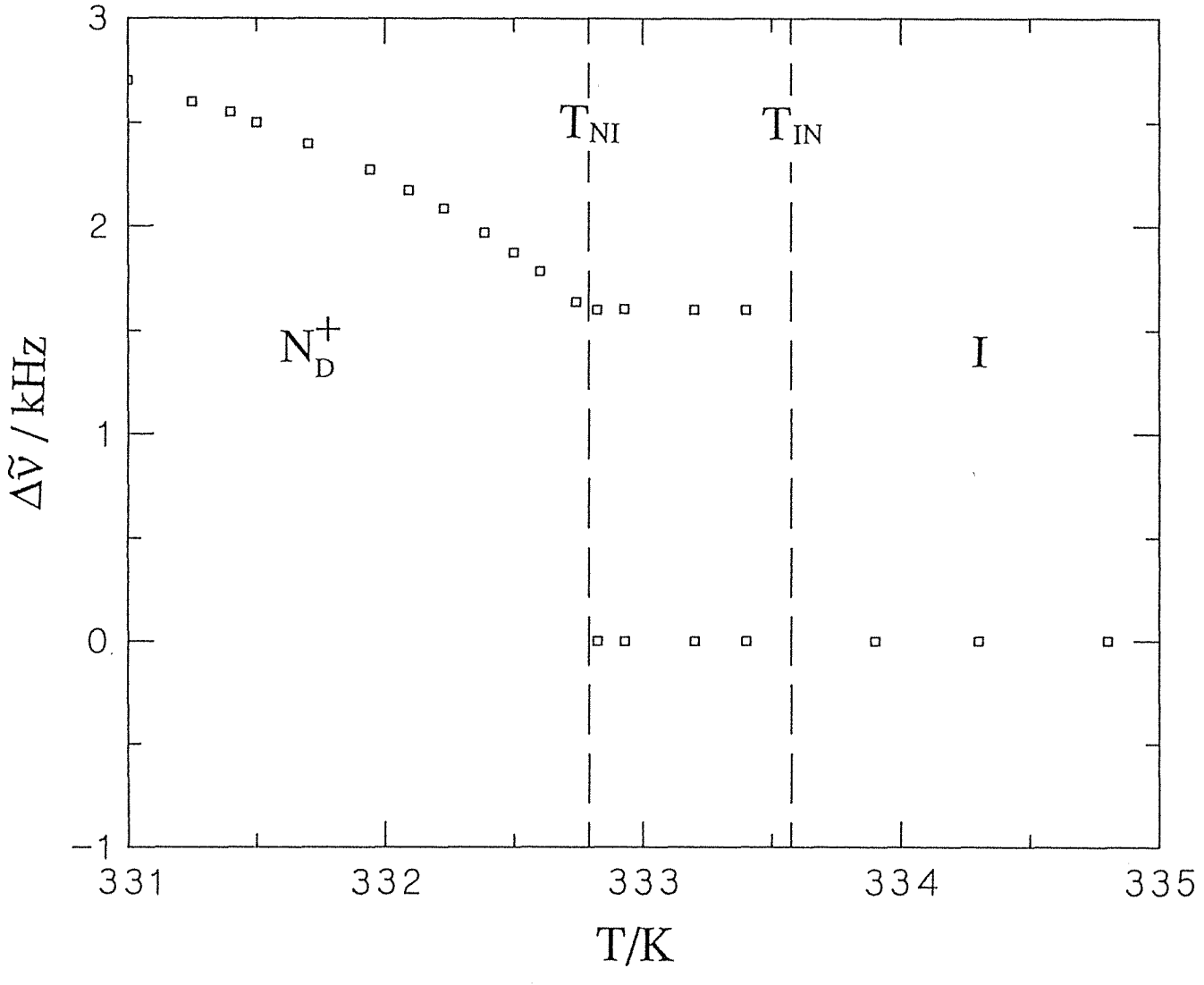
3
2
1
0
−1
331
332
333
334
335
T/K
Δν̃ / kHz
T_NI
T_IN
N_D^+
I

lamellar and nematic phases. The sequence of spectra observed when this sample is slowly cooled from the nematic phase across the nematic / lamellar biphasic region into the lamellar phase is shown in figure 15. Separate lamellar, and nematic signals are resolved, in the phase coexistence region, since the peak separation of nematic and lamellar signals is of the order of 40 Hz (cf. to quadrupole splittings of 5000 Hz). The outer peaks represent the lamellar phase spectrum while the inner peaks represent the nematic phase spectrum. It is interesting to compare the ^{133}Cs spectra with the ^{2}H spectra at the same temperatures for this sample [14] as shown in figure 16. This clearly indicates the greater resolving power of ^{133}Cs in the detection of the L_D and N_D^+ phases, the only indication from the ^{2}H spectra of $^{2}H_2O$ that a biphasic region exists is a slight broadening of the ^{2}H peaks in the mixed phase region. The appearance of the lamellar peaks on cooling, or nematic peaks on heating to determine T_{NL} or T_{LN}, is an imprecise method for reasons already discussed. A much better determination is achieved by observing the temperature dependence of the quadrupole splittings (figure 17a). A discontinuity in quadrupole splittings is observed at T_{NL} and T_{LN}, which clearly identifies these transition temperatures.

For all samples with added electrolyte there was no biphasic region observed for the nematic to lamellar transition. The implications of this are that the nematic to lamellar transition is second order for these samples, or else the intervening biphasic region is so narrow that the separate phases are unable to be resolved using caesium NMR. In any case the transition is second order within the precision of the experiment. A plot of $\Delta\nu$ versus temperature, figure 17b, shows a change in the temperature dependence of the quadrupole splitting at T_{LN}. The maximum slope indicates the T_{LN} transition [10,21] The downward turn in $\Delta\nu$ on the lamellar side of the transition and upward turn on the nematic side (figure 17a) are indications of strong pretransitional effects. Indeed on the

Figure 15. Sequence of ^{133}Cs NMR spectra as observed on cooling the $w_e = 0.00$ sample from the nematic phase N_D^+ to the lamellar phase L_D . The two distinct multiplets (b) indicate the presence of a nematic / lamellar biphasic region.

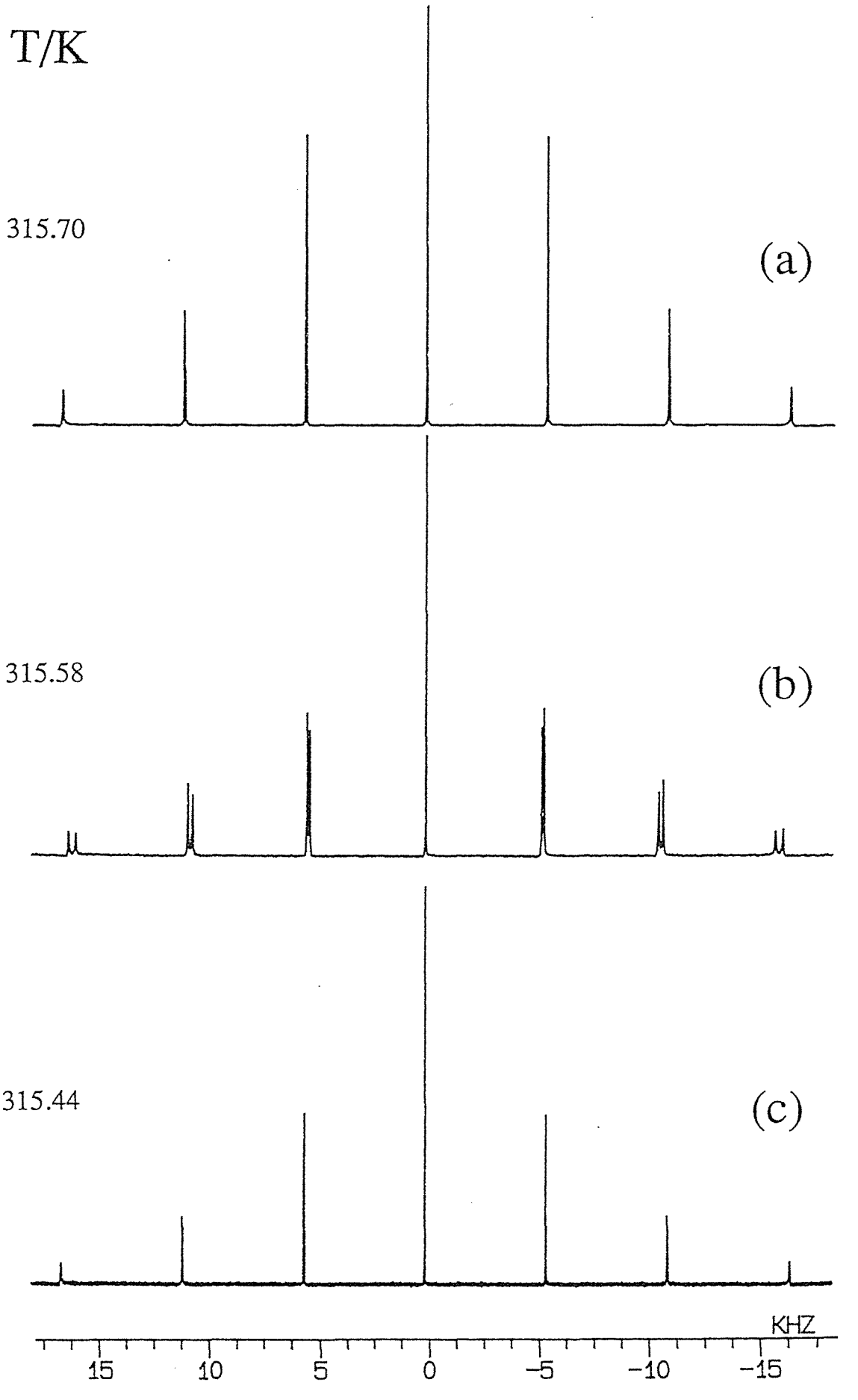
T/K
315.70
(a)
315.58
(b)
315.44
(c)
KHZ
15
10
5
0
-5
-10
-15

Figure 16. ^{2}H NMR spectra as observed on cooling the $w_e = 0.00$ sample from the nematic phase N_D^+ to the lamellar phase L_D. The ^{133}Cs NMR spectra for the same sample shows two distinct multiplets within the N_D^+ / L_D biphasic region (see previous figure) but the ^{2}H NMR spectra shows only a slight broadening of the doublet lines as an indication of a N_D^+ / L_D biphasic region. This comparison illustrates the greater resolving power of ^{133}Cs NMR compared to ^{2}H NMR .

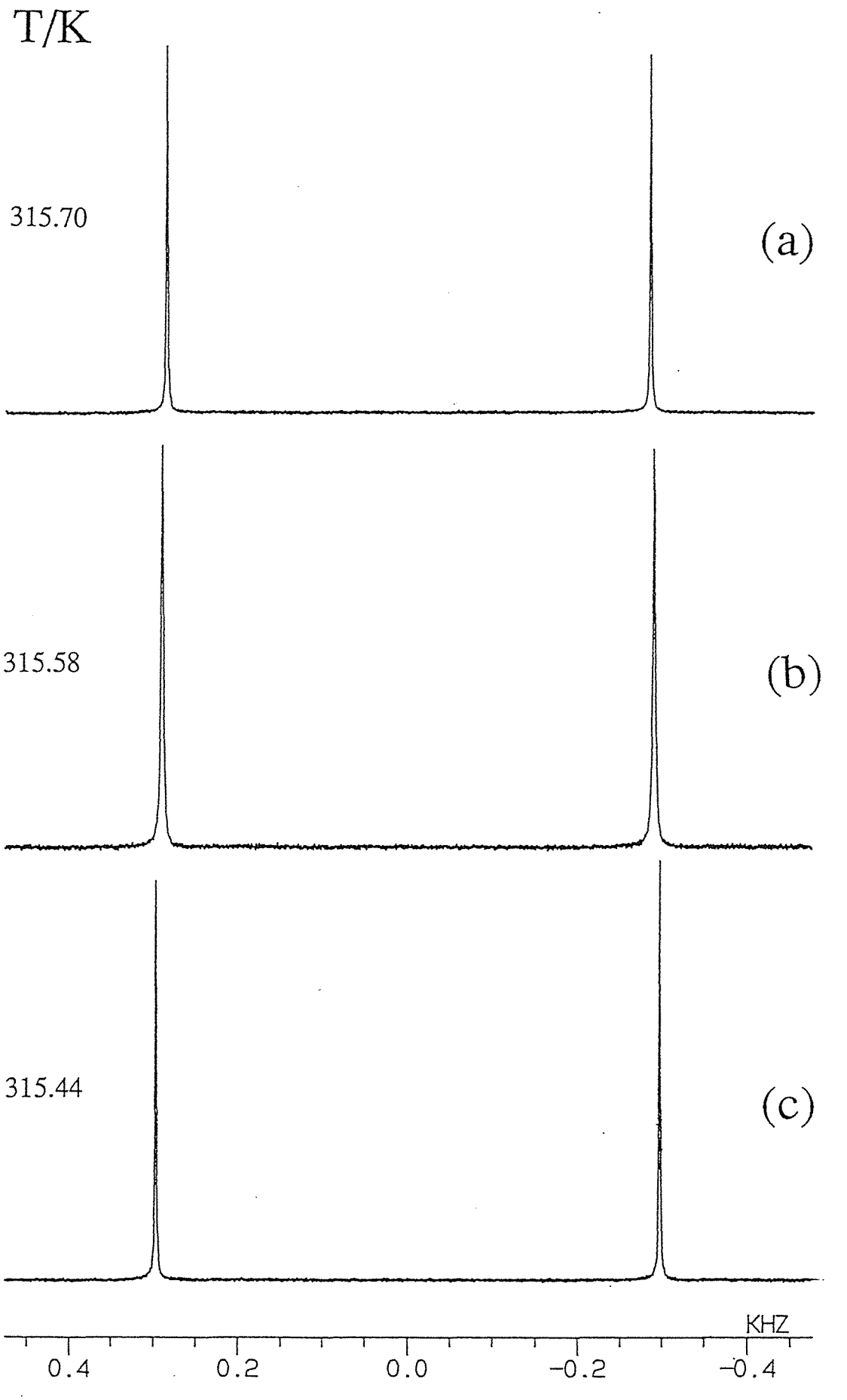
T/K
315.70
(a)
315.58
(b)
315.44
(c)
KHZ
0.4
0.2
0.0
−0.2
−0.4

Figure 17. Partially averaged ^{133}Cs quadrupole splitting $\Delta\nu$ versus temperature for the samples: (a) $w_e = 0.00$; illustrating the discontinuity in the quadrupole splitting at the T_{NL} and T_{LN} and (b) $w_e = 0.0434$; illustrating the change in the temperature dependence of the quadrupole splitting at the second order nematic to lamellar transition.

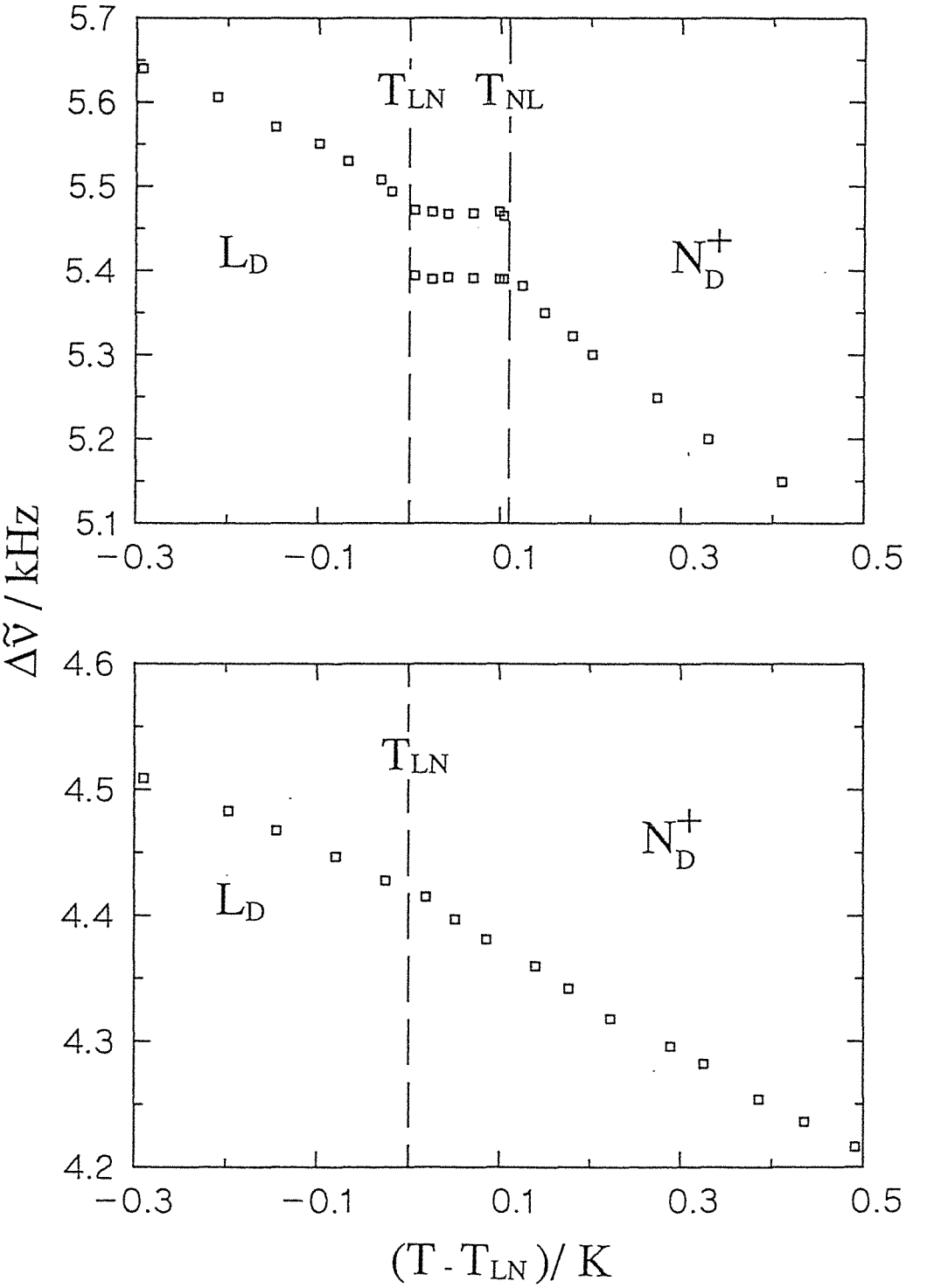
5.7
5.6
5.5
5.4
5.3
5.2
5.1
T_{LN} T_{NL}
L_D
N_D^+
−0.3
−0.1
0.1
0.3
0.5
$\Delta\tilde{\nu}$ / kHz
4.6
4.5
4.4
4.3
4.2
T_{LN}
L_D
N_D^+
−0.3
−0.1
0.1
0.3
0.5
$(T - T_{LN})$ / K

lamellar side the director rotates into alignment along the direction of the magnetic field for T_{LN} - T < 0.5 K for low w_e samples.

5.2.5 The determination of T_{LI}.

The width of the lamellar to isotropic transition varies from 4 K at Cep to 0.6 at w_e = 0.13. The transitions also occur at high temperature (high w_e) where the phases are quite mobile. The mobility of the phases coupled with the density differences between them leads to rapid phase separation. Any procedure that involves spending time in the I / L_D coexistence region will therefore result in large errors in T_{LI}. The best method to detect T_{LI} involves the generation of a polycrystalline sample by rapid cooling of an isotropic sample outside the magnetic field through the mixed phase region as discussed above in section 5.2.3. The quadrupole splittings are easily obtained from a polycrystalline sample as discussed previously and so a plot of $\Delta\nu$ verses temperature is readily constructed. On heating from the lamellar into the mixed phase there is a discontinuity in the quadrupole splitting (figure 18), similar to that observed in the detection of T_{NI} . It does not matter that phase separation occurs in the biphasic region as T_{LI} is identified by the discontinuity. An alternate method of preparation was to heat the polycrystalline sample to a temperature close to T_{LI} where reorientation of the lamellar director occurred to produce a macroscopically ordered lamellar phase. The sample was then cooled into the lamellar phase before obtaining $\Delta\nu$ on heating as before. The advantages of this latter method over measurements of $\Delta\nu$ from the polycrystalline spectrum is that a better signal to noise results, but in all other respects the techniques are identical.

Figure 18. The temperature dependence of the partially averaged ^{133}Cs quadrupole splitting $\Delta\nu$ versus temperature for a $w_e = 0.1015$ sample. The discontinuity in $\Delta\nu$ identifies T_{LI}.

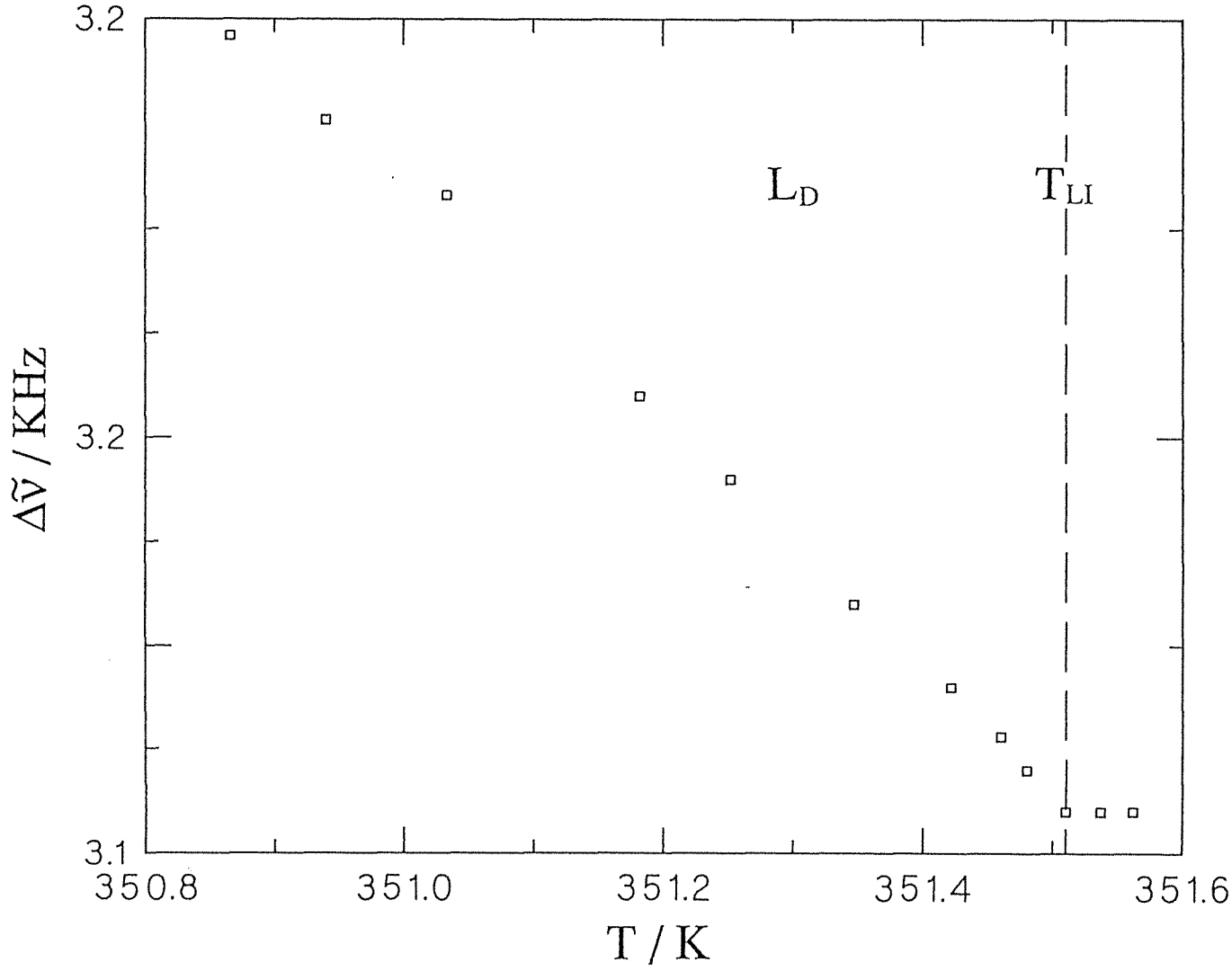
3.2
3.2
3.1
$\Delta\tilde{\nu}$ / KHz
L_D
T_{LI}
350.8
351.0
351.2
351.4
351.6
T / K

6. RELATIONSHIP BETWEEN QUADRUPOLE SPLITTING AND MESOPHASE STRUCTURE AND ORDER

6.1 MICELLAR STRUCTURE

The three quadrupole nuclei investigated in the study act as probes into the structure of the aggregate and the order of the mesophase. Each of the nuclei probe a distinctive aspect of the micelle-water interface, and it is the investigation of this region, intermediate to the micellar surface and the bulk which is of vital importance in determining the self association and self assembly properties of the mesophase. A wealth of information about the micellar structure is obtainable from the NMR of quadrupole nuclei.

From a consideration of equations (3), (5) and (7) it is clear that to obtain information on micellar structure it is necessary to deconvolute $|\bar{q}_{zz}|_s$ from the other terms in the expression for $\Delta\nu$. $|\bar{q}_{zz}|_s$ relates specifically to the aggregate surface through the shape factor $\langle P_2(\cos\alpha)\rangle_s$ and the fraction of ions or water bound at the surface.

6.1.1 Size and shape of the aggregates.

The equation defining $\Delta\nu$ for the ^2H nuclei of heavy water (equation (3)) contains a number of terms which may show a temperature dependence. It is possible to show that only S and $\langle P_2(\cos\alpha)\rangle_s$ contribute to the temperature variation of the quadrupole splittings, and that all other terms are constants for a particular w (i.e. x_A/x_w is constant), by using order parameter and micellar axial ratio data obtained from electrical conductivity and x-ray studies [21,34]. From x-ray studies the ratio $\frac{a}{b}$ of the micelles can be obtained, where a is the semi-minor and b is the semi-major axis of the micelle. This

enables the quantity $\langle P_2(\cos\alpha)\rangle_s$ to be calculated [10,34]. Conductivity measurements in conjunction with the x-ray structural data enable the orientational order parameter S to be calculated [21]. Assuming a constant $\chi_D n_b S_{OD}$ equations (3) and (4) can be used to obtain an expression for the reduced ^2H quadrupole splittings ($\Delta\nu_r$) at a given temperature relative to the value at T_{NI}.

$$\Delta\nu_r = \frac{\Delta\nu_T}{\Delta\nu_{T_{NI}}} = \frac{(S\langle P_2(\cos\alpha)\rangle_s)_T}{(S\langle P_2(\cos\alpha)\rangle_s)_{T_{NI}}} \qquad (11)$$

A plot of $\Delta\nu_r$ against the right hand side of equation (11) should therefore result in a straight line of slope 1 which passes through the origin. This plot is given in figure 19, over the temperature range T_{NI} to T_{LN} - 18.3 K (24.3 K) for $w_e = 0$,which shows that this is so and provides a strong affirmation of our model. The small difference could well be explained by the fact that samples of slightly different concentrations were used for the NMR, x-ray and conductivity measurements and there is also a high degree of scatter in the x-ray data. Taking $\chi_D \approx 215$ kHz as for heavy ice [37] gives $n_b S_{OD} = 0.12$ over the full temperature range, which is in the expected range for this quantity [38]. We can therefore conclude that the temperature dependence of $\Delta\nu$ (^2H) is determined by S and $\langle P_2(\cos\alpha)\rangle$ alone. Thus ^2H NMR of heavy water acts as a probe of micelle structure and order in lyotropic mesophases.

6.1.2 Fraction of ions bound to the micelle.

6.1.2(i) Temperature dependence of $\Delta\nu$ at constant w_e

It has been shown that $\Delta\nu(^2H)$ reflects the temperature variation of S and $\langle P_2(\cos\alpha)\rangle_s$ but the temperature dependence of $\Delta\nu(^{133}Cs)$ and $\Delta\nu(^{35}Cl)$ also depends on the bound fraction of ions (equations (5) to (8)). This is obvious from a comparison of the

Figure 19. Plot of equation (11). The diagonal has a slope of 1 and an intercept of zero as predicted by equation (11). The temperature range of the comparison is from T_{NI} to T_{NI} - 18.3 K.

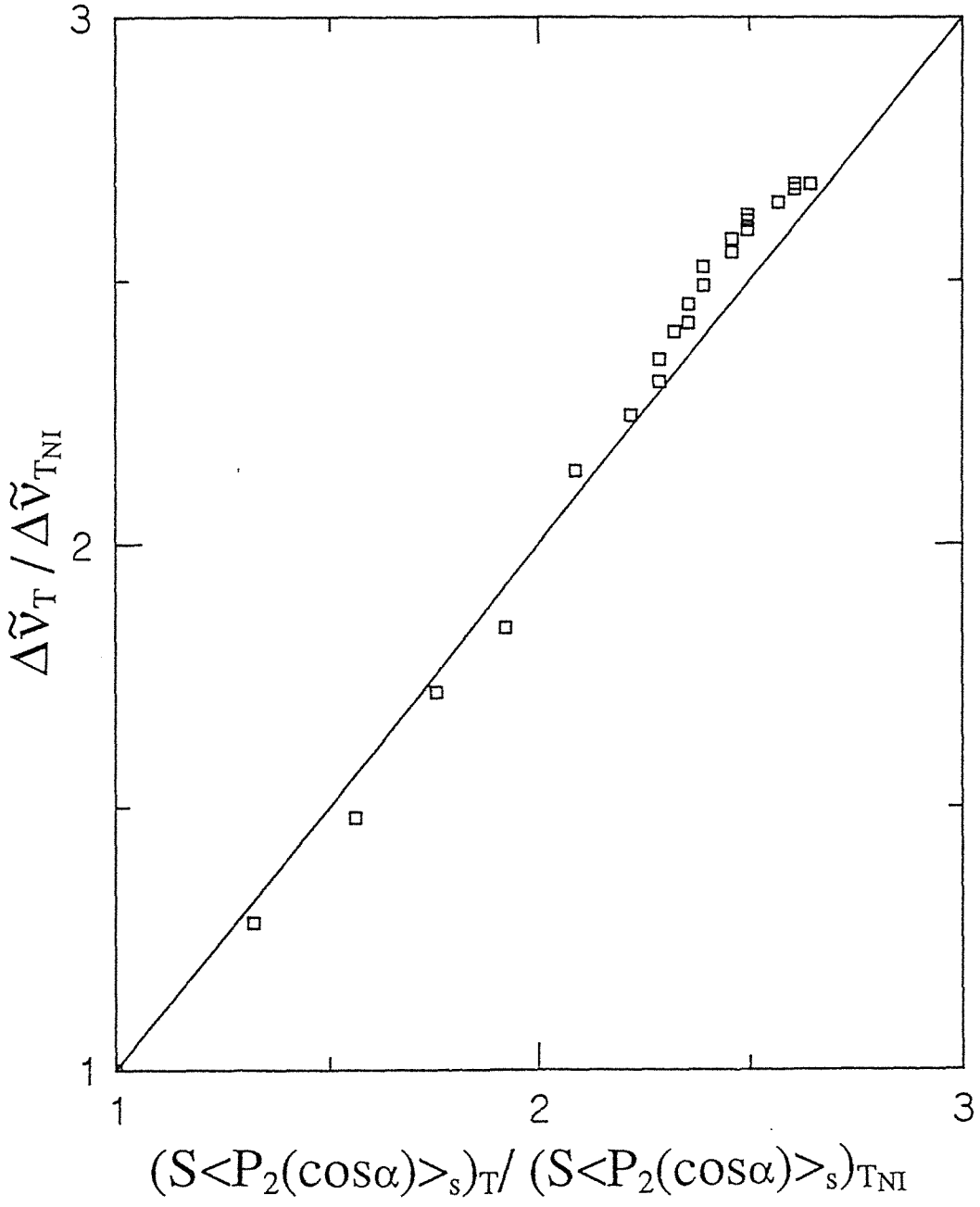
3
2
1
1
2
3
$\Delta\tilde{\nu}_T / \Delta\tilde{\nu}_{T_{NI}}$
$(S<P_2(\cos\alpha)>_s)_T / (S<P_2(\cos\alpha)>_s)_{T_{NI}}$

temperature dependence of the quadrupole splittings of ^{133}Cs, ^{2}H, and ^{35}Cl as shown in figure 20 for a sample with $w_e = 0.0294$. To enable all three temperature dependences to be presented on one graph the values have all been reduced to their respective values at T_{NI}. From the plot it is obvious that $\delta\Delta\nu(^{133}Cs)/\delta T$ is greater and $\delta\Delta\nu(^{35}Cl)/\delta T$ lesser than $\delta\Delta\nu(^{2}H)/\delta T$ at any temperature. To prove that this is due to changes in the fraction of bound ions it is first of all necessary to show that χ_{Cs} and χ_{Cl} are temperature independent over the range considered here. This can be done by a comparison of the ^{133}Cs quadrupole couplings with the chemical shift anisotropies. In this study $\Delta\sigma$ was measured as a function of temperature in two ways. For a ordered sample the parallel component was measured with respect to the isotropic peak at T_{IN} equation (10), for disordered samples it was measured directly from the central peak of the polycrystalline sample in the lamellar phase as shown in figure 21. The plot of $\Delta\sigma$ versus temperature is shown in figure 22. The fact that the ordered and polycrystalline data overlaps justifies the assumption that the temperature dependence of the isotropic component can be ignored. The plot has all the features of the $\Delta\nu$ versus temperature curve. In fact the ratio $\Delta\nu(^{133}Cs)/\Delta\sigma(^{133}Cs)$ is constant over the whole temperature range. This is graphically illustrated in figure 23 where the reduced values of the quadrupole splittings $\Delta\nu_r$ is plotted against that for the chemical shift anisotropy $\Delta\sigma_r$.

From equation (5) and (9) at any given temperature,

$$\frac{\Delta\nu_r(^{133}Cs)}{\Delta\sigma_r(^{133}Cs)} = \{(\chi_{Cs})_T / (\chi_{Cs})_{T_{NI}}\} / \{(\sigma_{//}-\sigma_{\perp})_T / (\sigma_{//}-\sigma_{\perp})_{T_{NI}}\}$$

The plot of $\Delta\nu_r(^{133}Cs)$ versus $\Delta\sigma_r(^{133}Cs)$ figure 23 has a slope of 1, and an intercept of zero. The simplest explanation for this is that all the quantities in the expression for the slope are temperature independent. The alternative explanation is that χ_{Cs} and $(\sigma_{//}-\sigma_{\perp})$ have the same temperature dependence, although this is extremely unlikely since χ_{Cs} is a

Figure 20. Reduced partially averaged quadrupole splittings $\Delta\nu_r$ versus temperature as observed on cooling the $w_e = 0.0294$ sample from the isotropic phase I into the nematic phase N_D^+ and from N_D^+ into the lamellar L_D for; ^2H, ^{133}Cs and ^{35}Cl as indicated on the graph. The splittings have been reduced to their respective values at T_{NI} to illustrate the difference in temperature dependence for each of the three nuclei. The values for the $\Delta\nu$ at T_{NI} are 3.5, 0.232 and 1.61 kHz for the ^{35}Cl, ^2H and ^{133}Cs nuclei respectively.

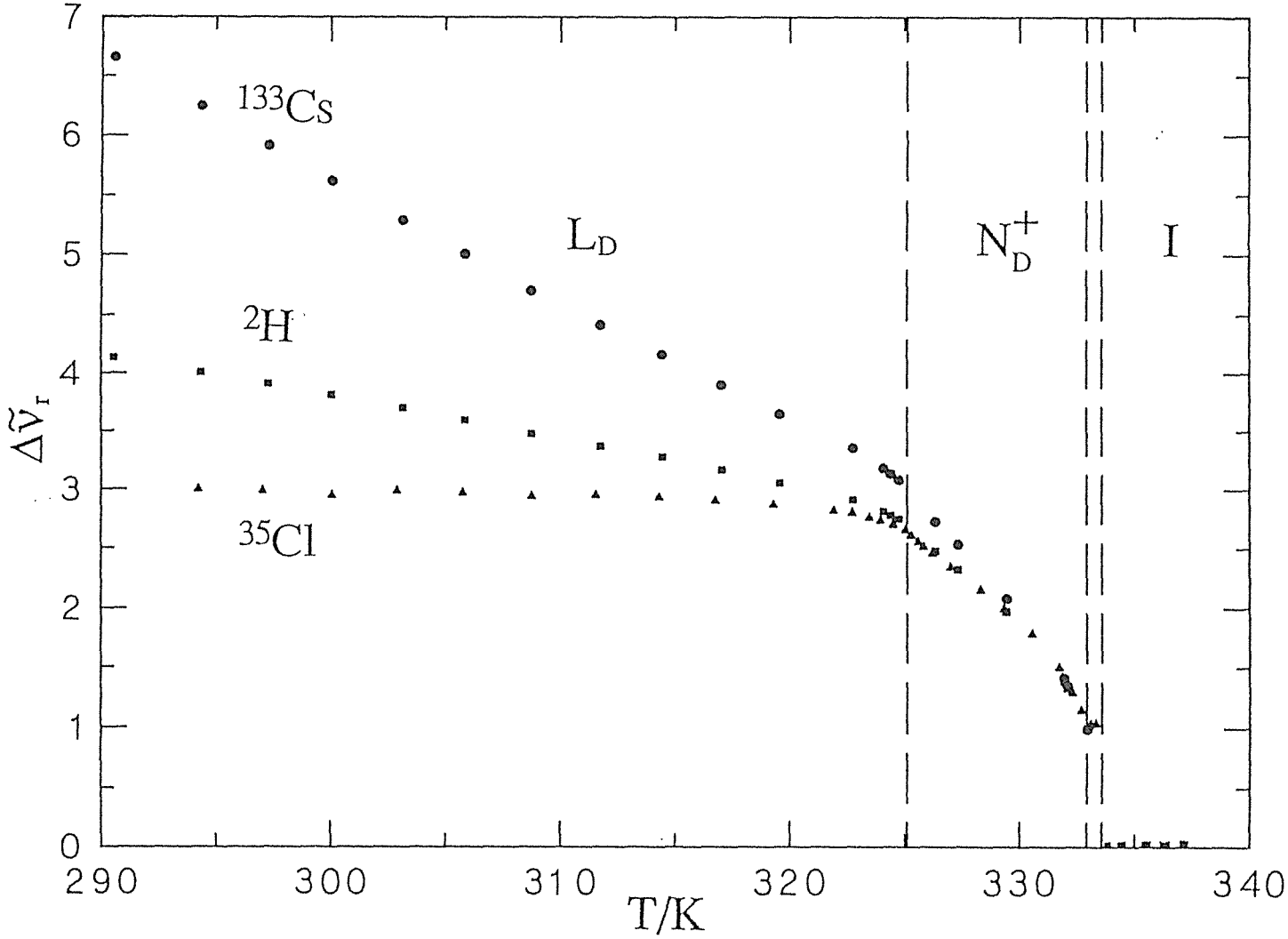
7
6
5
4
3
2
1
0
290
300
310
320
330
340
T/K
$\Delta\tilde{\nu}_r$
^{133}Cs
^{2}H
^{35}Cl
L_D
N_D^+
I

Figure 21. ^{133}Cs NMR spectra of the -1/2 to +1/2 transition for a w_e = 0.0434 sample at 321.03 K in the lamellar phase. $\sigma_\perp$ and $\sigma_{//}$ as indicated have been determined from this polycrystalline spectrum according to the method of reference 31 using the Lorentzian line shape option.

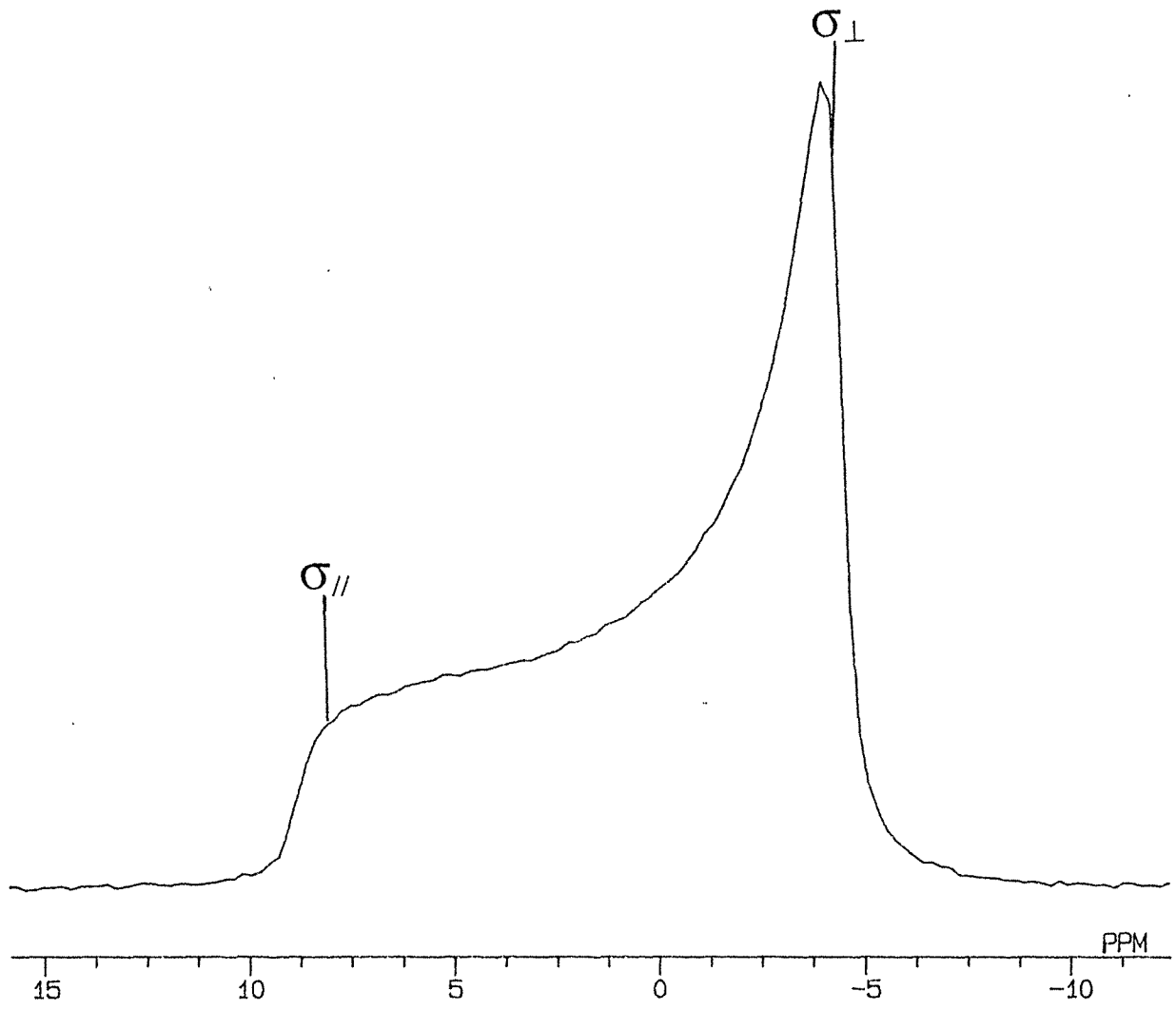
σ⊥
σ//
PPM
15
10
5
0
-5
-10

Figure 22. ^{133}Cs chemical shift anisotropy $\Delta\sigma$ as observed on cooling the $w_e = 0.00$ sample from the isotropic I into the nematic phase N_D^+ and from N_D^+ into the lamellar L_D . This plot illustrates the similarity in the plots of the chemical shift and the partially averaged quadrupole splittings figure 10. Note the nematic / lamellar biphasic region is not resolved. This is because it was beyond the resolution of the NMR to identify separate parallel components of the chemical shielding tensor for the nematic and lamellar phases.

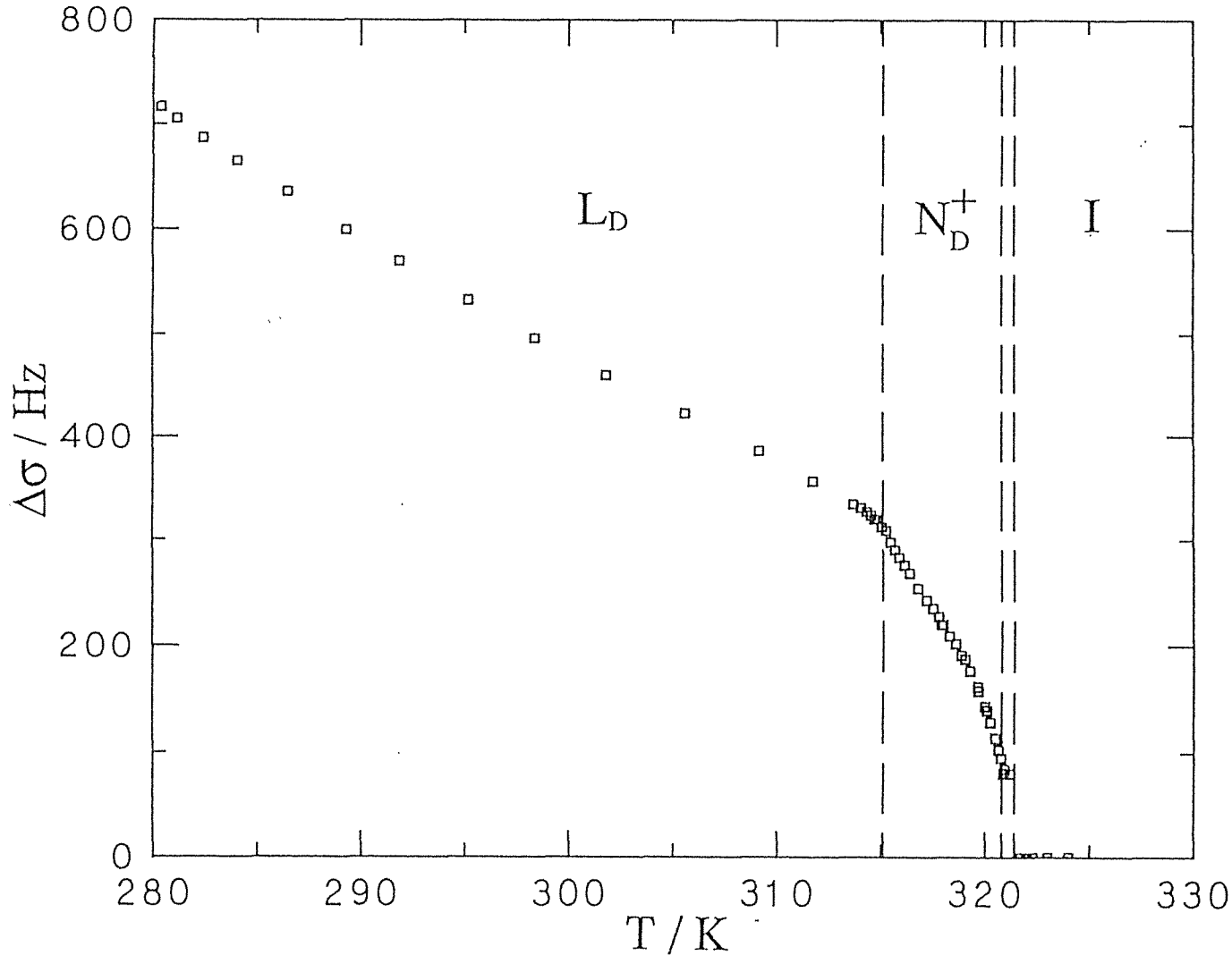
800
600
400
200
0
Δσ / Hz
280
290
300
310
320
330
T / K
L_D
N_D^+
I

Figure 23 Plot of $\Delta\sigma_T / \Delta\sigma_{T_{NI}}$ ($\Delta\sigma_r$) versus $\Delta\nabla_T\Delta\nabla_{T_{NI}}$ ($\Delta\nabla_r$) for the $w_e = 0.00$ sample over the temperature range T_{NI} to T_{NI} - 40 K. The plot has a slope of 1 and an intercept of zero showing that the temperature dependence of both the ^{133}Cs quadrupole splitting and the ^{133}Cs chemical shift anisotropies are determined by the same factors.

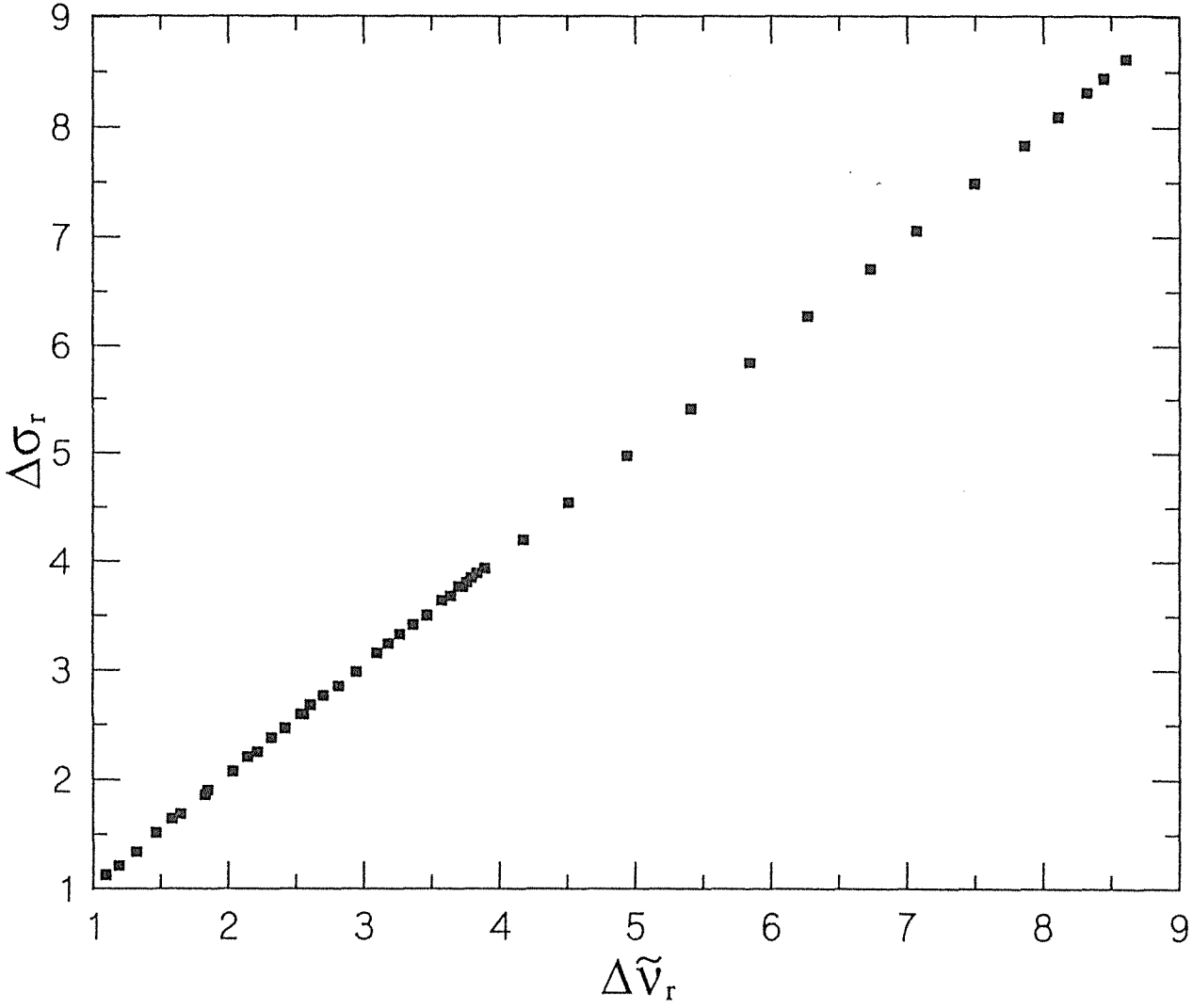
9
8
7
6
5
4
3
2
1
$\Delta\sigma_r$
1
2
3
4
5
6
7
8
9
$\Delta\tilde{\nu}_r$

nuclear property, and $(\sigma_{//}-\sigma_{\perp})$ is an electronic property [39]. Since both χ_D and χ_{Cs} have been shown to be temperature independent it is reasonable to assume that χ_{Cl} also possesses that property. This assumption allows us to write expressions for $\Delta\nu_r(^{133}Cs)$ and $\Delta\nu_r(^{35}Cl)$ i.e.

$$\Delta\nu_r(^{133}Cs)=\frac{\Delta\nu_T}{\Delta\nu_{T_{NI}}} = \{(S<P_2(\cos\alpha)>_s)_T\,(\beta_{Cs})_T\} \,/\, \{(S<P_2(\cos\alpha)>_s)_{T_{NI}}\,(\beta_{Cs})_{T_{NI}}\}$$

and similarly for ^{35}Cl. So in addition to the S and $<P_2(\cos\alpha)>_s$ terms which govern the temperature dependence of the deuterium quadrupole splittings, there is a contribution to the temperature dependence of the ^{133}Cs and ^{35}Cl splittings from the fraction of bound ions.

Thus for the two nuclei ^{133}Cs and ^{35}Cl (figure 20) the differences in the $\Delta\nu$ temperature dependence is explained in terms of changes in the bound ion fraction. Therefore, with decreasing temperature there is an increase in the number of bound caesium ions relative to the value at T_{NI} and vice versa for the chloride ions. The variation of β with respect to the values at T_{IN} is obtained from a consideration of the quantities $\Delta\nu_r / \Delta\nu_r(^2H)$ (= $\beta_T / \beta_{T\,NI}$) for the two nuclei, as shown in figure 24. The figure shows an increase in β_{Cs} of 30 % in the temperature range T_{NI} to T_{NI} - 22 K which compares with a value of 19 % [34] obtained from conductivity measurements (for the $w_e = 0$ sample) over the same temperature range. The agreement is pleasing in view of the fact that what conductivity "sees " as bound ions is not necessarily the same as that seen by NMR. The increase in β_{Cs} and the concomitant decrease in β_{Cl} with decreasing temperature is consistent with the low energy state being favoured. This state would tend to have a layer of Cs^+ ions as nearest neighbours to the carboxylate ions, with the Cl^- ions as next nearest neighbours. It is worth noting that this increase in β_{Cs} is paralleled by an increase in the micelle size on cooling [22]. Thus a reduction in the micellar surface

Figure 24. The fraction of bound ions β as observed on cooling the $w_e = 0.0294$ sample from T_{NI} through the nematic phase N_D^+ and from N_D^+ into the lamellar phase L_D, reduced to the fraction of ions bound at T_{NI}.

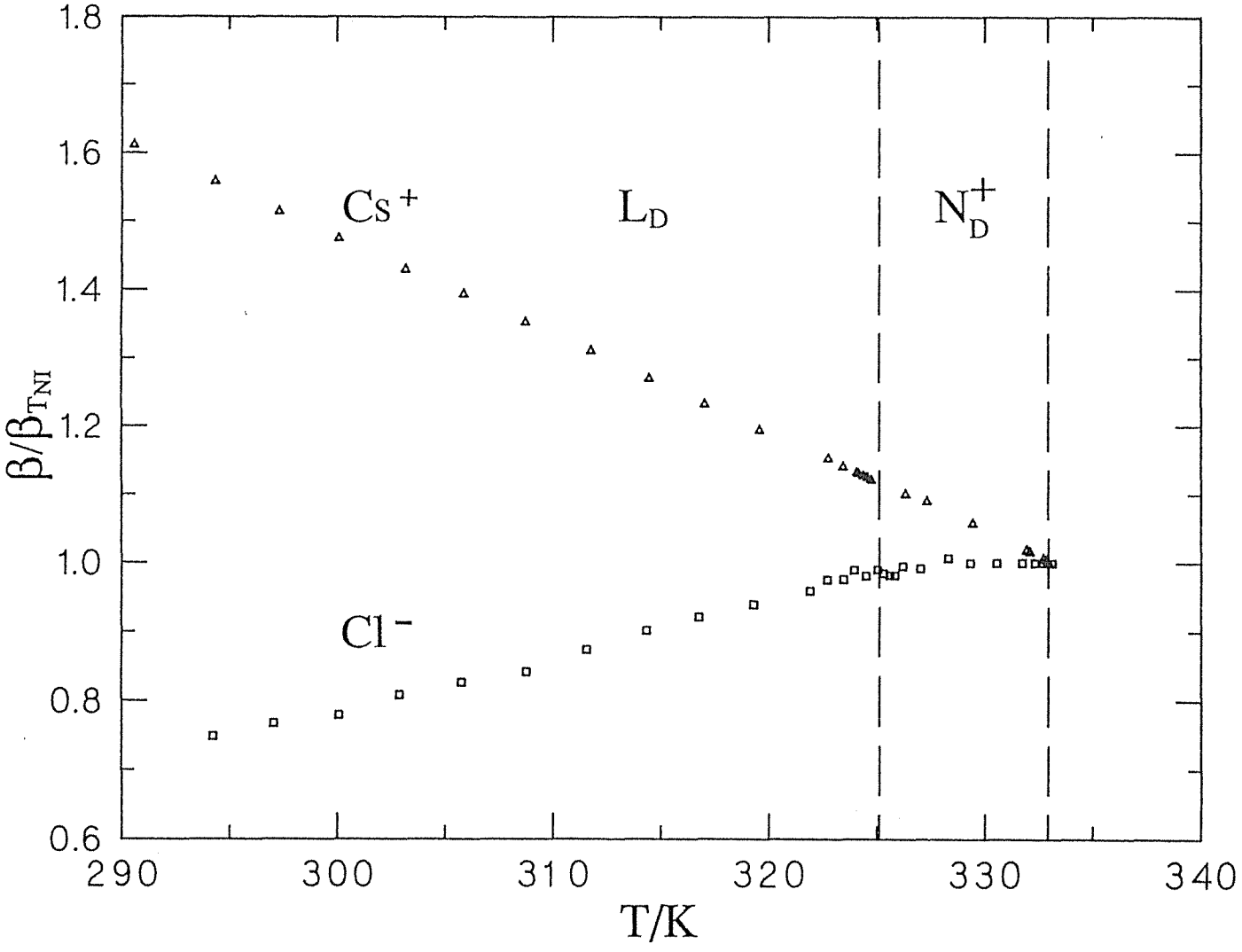
1.8
1.6
1.4
1.2
1.0
0.8
0.6
β/β$_{T_{NI}}$
Cs$^+$
L$_D$
N$_D^+$
Cl$^-$
290
300
310
320
330
340
T/K

charge density is coupled to an increase in micelle size. The behaviour illustrated in figure 24 for the $w_e = 0.0294$ sample is typical of all the samples studied.

6.1.2(ii) Concentration dependence of $\Delta\nu$ at constant temperature.

The concentration dependence of the quadrupole splittings of ^2H, ^{133}Cs and ^{35}Cl at various constant temperatures within the lamellar phase is given in figures 25,26 and 27 respectively. Data below 310 K is not shown as the higher w_e samples crystalise out at around 305 K. Information about the orientational order parameter in the lamellar phase has been obtained from x-ray studies conducted on the binary CsPFO/ water system [21]. It was established that throughout the lamellar phase S is essentially constant, so the $\Delta\nu$ concentration dependence in this phase is determined by changes in $\langle P_2(\cos\alpha)\rangle_s$ and the fraction of bound water or ions. It has been shown that $n_b S_{OD}$ is constant over a wide temperature and composition range [10] and thus the increase in $\Delta\nu(^2H)$ with increasing w_e at constant temperature (figure 25), implies a growth in the average size of the micelles (i.e. increase in $P_2(\cos\alpha)>_s$). This is a consequence of a decrease in the ratio of the minor axis (a) to the major axis (b). Since a is constant [14] this must mean that b increases, that is , the micelle grows. Also as the temperature increases there is a reduction in the size of the micelles.

For the ^{133}Cs quadrupole splittings the data is complicated by the changing caesium ion concentration as w_e is varied, this complication can be removed if instead of considering the change in the bound fraction of ions the change in the number of ions bound per amphiphile is considered. This can be calculated in the following way. The ratio $\Delta\nu(^{133}Cs) / \Delta\nu(^2H)$ at a given temperature is equal to $k\,\beta_{Cs}$, where the constant k includes all the constant terms in equations (4) and (6). The quantity β_{Cs} can be written $n_b /(n_A + n_S)$ where n_b is the number of moles of bound ions and the total number of

Figure 25. Partially averaged ^2H quadrupole splittings $\Delta\nu(^2H)$ at various constant temperatures within the lamellar region versus weight fraction of CsCl w_e

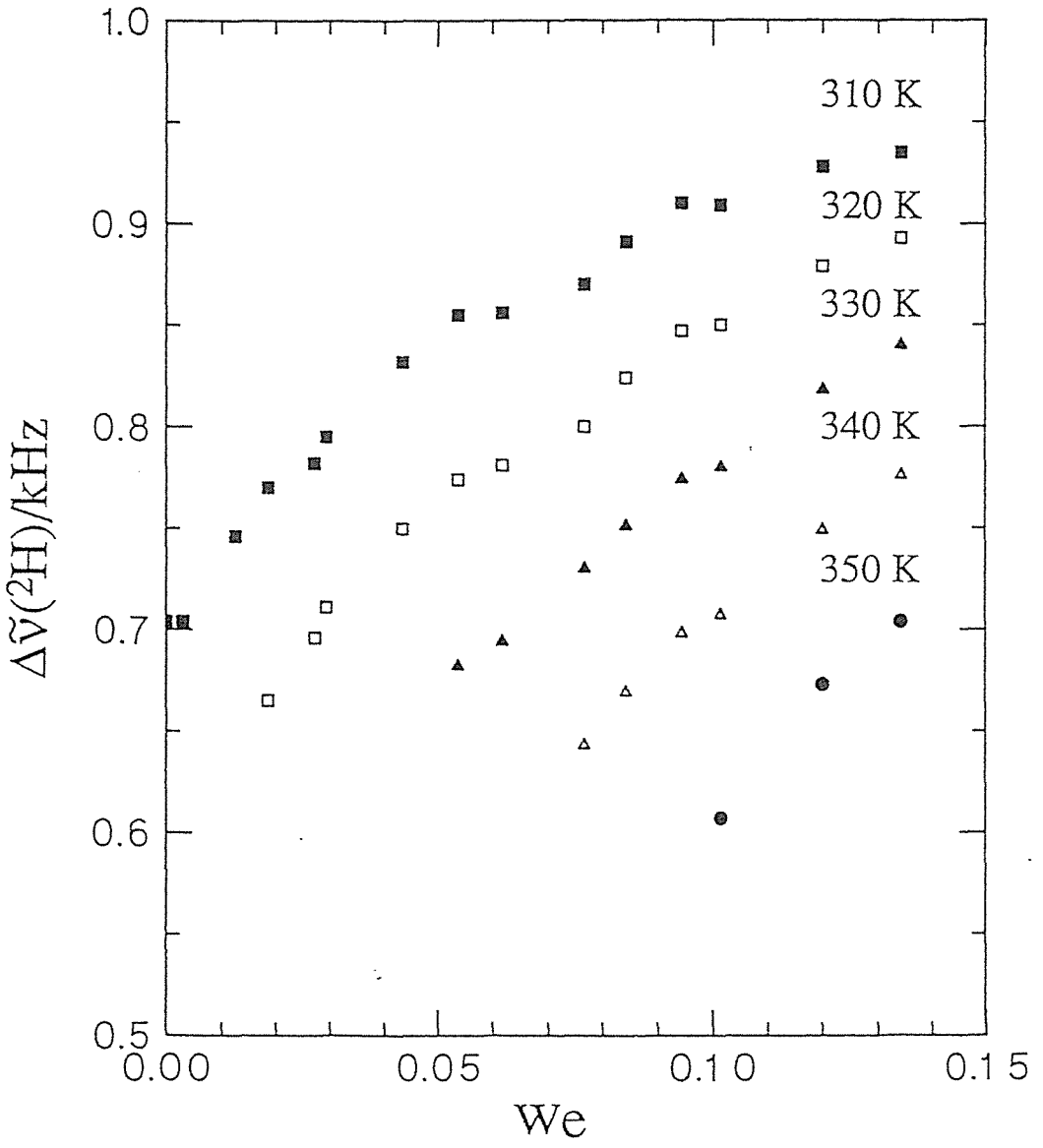
1.0
0.9
0.8
0.7
0.6
0.5
0.00
0.05
0.10
0.15
We
$\Delta\tilde{\nu}(^2H)$/kHz
310 K
320 K
330 K
340 K
350 K

Figure 26. Partially averaged ^{133}Cs quadrupole splittings $\Delta\nu(^{133}Cs)$ at various constant temperatures within the lamellar region versus weight fraction of CsCl w_e.

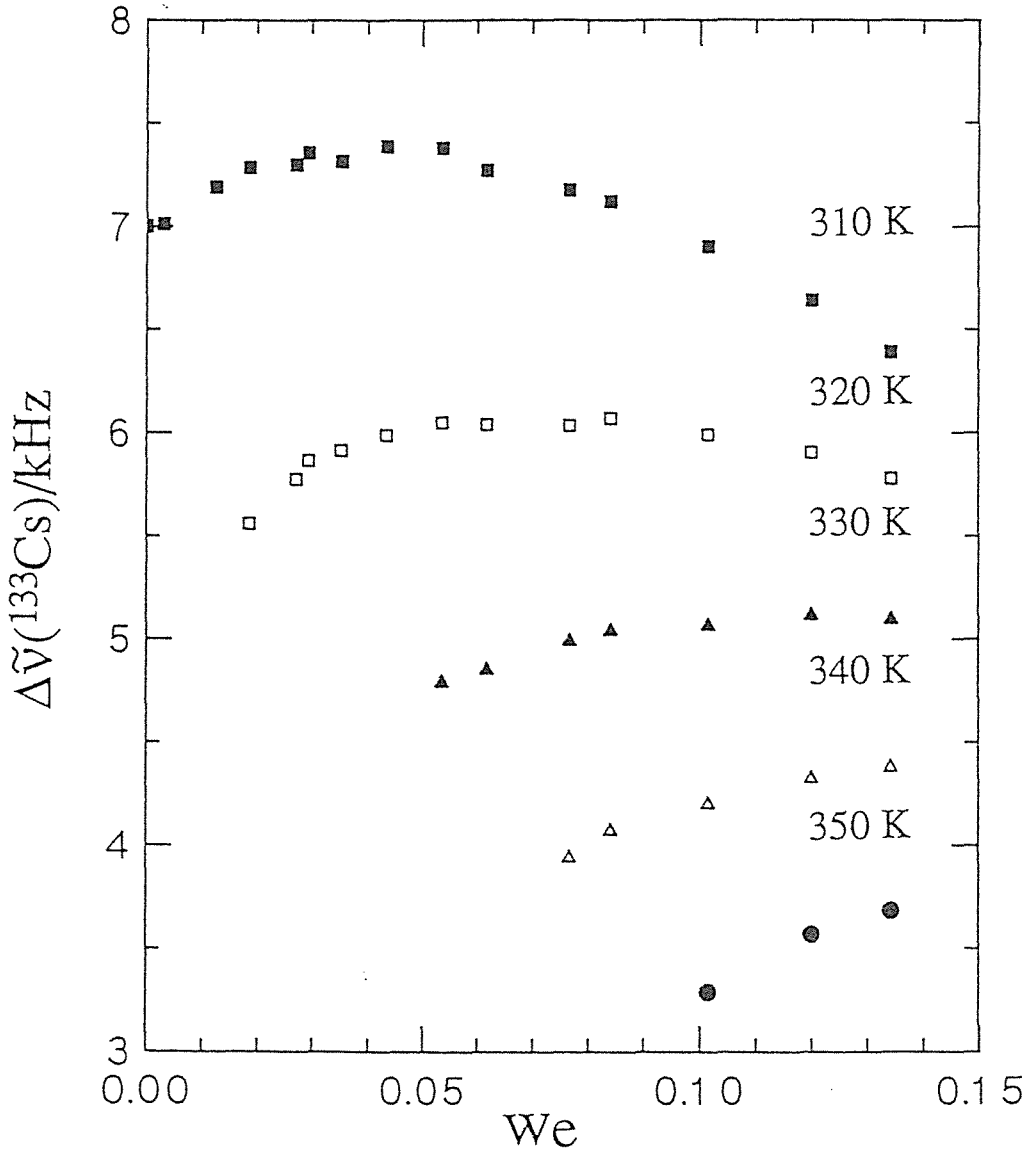
8
7
6
5
4
3
0.00
0.05
0.10
0.15
We
$\Delta\tilde{\nu}(^{133}Cs)$/kHz
310 K
320 K
330 K
340 K
350 K

Figure 27. Partially averaged ^{35}Cl quadrupole splittings $\Delta\nu(^{35}Cl)$ at various constant temperatures within the lamellar region versus weight fraction of CsCl w_e

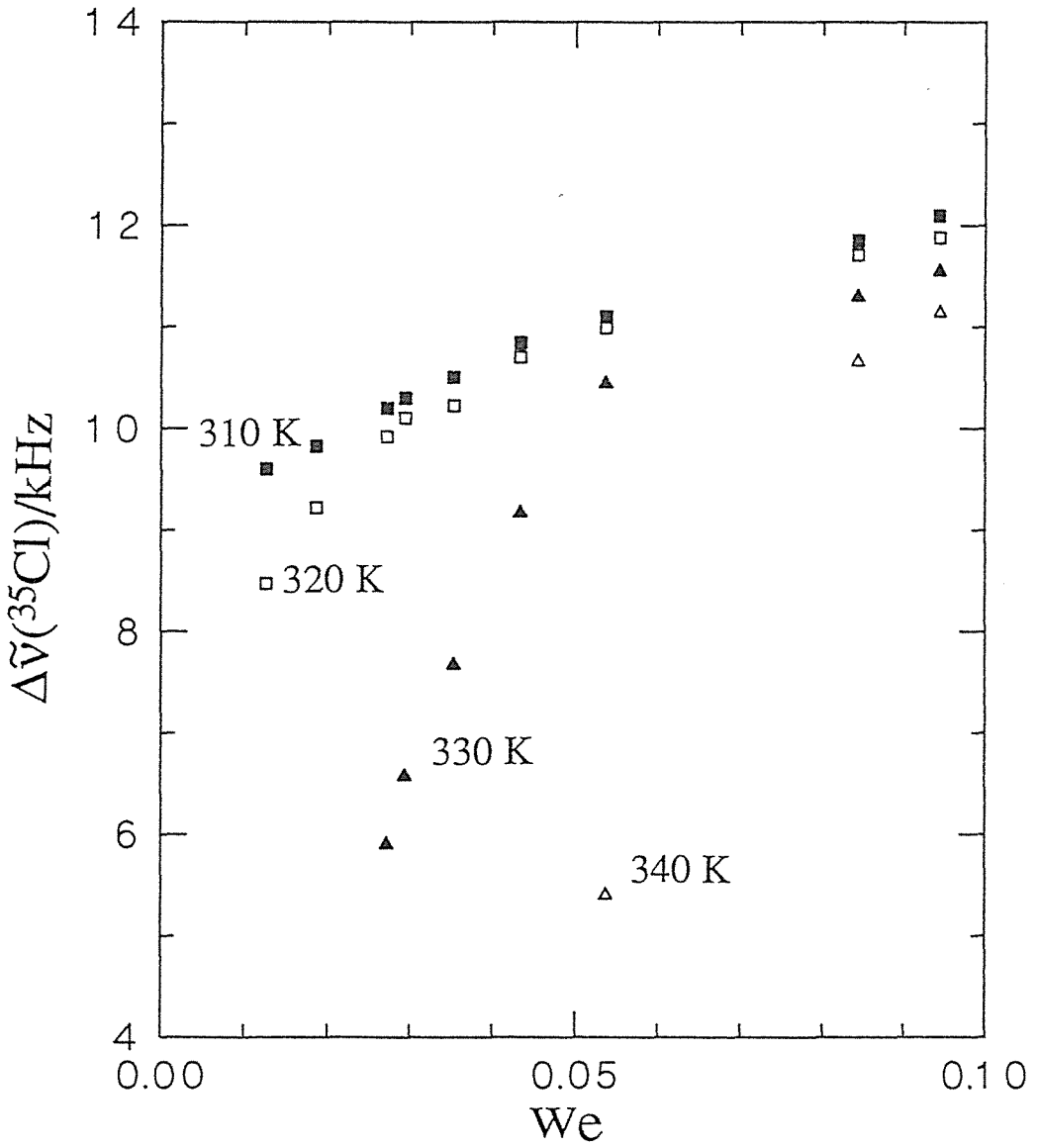
14
12
10
8
6
4
0.00
0.05
0.10
We
Δν̃(35Cl)/kHz
310 K
320 K
330 K
340 K

moles of caesium ions is the sum of the moles of amphiphile (n_A) and the moles of salt (n_S). To obtain the number bound per amphiphile molecule (n_b / n_A) requires that β_{Cs} be multiplied by $(n_A + n_S) / n_A$. Furthermore to represent the change in n_b / n_A with added electrolyte at various temperatures the data is normalized to the $w_e = 0$ point at 310 K i.e. the quantity

$$\frac{(\{\Delta\nu\ (^{133}Cs)/\ \Delta\nu\ (^{2}H)\}_{w_e,T})\ (n_A + n_S)}{(\{\Delta\nu\ (^{133}Cs)/\ \Delta\nu\ (^{2}H)\}_{0,310\ K})\quad n_A} = \frac{(n_b / n_A)_{w_e;T}}{(n_b / n_A)_{0;310\ K}}$$

reflects changes in n_b / n_A with the value at $w_e = 0$ and T = 310 K set equal to 1. A plot of this quantity versus w_e at several temperatures is shown in figure 28. From this graph we can see that the caesium binding increases as w_e increases at constant temperature for all five temperatures considered. It is also clear that the n_b / n_A decreases with increasing temperature, consistent with a "boil off" of Cs^+ ions at the higher temperatures.

As the caesium bound per amphiphile increases with increasing w_e, the charge density at the micellar surface decreases, which is consistent with the extra Cs^+ ions binding between the carboxylate groups and in so doing, shielding neighbouring carboxylate groups from each other. This reduction in head group repulsion, promotes a flat surface as opposed to a curved surface for the micelle which in turn allows the micelles to grow. In fact the only way the micelle can grow and remain an oblate ellipsoid is for the a/b ratio to decrease. This growth in micellar size is reflected by the increase in $\Delta\nu(^2H)$ with increasing w_e (figure 25).

This same method can be used to determine the ratio n_b / n_A for the Cl^- ions but in this case the data must obviously be relative to a sample other than $w_e = 0.0$ because there are no chloride ions present in this sample. Figure 29 shows the number of chloride ions

Figure 28. The number of caesium ions bound per amphiphile molecule n_b^{Cs} versus w_e at constant temperatures within the lamellar phase. The data has been reduced the n_b^{Cs} at 310 K and $w_e = 0.00$.

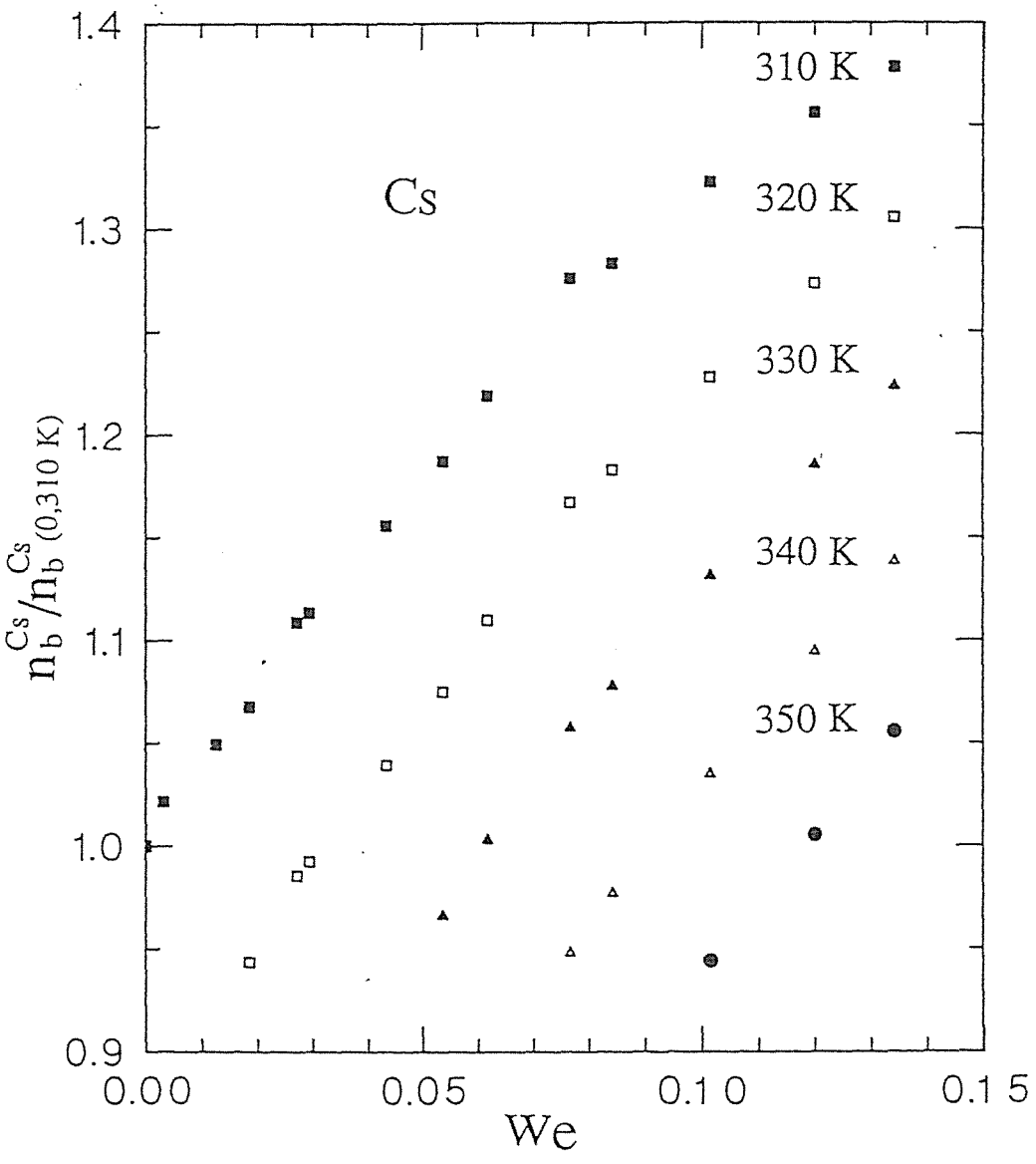
1.4
1.3
1.2
1.1
1.0
0.9
0.00
0.05
0.10
0.15
We
$n_b^{Cs}/n_b^{Cs}{}_{(0,310\ K)}$
Cs
310 K
320 K
330 K
340 K
350 K

Figure 29. The number of chloride ions bound per amphiphile molecule n_b^{Cl} versus w_e at constant temperatures within the lamellar phase. The data has been reduced the n_b^{Cs} at 310 K and $w_e = 0.0126$.

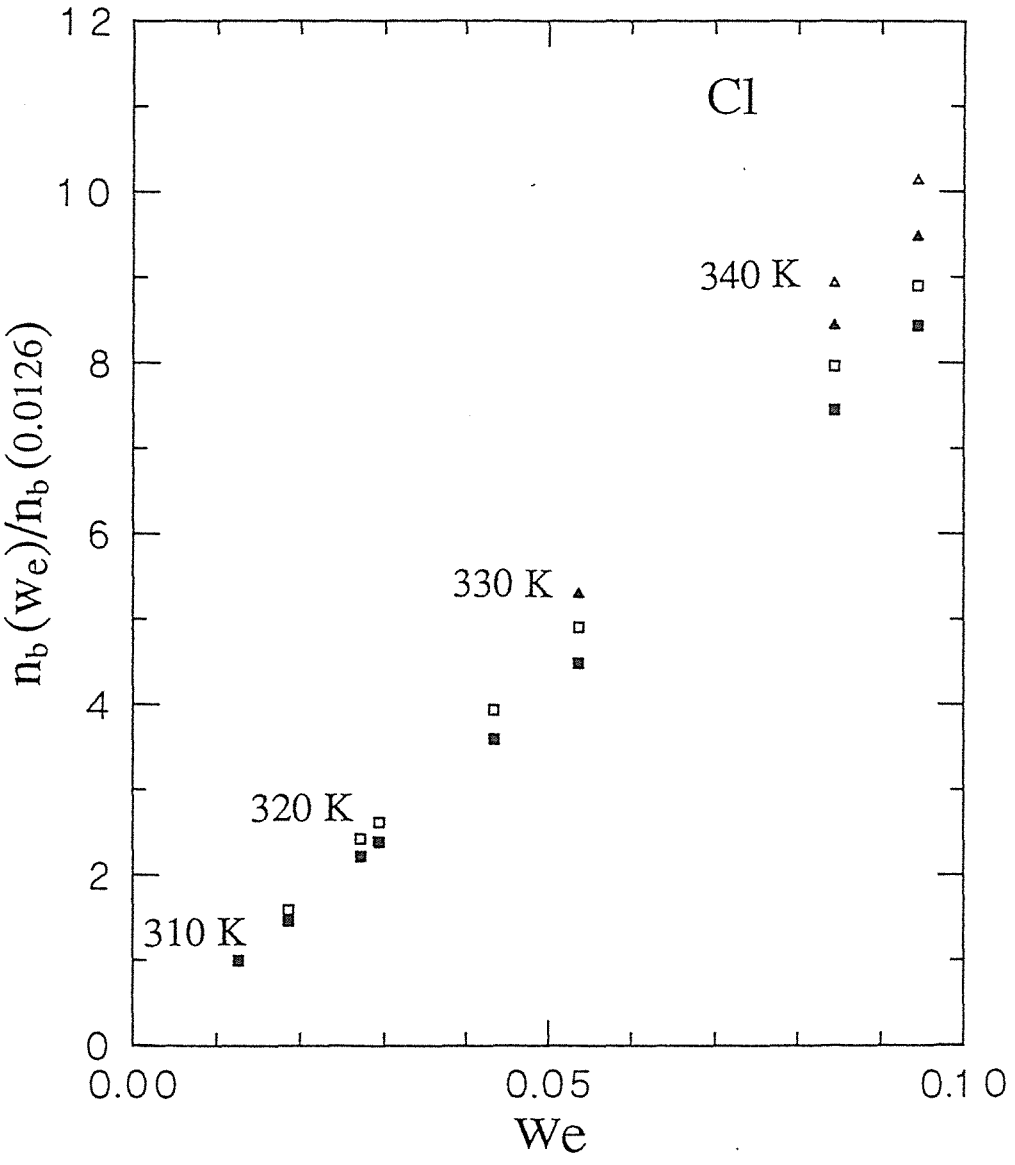
Cl
340 K
330 K
320 K
310 K
$n_b(We)/n_b(0.0126)$
We
0
2
4
6
8
10
12
0.00
0.05
0.10

bound per amphiphile as a function of w_e at constant temperature, relative to n_b/n_A at w_e = 0.0126 at 310 K. There is an increase in n_b/n_A as w_e increases, which is probably caused simply by the increase in the chloride ion concentration resulting in more Cl^- ions in the vicinity of the micelle surface. An interesting observation is that more Cl^- ions are bound at high than low temperatures. There is symmetry here as there must be, since as more Cs^+ ions become bound they will be displacing Cl^- ions and vice versa. The concept of "bound" Cl^- ions is problematical . The increase in Cl^- ion bound fraction bears a very close relationship to the increase to the total Cl^- ion concentration. It appears that the Cl^- ion concentration in the vicinity of the micellar surface is therefore simply reflecting the bulk Cl^- ion concentration, i.e. there are no specific interactions at the surface. This does not imply that a change in the coion will not affect the phase behaviour, since other interactions such as between ion pairs could affect the fraction of Cs^+ ions bound. It appears at this stage that this is the determining factor in controlling the micelle size and hence the macroscopic phase behaviour.

6.1.2(iii) $\Delta\nu$ at the phase transition temperature.

(a) Lamellar to nematic and lamellar to isotropic transition lines.

Figure 30 shows the quadrupole splittings at the phase transition temperatures for the three nuclei as a function of w_e. The deuterium quadrupole splittings are seen to decrease slightly (after an initial increase) along the transition line as w_e increases. $\Delta\nu(^2H)$ is a function of S and $\langle P_2(\cos\alpha)\rangle_s$, and as S is assumed to be constant at T_{LN} then, $\langle P_2(\cos\alpha)\rangle_s$ must change only slightly along the transition line. The implication of this is that the micellar size and shape is about the same along these transition boundaries. The addition of salt causes growth in the micellar size as indicated above, so in order to bring about a transition to the nematic phase the micelle size must decrease

Figure 30. Partially averaged quadrupole splittings at the phase transition temperature versus w_e.

(a) $\Delta\nu(^2H)$

(b) $\Delta\nu(^{133}Cs)$

(c) $\Delta\nu(^{35}Cl)$

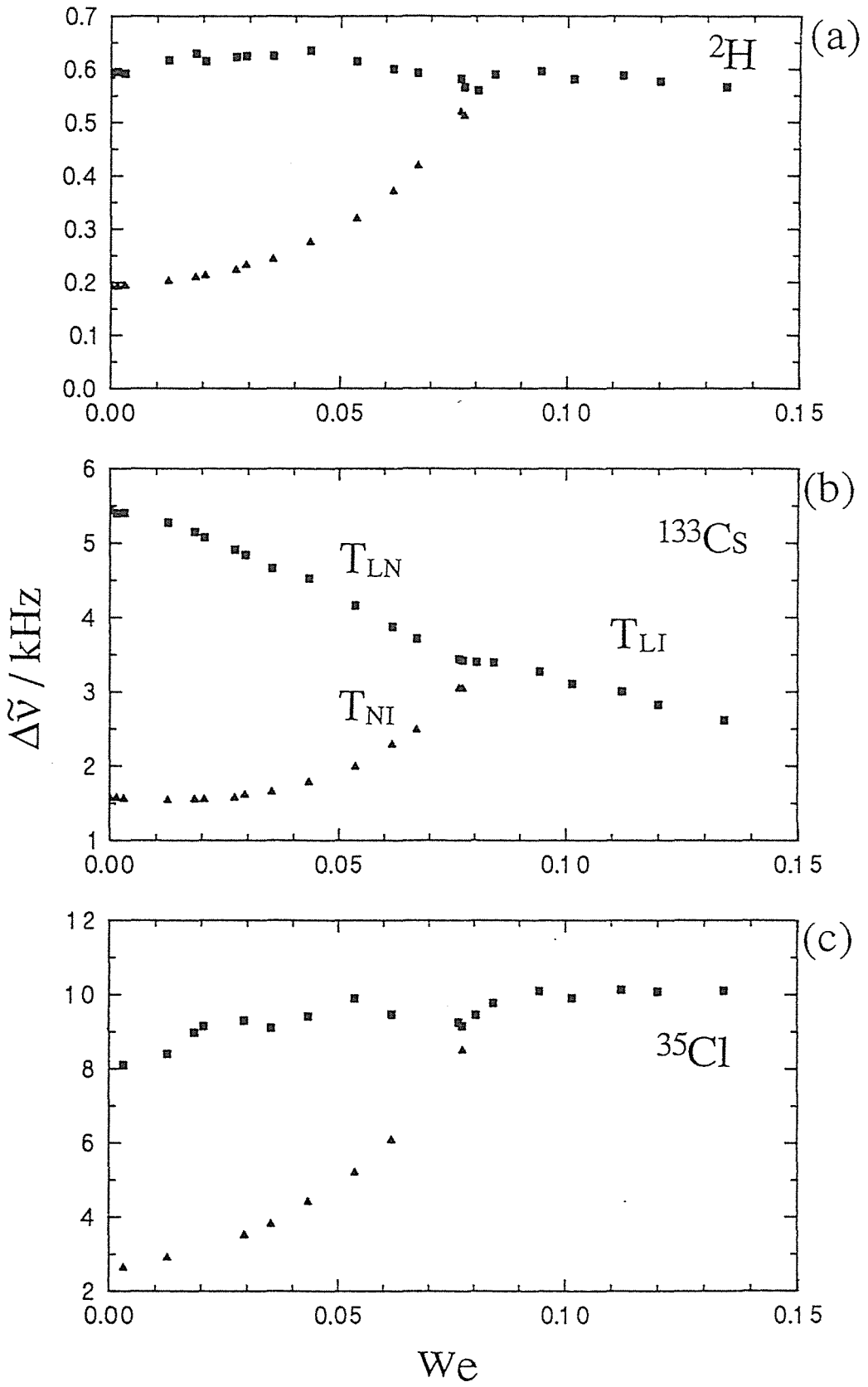
(a)
^{2}H
(b)
^{133}Cs
T_{LN}
T_{LI}
T_{NI}
(c)
^{35}Cl
$\Delta\tilde{\nu}$ / kHz
We
0.0
0.1
0.2
0.3
0.4
0.5
0.6
0.7
1
2
3
4
5
6
2
4
6
8
10
12
0.00
0.05
0.10
0.15

and this is done by raising the temperature, as increased temperature leads to smaller micelles. Once the micelle reaches a certain size at a given volume fraction a transition from the lamellar phase into the nematic phase will occur. It must be remembered that the concentration and temperature are changing along the transition line, so high w_e also corresponds to high temperature.

The ^{133}Cs quadrupole splittings decrease with increasing w_e at T_{LN} and T_{LI} (figure 30b). Since the ^{2}H quadrupole splittings indicate that the product $S \langle P_2(\cos\alpha)\rangle_s$ is roughly constant along the transition line, the reason for this must be the extra Cs^+ ions that are being added which causes an increase in the fraction of free ions. This effect can again be removed by investigating the change in Cs^+ ions associated per amphiphile molecule as in the previous section. The plot of n_b / n_A normalized to $w_e = 0.00$ and T_{LN} for the $w_e = 0.00$ (315.55 K) sample is given in figure 31. The bound ion fraction remains relatively constant with increasing w_e. So the surface charge density remains constant and this is associated with the micelle size remaining relatively constant at this transition as witnessed by the ^{2}H quadrupole splittings.

The ^{35}Cl quadrupole splittings increase steadily with increasing w_e (figure 30c). To remove the effects of increasing the Cl^- concentration it is better to plot the bound fraction per amphiphile normalizing to the $w_e = 0.0126$ sample at its T_{LN} (319.72 K). This is done in figure 32 and shows the spectacular increase in this quantity with increasing w_e (and temperature) but it is straightforward to demonstrate there is still a large excess of Cs^+ ions to bound at the micellar surface. The ratio $\Delta\nu(^{35}Cl)/\Delta\nu(^{133}Cs) = 7(\chi_{Cl}/\chi_{Cs})(\beta_{Cl}/\beta_{Cs})$. If it is assumed that the χ ratio is equal to that of the ratio of electric quadrupole moments then β_{Cl}/β_{Cs} can be determined. This quantity can be related to the ratio of number bound (n_b) by recalling that $\beta_{Cl} = n_b^{Cl} / n_s$ and $\beta_{Cs} = n_b^{Cs} / (n_A + n_s)$ where

Figure 31. The number of caesium ions bound per amphiphile molecule n_b^{Cs} versus w_e along the lamellar transition line. The values have all been reduced to n_b^{Cs} at T_{LN} for the $w_e = 0.00$ sample (315.52 K).

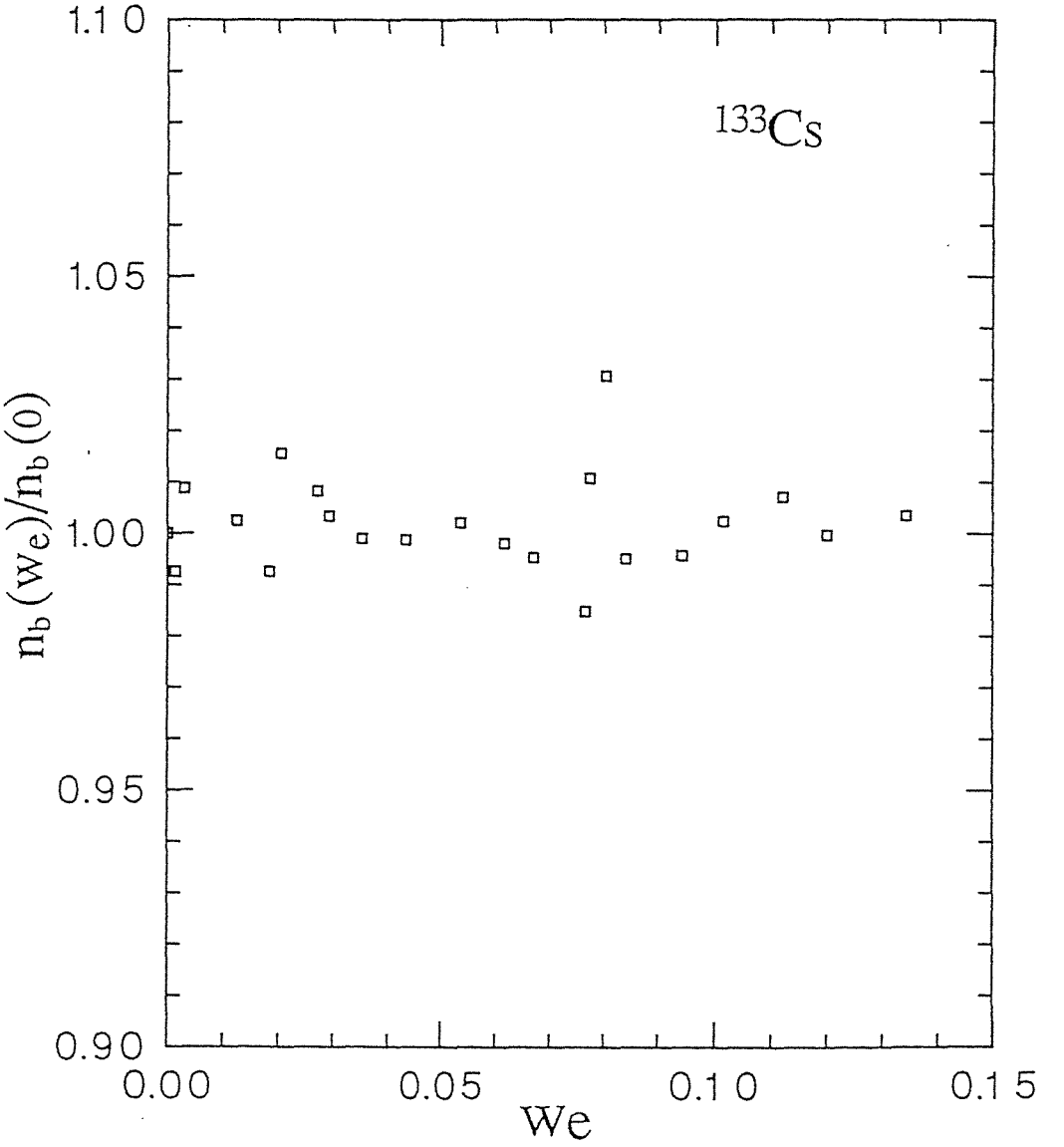
1.10
1.05
1.00
0.95
0.90
$n_b(We)/n_b(0)$
^{133}Cs
0.00
0.05
0.10
0.15
We

Figure 32. The number of chloride ions bound per amphiphile molecule n_b^{Cl} versus weight fraction CsCl w_e along the lamellar transition line. The values have all been reduced to n_b^{Cs} at T_{LN} for the $w_e = 0.0126$ sample (319.72 K).

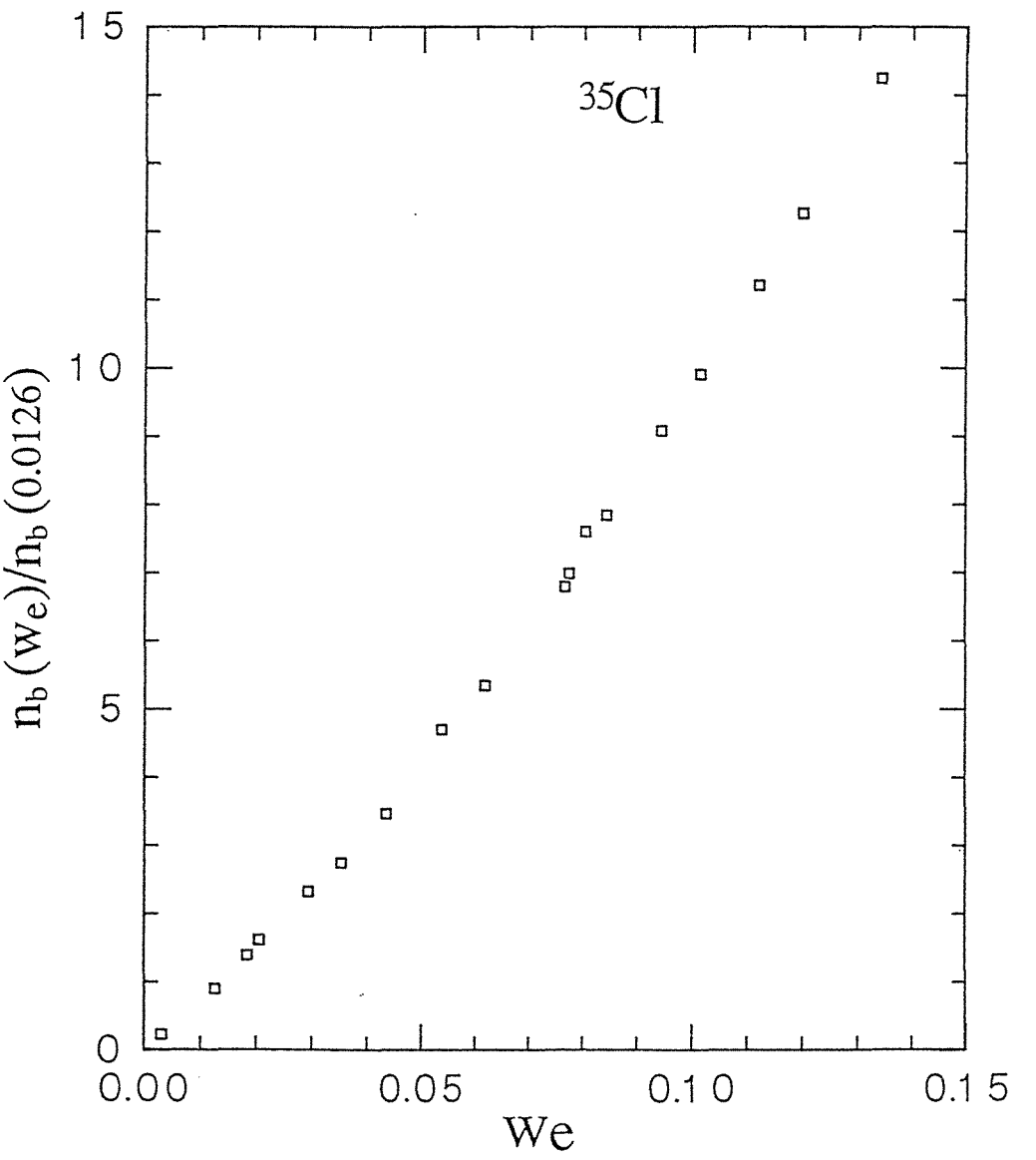
15
10
5
0
0.00
0.05
0.10
0.15
^{35}Cl
$n_b\,(w_e)/n_b\,(0.0126)$
We

n_s and n_A are, as before, the number of moles of salt and amphiphile respectively, and n_b^{Cl} and n_b^{Cs} are respectively the number of bound Cl^- and Cs^+ ions. n_b^{Cl}/n_b^{Cs} is therefore equal to (β_{Cl}/β_{Cs})($n_s/(n_A + n_s)$). This quantity is plotted in figure 33, where it is seen that at T_{LN} there is a 10 fold increase in n_b^{Cl}/n_b^{Cs} but even at the highest temperature n_b^{Cl} is only 1 % of n_b^{Cs}. Even if the assumption regarding χ_{Cl}/χ_{Cs} is not correct, the relative change in n_b^{Cl}/n_b^{Cs} is not affected since χ_{Cl}/χ_{Cs} is temperature independent,

(b) Nematic to isotropic transition line

At this transition S is not constant, so $\Delta\nu_{T_{NI}}$ is a function of $|q_{zz}|_s$ and S. For all three nuclei $\Delta\nu_{T_{NI}}$ increases with w_e, an increase that is paralleled by the increase in the temperature width of the I/N_D^+ coexistence region. A plot of this temperature width is given in figure 34. In the CsPFO / ^2H_2O system the width of the isotropic / nematic coexistence region increases with increasing weight fraction of amphiphile and the plot is not unlike figure 34. The magnitude of $T_{IN} - T_{NI}$ has been shown to be proportional to the strength of the transition. The value of the order parameter and probably the size of the aggregate ($<P_2(\cos\alpha)>_s$) also increase at T_{NI} as w_e increases. At Cep, $S<P_2(\cos\alpha)>_s$ has increased to such an extent that it cannot be distinguished from the lamellar phase. This is the upper limit of the N_D^+ phase.

Figure 33 Ratio of fraction of chloride ions bound relative to the fraction of caesium ions bound, expressed as the ratio per amphiphile molecule, versus the w_e.

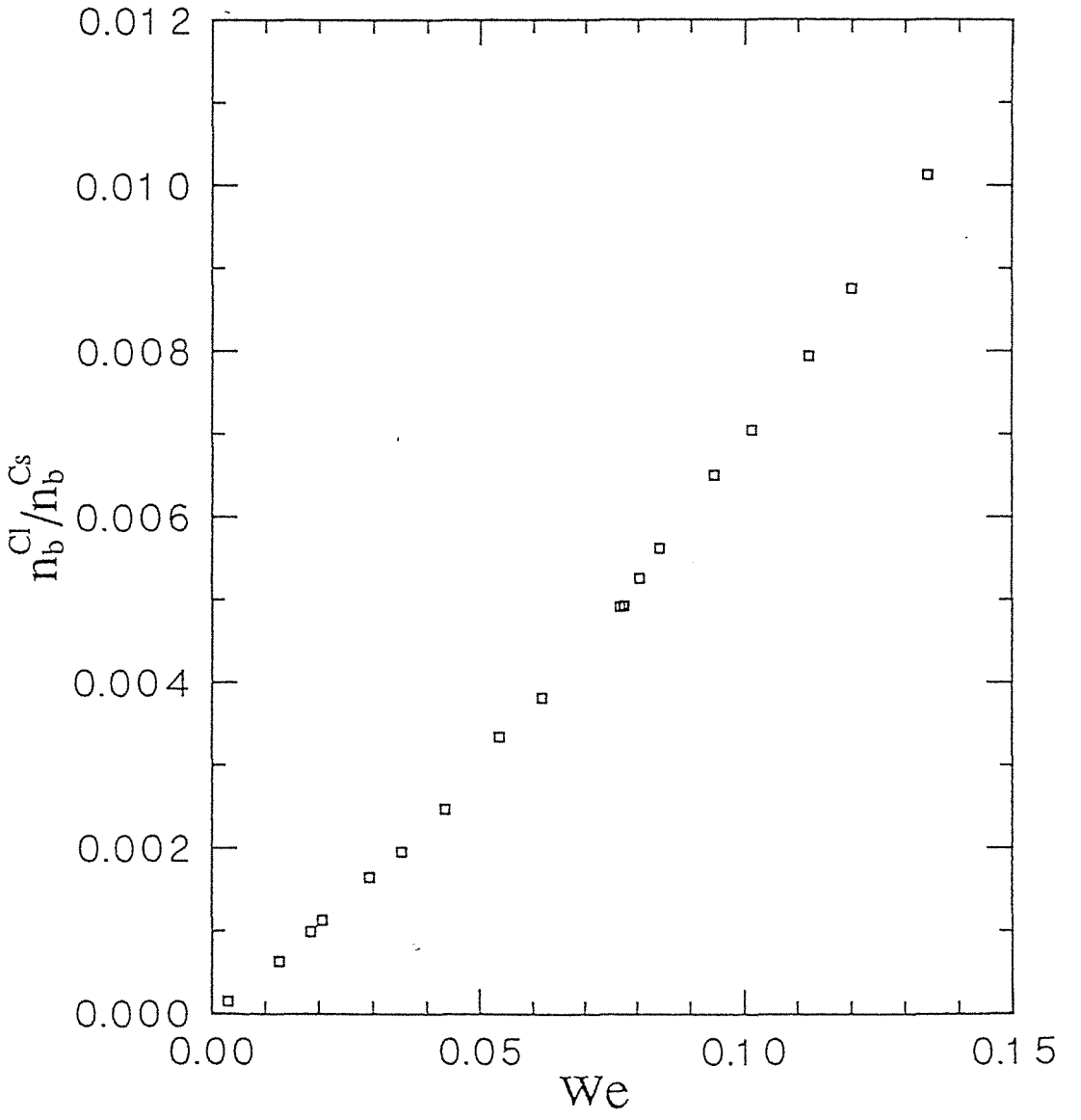
0.012
0.010
0.008
0.006
0.004
0.002
0.000
n_b^{Cl}/n_b^{Cs}
0.00
0.05
0.10
0.15
We

Figure 34. Plot of T_{IN} - T_{NI} versus w_e, showing the increase in the temperature width of the isotropic / nematic biphasic region with increasing w_e.

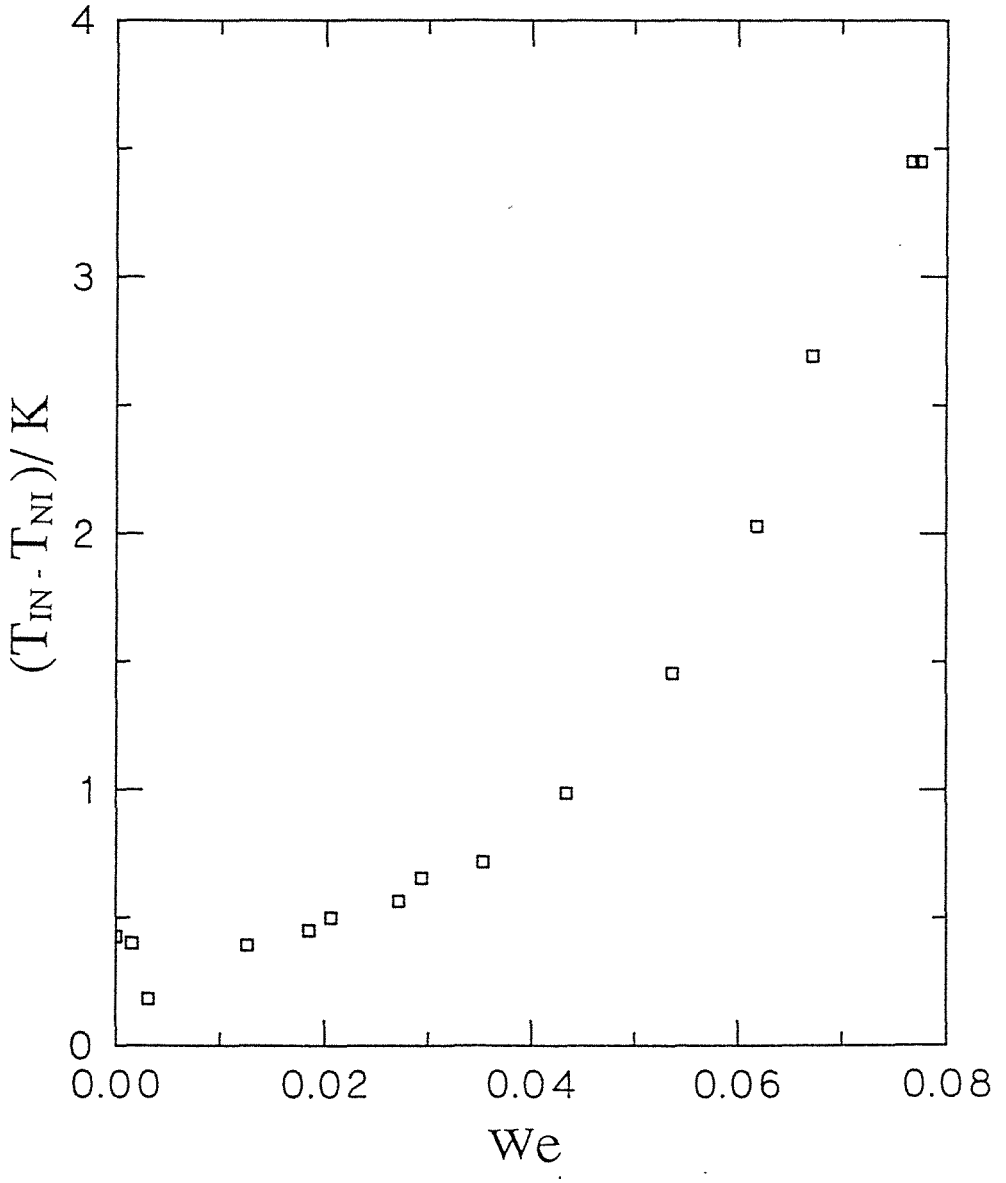
4
3
2
1
0
0.00
0.02
0.04
0.06
0.08
$(T_{IN} - T_{NI})$ / K
We

7. CONCLUSION

It has been shown that the phase behaviour of the CsPFO/^2H_2O/CsCl system can be understood in terms of change to the aggregate size on the addition of the salt. At constant temperature the effect of the salt is to increase the aggregation number of the micelle. The way the micelle grows is to increase the length of the semi-major axis, i.e. the micelle becomes more anisometric and the intermicellar anisotropic interaction is increased [40]. The reason for the growth in micelle size is due to increased counter-ion binding which lowers the charge density on the micelles surface. In fact there is a strong coupling between micelle size and the surface charge density. A lower charge density enables the carboxylate head groups to get closer together and encourages the formation of planar surfaces over curved surfaces (i.e. repulsion between head groups leads to curved surfaces as these allow maximum separation of the head groups in a micelle).

Thus at any given temperature the micelles will increase in size with an increase in w_e, but the ^2H NMR tells us that the micelles are about the same size and shape at the L_D to N_D^+ transition. Thus the phase transition temperature increases with w_e , since the temperature has to be increased by successively greater amounts in order to decrease the micellar size so as to bring about the phase transition. Thus it is possible to follow change in aggregate size simply by observing the phase behaviour. This can be done quickly and cheaply using a polarizing microscope equipped with a hot stage. The effects of various types of additives (alcohols, salts, acids, bases, etc.) on aggregate size can therefore be determined quickly and through this a better understanding of the nature of the surface interactions will result.

It has also been shown that the temperature range of the nematic phase first increases at small w_e, then starts to decrease as the CsCl concentration is increased further until it eventually disappears altogether at Cep. This behaviour compares with that of the hydrocarbon liquid crystal system DACl / ammonium chloride /water [8], some phase diagrams for which are given in figure 35. In the absence of salt the nematic range is very small (in fact at one time it was thought that the salt was essential for the nematic phase). The addition of salt extends the nematic phase region and decreases the range of the hexagonal phase (figures 35(a) and (b)). Eventually the hexagonal phase disappears altogether (figure 35(c) and (d)) and an extensive nematic phase results. Thus the addition of salt promotes the N_D phase and discourages the hexagonal phase (i.e. the salt promotes the production of discoid micelles). At a constant DACl: water ratio of 1.16 by weight the phase behaviour on the addition of NH_4Cl (figure 36) is very similar to that of our system (i.e. the temperature range of the nematic phase is initially extended by salt, before decreasing and finally disappearing at Cep ($w_e = 0.74$; $T = 67^oC$) and the L to N_D is thought to be second order). This suggests the possibility of some universal behaviour of micellar liquid crystals.

For our fluorocarbon system we do not need salt for an extensive nematic phase but like the hydrocarbon small amounts of salt do stabilize the phase. What is the difference between hydrocarbons and fluorocarbons? Maybe it has something to do with the water-hydrocarbon (fluorocarbon) interfacial energy. Fluorocarbons have a larger cross section area, and are rigid which may enable the water to get close to the fluorocarbon core. This will give rise to a high interfacial tension which the system will reduce by reducing the surface curvature i.e. by producing discoidal micelles. Further work is necessary to understand this. An obvious experiment is to compare the phase behaviour of hydrocarbons, and fluorocarbons in H_2O and ^2H_2O [14].

Figure 35. Sequence of phase diagrams for the decylammonium chloride (DACl) / NH_4Cl / water system. The presence of salt (NH_4Cl) favours the nematic phase over the hexagonal phase ((a) to (d)) (from reference 8).

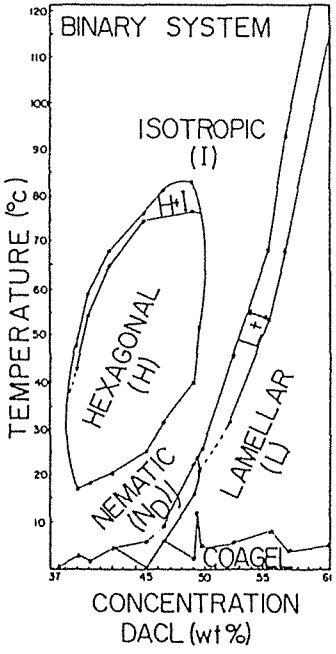
BINARY SYSTEM
ISOTROPIC
(I)
H+I
HEXAGONAL
(H)
L+I
LAMELLAR
(L)
NEMATIC
(N,D)
COAGEL
TEMPERATURE (°c)
CONCENTRATION
DACL (wt%)

(a)

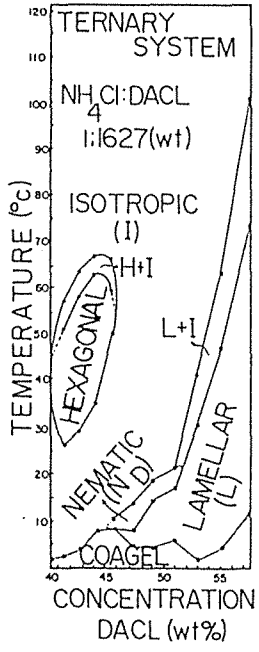
TERNARY
SYSTEM
NH4CI:DACL
1:1627(wt)
ISOTROPIC
(I)
H+I
HEXAGONAL
L+I
LAMELLAR
(L)
NEMATIC
(N,D)
COAGEL
TEMPERATURE (°c)
CONCENTRATION
DACL (wt%)

(b)

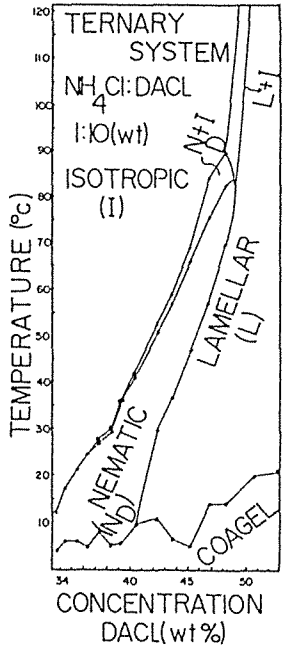
TERNARY
SYSTEM
NH4CI:DACL
1:10(wt)
ISOTROPIC
(I)
N+I
D
L+I
LAMELLAR
(L)
NEMATIC
(N,D)
COAGEL
TEMPERATURE (°c)
CONCENTRATION
DACL(wt%)

(c)

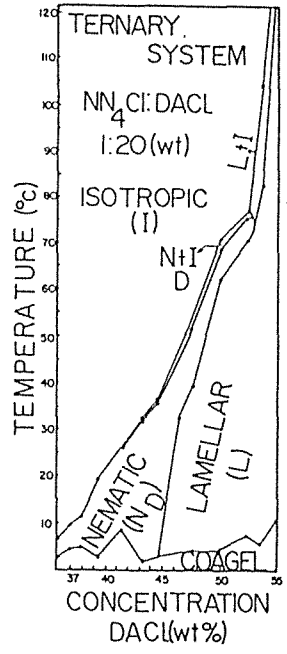
TERNARY
SYSTEM
NH4CI:DACL
1:20(wt)
ISOTROPIC
(I)
N+I
D
L+I
LAMELLAR
(L)
NEMATIC
(N,D)
COAGEL
TEMPERATURE (°c)
CONCENTRATION
DACL(wt%)

(d)

Figure 36. Partial phase diagram showing the effect of added salt (NH_4Cl) at a constant DACl : water ratio (from reference 8).

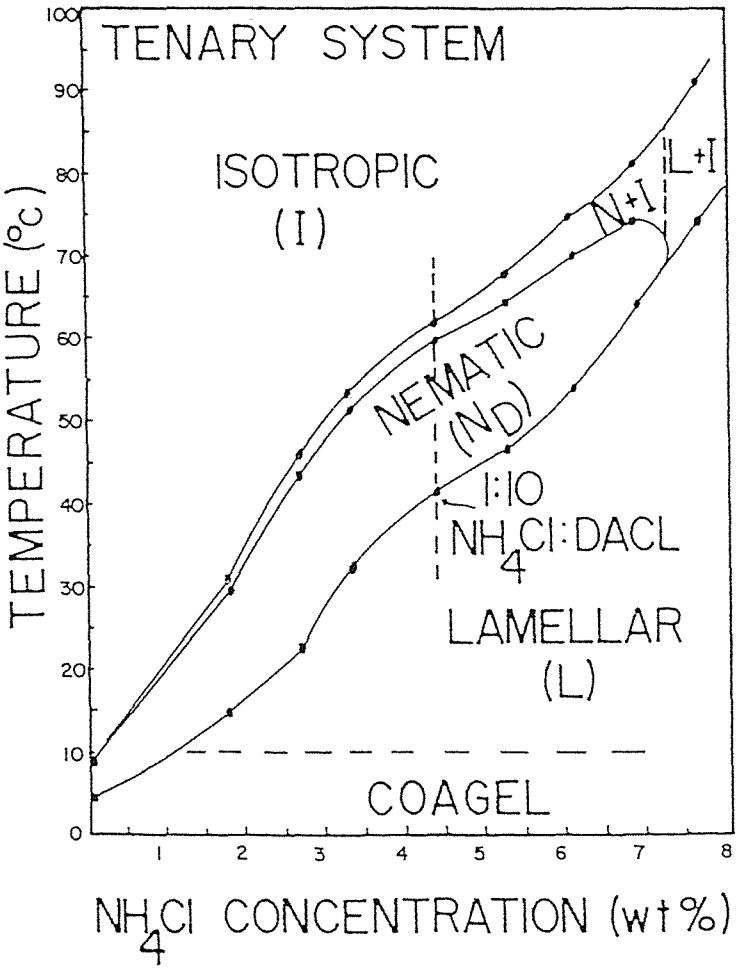
TENARY SYSTEM
ISOTROPIC
(I)
N+I
L+I
NEMATIC
(ND)
1:10
NH4CI:DACL
LAMELLAR
(L)
COAGEL
TEMPERATURE (°C)
NH4CI CONCENTRATION (wt%)
0
10
20
30
40
50
60
70
80
90
100
1
2
3
4
5
6
7
8

The eventual disappearance of the nematic phase is related to the strength of the isotropic to nematic transition, which is proportional to $T_{IN} - T_{NI}$. As w_e increases so does $T_{IN} - T_{NI}$ and the micelle order parameter and size at T_{NI} also increase. At Cep the nematic and lamellar phases are no longer distinguishable, and this point represents the upper limit of nematic stability.

An interesting and unexpected observation was the presence of quadrupole splittings in the ^{35}Cl coion. With hindsight this may be obvious, but the presence of Cl^- ions at the surface of the negatively charged micelle could suggest that they have a part to play in the surface interactions. However, since the calculated value of the moles of bound Cl^- ions per amphiphile molecule has been shown to reflect the bulk Cl^- ion concentration, the effect is probably not a specific interaction. It probably effects the phase behaviour by modifying the fraction of bound Cs^+ ions which is the factor that determines the micelle size and shape and hence the macroscopic phase behaviour. It would be interesting to investigate the role of the coion on the phase behaviour by for example, choosing a sample with an extensive nematic range and examining the effect on the phase behaviour of substituting F^-, Br^-, and I^- for the Cl^- ions. A simple polarizing microscope experiment will give a broad picture of what is happening, and the specific effects at the micellar surface can be investigated by studying the NMR of the possible quadrupole nuclei.

8. REFERENCES

1. B. Lindman and H. Wennerström,
   In *Topics in Current Chemistry* ; Springer-Verlag : Berlin **87**, pp 1-84 (1980).

2. P. Ekwall,
   In *Advances in Liquid Crystals* ; Ed. G.H.Brown; Academic : New York
   1, pp 1-142 (1975).

3. G.J.T. Tiddy,
   Phys. Rep. **57**, 1 (1980).

4. P.S. Pershan,
   Phys. Today **35**, 34 (1982).

5. F. Reintzer,
   Monatsh Chem. **9**, 1

6. K.D. Lawson and T.J. Flautt,
   J. Am. Chem. Soc. **89**, 5490 (1967).

7. L.J. Yu and A. Saupe,
   J. Am. Chem. Soc. **102**, 4879 (1980).

8. M.R. Rizzatti and J.D. Gault,
   J. Colloid Inerface Sci. **110**, 258 (1985).

9. H. Lee and M.M. Labes,
Mol. Cryst. LIq. Cryst. **84**, 137 (1982).

10. N. Boden, S. Corne and K.W. Jolley,
J. Phys. Chem. **91**, 4092 (1987).

11. N. Boden, K.W. Jolley and M.H. Smith,
To be published.

12. K. Fontell and B. Lindman,
J. Phys. Chem. **18**, 3289 (1983).

13. H. Hoffman,
Ber. Bunsengers. Phys. Chem. **88**, 1074 (1984).

14. N. Boden, K.W. Jolley and M.H. Smith,
Liq. Cryst. **6**, 481 (1989).

15. A. Saupe,
J. Colliod Interface Sci. **58**, (1977).

16. J. Charvolin, A. Levelut and E.T. Samulski,
J. Physique Lett. **40**, L- 587 (1979).

17. N. Boden, R.J. Bushby, K.W. Jolley, M.C. Holmes and F. Sixl,
Mol. Cryst. Liq. Cryst. **152**, 37 (1987).

18. N. Boden, R.J. Bushby, L. Ferris, C. Hardy and F. Sixl,
Liq. Cryst. **1**, 109 (1986).

19. L.J. Yu and A. Saupe
Phys. Lett. **45**, 1000 (1980).

20. N. Boden, R.J. Bushby and C. Hardy,
J. Physique Lett. **46**, L- 325 (1985).

21. N. Boden, S. Corne, M.C. Holmes, P.H. Jackson, D. Parker and K.W. Jolley
J. Physique **47**, 2135 (1986).

22. M.C. Holmes, D.J. Renolds and N. Boden,
J. Phys. Chem. **91**, 5257 (1987).

23. K. Radley,
Mol. Cryst. Liq. Cryst. **102**, 317 (1984).

24. C. Rosenblatt,
J. Physique Lett. **46**, L- 1191 (1985).

25. C. Rosenblatt,
J. Chem. Phys. **89**, 5033 (1988)

26. C. Rosenblatt,
J. Phys. Chem. **92**, 5770 (1988).

27. N. Boden and S.A. Jones,
N.A.T.O. ASI. Sci. C. Maths Phys. Sci. **141** 437 (1985).

28. H. Wennerström, G. Lindblom and B. Lindman,
Chem. Scr. **6**, 97 (1974).

29. A.D. Buckingham and K.D. McLauchlan ,
In *Progress in NMR Spectroscopy, Vol. 2* ; Ed. J.W Emsley, J. Feeney and L.H. Sutcliffe, Pergaman. Oxford, p 63 (1967).

30. H. Wennerström and G. Lindblom,
Q. Rev. Biophys. **10**, 67 (1977).

31. R. Dietrich and L Trahms,
J. Magn. Reason. **71**, 337 (1987).

32. W.L. McMillian,
Phys. Rev. A **4**, 1238 (1971).

33. W.L. McMillian,
Phys. Rev. A **6**, 936 (1972).

34. D. Parker,
PhD Thesis, University of Leeds (1988).

35. D.M. Chen, F.Y. Fujiwara and L.W. Reeves,
Can. J. Chem. **55**, 2396 (19770.

36. K.W. Jolley, M.H. Smith and N. Boden,
Chem. Phys. Lett. **162**, 152 (1989).

37. P. Waldstein, S.W. Rabideam and J.A. Jackson,
J. Phys. Chem. **41**, 3407 (1964).

38. N.O. Perrson and B.J Lindman,
J. Phys. Chem. **79**, 1410 (1975).

39. N.O. Perrson and B.J Lindman,
J. Phys. Chem. **83**, 3015 (1979).

40. N. Boden and M.C Holmes,
Chem. Phys. Lett. **109**, 76 (1984).